universität wien

Diplomarbeit

Titel der Diplomarbeit

On the localizability of atmospheric tracer sources using a Lagrangian particle dispersion model in backward mode

Verfasser

Rainer Kaltenberger

Angestrebter akademischer Grad

Magister der Naturwissenschaften (Mag. rer. nat.)

Wien, 2013

"Peace cannot be kept by force;
it can only be achieved by understanding."

Albert Einstein (1879–1955)

Contents

List of Figures

List of Tables

List of Acronyms

4DVAR Four dimensional variational data assimilation

^{85}Kr Krypton-85

ACM Association for Computing Machinery

AOI Area Of Interest

AP Additional Protocol (to the NPT)

ASCII American Standard Code for Information Interchange

ATM Atmospheric transport model/modelling

ATMES-II 2nd Atmospheric Transport Model Evaluation Study

ATTA Atomic trap trace analysis

BfS German Federal Office for Radio Protection

BOKU University of Natural Resources and Life Sciences, Vienna

Bq Bequerel

COGEMA Compagnie générale des matières nucléaires

CRESP Consortium for Risk Evaluation with Stakeholder Participation

CTBT Comprehensive Nuclear-Test-Ban Treaty

CTBTO Comprehensive Nuclear-Test-Ban Treaty Organisation

CWC Convention on the Prohibition of the Development, Production, Stockpiling and Use of Chemical Weapons and on their Destruction

DWD Geman Weather Service

ECHAM5 5th generation of the ECHAM general circulation model (*EC*MWF based, developed in *Ham*burg)

ECMWF European Centre for Medium-range Weather Forecast

EMIS Electromagnetic isotope separation

ESARDA European Safeguards Research and Development Association

ETEX European Tracer Experiment

ETEX-1 1st European Tracer Experiment

FMCT Fissile Material Cutoff Treaty

GCM General circulation model

GEM Global Environmental Multiscale Mode

GFS Global Forecast System

GNU GNU's not Unix

GRIB Gridded Binary

GUI Graphical user interface

HYSPLIT Hybrid Single Particle Lagrangian Integrated Trajectory Model

IAEA International Atomic Energy Agency

IDC International Data Centre (division to the PTS)

IDW Inverse distance weighting

iGSE Independent Group of Scientific Experts on the detection of clandestine nuclear-weapons-usable materials production

IMS International Monitoring System (of the CTBTO)

INESAP International Network of Engineers and Scientists Against Proliferation

INFCIRC IAEA Information Circular

IPFM International Panel on Fissile Materials

JRC Joint Research Centre (of the European Comission)

Kr-85 Krypton-85

LIDAR Light Detection And Ranging

LPDM Lagrangian particle dispersion model/modelling

maxcor Maximum correlation

MM Mesoscale model

MM5 Mesoscale Model 5

NCEP National Centers for Environmental Predictions

NDC National Data Centre (of a Signatory State to the CTBTO)

netCDF Network Common Data Form

NGO Non-governmental Organisation

NOAA National Oceanic and Atmospheric Administration

NPT Non-Proliferation Treaty

NWP Numerical weather prediction

PFC Perfluorcarbon compounds

PMCH Perfluormethylcyclohexane

POPs Persistent Organic Pollutants

PSR Potential source region

PTS Provisional Technical Secretariat (of the CTBTO)

Pu-238 Plutonium-238

RN Radionuclide

RSMC Regional Specialized Meteorological Centre

s-r Source-receptor

SEA Special event analysis

SODAR Sound Detection And Ranging

SRM Source-receptor matrix

SRS Source-receptor sensitivity

SW Southwest

UNODA United Nations Office for Disarmament Affairs

UF$_6$ Uranium hexafluoride

UTC Coordinated Universal Time

v/v volume to volume

WAES Wide-area environmental sampling

Web-Grape Web-connected Graphics Engine

WISE World Information Service on Energy

WMO World Meteorological Organisation

WRF Weather Research and Forecasting

ZAMG Central Institute for Meteorology and Geodynamics, Austria

ZNF Carl Friedrich von Weizäcker Center for Science and Peace Research at the University of Hamburg

Abstract

The localizability of atmospheric tracer sources can be assessed using atmospheric transport models in backward mode. With the Additional Protocol to the Non-Proliferation Treaty (NPT), whose compliance of ratified states is monitored by the International Atomic Energy Agency (IAEA), atmospheric sampling analysis of the noble gas Krypton-85 (Kr-85), which is a suitable tracer for plutonium separation activities, was introduced. A novel sensor technology, called ATTA (atomic trap trace analysis), will soon allow a radical cost reduction of currently expensive sampling- and analyzing methods and thus will enable higher refined sampling intervals e.g. of 6h or 12h. The main target of this thesis is to investigate the effects of different temporal sampling resolutions on the localizability of tracer sources using backtracking methods, which have already been set up operationally to support the verification of the Comprehensive Nuclear-Test-Ban Treaty (CTBT).

Predefined weekly quantities of Kr-85 were hypothetically released in 2009 over the La Hague reprocessing plant and forward dispersed using the Lagrangian particle dispersion model Flexpart. In so-called "catch-the-plume" scenarios, pseudo concentration samples were generated at two fictitious sampling stations. For each of the virtual samples, source-receptor sensitivity (SRS) fields were simulated and averaged to yield backward sensitivities of different temporal sampling resolutions. Afterwards, backward correlation fields, so-called "possible source regions" (PSR) of the multiple measurement scenario, were calculated to compute localizability parameters, e.g. the distance between the spatio-temporal correlation maximum and the release point or the size of a user-defined PSR.

All methods applied within this thesis were validated using real tracer measurement data of the 1th European Tracer Experiment. A cost-benefit analysis yields optimum spatial localization results for a sampling interval of 12h, where in 86% of all simulations the error of the estimated release point location was < 350km and correlation values ranged ≥ 0.7 at La Hague in 61% of all cases. The tracer origin stayed well locatable, i.e. had an localization error <111 km, up to 2000km away from the source in synoptic weather conditions, where advection processes dominate over diffusion yielding sharp concentration peaks at the sampling stations. Temporal localization within ±6h can be achieved in around 70% of all cases and intervals. Further research is needed to improve the localizability in diffusive weather situations and to assess the minimum detectable source strength. The findings of this thesis might contribute to the adaption of the presented methods for monitoring the compliance of other treaties. NGOs can operate Flexpart to confirm the independence of statements published by international organizations in divisive issues.

Kurzfassung

Im Rückwärtsmodus eignen sich atmosphärische Transportmodelle, um die Lokalisierbarkeit von Quellen atmosphärischer Tracer zu ermitteln. Durch das Zusatzprotokoll zum Atomwaffensperrvertrag (NPT), dessen Einhaltung von der Internationalen Atomenergie-Organisation (IAEO) überwacht wird, sind Messungen des chemisch inaktiven, radioaktiven Edelgases Krypton-85 (Kr-85) rechtlich vorgesehen. Krypton-85 eignet sich als Indikator zur Herstellung von Plutonium. Eine neue Messtechnik, genannt ATTA (Atomic Trap Trace Analysis), wird in naher Zukunft die Kosten der zurzeit aufwändigen Sampling- und Analysemethoden stark reduzieren und höher aufgelöste Samplingintervalle, z.B. 6-stündig oder 12-stündig, ermöglichen. Das Ziel dieser Diplomarbeit ist die Untersuchung der Auswirkung von verschiedenen zeitlichen Messintervallen auf die Lokalisierbarkeit von Tracerquellen mittels atmosphärischer Rückverfolgungsmethoden, welche bereits operationell zur Verifikation des Kernwaffenteststopp-Vertrages (CTBT) eingesetzt werden.

Hierzu wurden 2009 wöchentliche Emissionen von Kr-85 über der Wiederaufbereitungsanlage La Hague fiktiv freigesetzt und Vorwärtssimulationen mit dem Lagrange'schen Partikelausbreitungsmodell Flexpart durchgeführt. In sogenannten "Catch-the-plume" Szenarien wurden Pseudokonzentrationsmesswerte an jeweils zwei virtuellen Messstationen generiert und die zugehörigen Quell-Rezeptorfelder (SRS-Felder) durch Flexpart im Rückwärtsmodus berechnet. Diese wurden anschließend gemittelt, um Sensitivitätsfelder für unterschiedliche Messintervalle der Pseudomessungen zu erhalten. Danach wurden mittels eines "try-and-error" Ansatzes Rückwärtskorrelationsfelder, sogenannte "PSR-Felder" der jeweiligen Messszenarien berechnet, um Lokalisierbarkeitsparameter z.B. die Distanz zwischen räumlich-zeitlicher Maximalkorrelation und dem Freisetzungspunkt oder der Größe der Fläche eines benutzerdefinierten Korrelationswertes zu bestimmen.

Die verwendeten Methoden wurden im Anschluß anhand von echten Tracermessdaten des ersten Europäischen Tracer Experiments (ETEX-1) validiert. Eine Kosten-Nutzen Analyse identifizierte als ideale Zeitauflösung zwölf Stunden, wobei der Lokalisierungsfehler der berechneten Position des Quellpunktes in 86% aller Simulationen kleiner als 350km war und in 61% der Fälle der Korrelationswert bei La Hague 0.7 überstieg. Der Ursprung des Tracers war auf bis zu 2000km Entfernung von der Quelle gut lokalisierbar (Lokalisierungsfehler <111 km) insbesondere bei Wetterlagen, bei denen Advektionsprozesse im Vergleich zur Diffusion dominierten und zu scharfen Signalen bei den Samplingstationen führten. Innerhalb einer Toleranz von ±6h waren ca. 70% der Simulationen aller Samplingintervalle zeitlich lokalisierbar. Weitere Untersuchungen sind nötig um die Lokalisierbarkeit bei gra-

dientschwachen Wetterlagen zu verbessern. Die Ergebnisse können bei möglichen zukünftigen Adaptionen der Methoden im Rahmen von anderen internationalen Verträgen, bei welchen atmosphärische Rückverfolgungsmethoden anwendbar sind, nützlich sein. Nichtregierungsorganisationen könnten Flexpart verwenden, um bei polarisierenden Themen die Unabhängigkeit internationaler Organisationen hervorzuheben.

Preface

This diploma-thesis was initiated by the research project "Simulations of atmospheric Noble Gas Concentrations to Assess Sampling Procedures for the Detection of Clandestine Nuclear Reprocessing" (IAEA GER 1643 (C.38)) funded by the Government of the Federal Republic of Germany within the Joint Programme on the Technical Development and Further Improvement of IAEA Safeguards between the Federal Republic of Germany and the IAEA. Based on findings of phase I/part III of this project which were achieved by Rainer Kaltenberger (ZAMG, Uni Wien), supervised by Prof. Martin B. Kalinowski (ZNF-Hamburg) and Dr. Gerhard Wotawa (ZAMG) in 2012, the results were subsequently generalized and further evaluated within this thesis. The framework project of this thesis is briefly described in Chap. 1.4.1.

Notice: Neither the author of this thesis, nor the organization, nor the Federal Government of Germany assume any liability whatsoever for any use of this thesis or parts of it. Moreover, the content of this thesis does not represent any policy of the Federal Government of Germany.

Chapter 1

Introduction

Environmental sample analysis becomes increasingly important for the verification of international treaties. Atmospheric backtracking of tracer substances, i.e. particles or noble gases, released by clandestine processes provide a valuable approach for international organisations to verify the compliance of ratified state parties which is generally foreseen by a number of treaties. Apart from legal considerations, a variety of technical aspects have to be investigated to qualify a tracer being capable for backtracking purposes.

In a *receptor-orientated* view, i.e. if an ad hoc measurement during a field-campaign yields suspicious concentration levels of a tracer substance, the detectability of the origin of the tracer depends on several factors (Fig. 1.1). Since the physical laws which control dispersion result in a very complex multimodal distribution that can hardly be described completely by a parametric model, a way to approach this distribution is to generate realisations by simulations with an atmospheric transport model (ATM) (Helle and Pebesma (2013)). Thus the localizability of a tracer source can be determined by analyzing the accuracy of localization of realisations through ATMs usually driven by weather data from one year and based on specific sampling setups.

Different synoptic weather patterns, more specifically the influence of advection, diffusion and deposition, heavily affect the dispersion process of the tracer substance. Atmospheric conditions which are unsuitable for tracing substances can be favourable for a violator of a treaty. This has to be recognized along with other potential countermeasures when assessing the detectability. In addition, the ability to discover a suspicious activity based on sample analysis is limited by its minimum detectable concentration - a threshold value, which is predominantely defined by the atmospheric background and the minimal source strength of the respective tracer substance. Moreover, the atmospheric tracer sub-

stance has to be well above the detection limit specified by the applied sample analyzing technique.
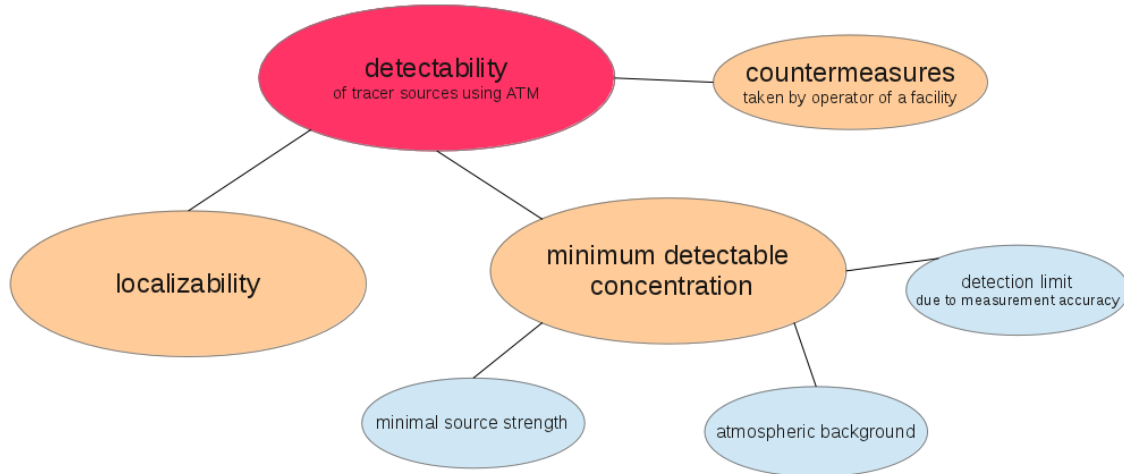
Figure 1.1 – Simplified sketch of aspects which have to be considered when assessing the detectability of tracer substances. Focus of this work is localizability. A more detailed chart is printed on page 16.

Like the Comprehensive Nuclear-Test-Ban Treaty (CTBT), where this concept is already implemented operationally, the Non-Proliferation Treaty (NPT) legally forsees environmental sample analysis which was manifested as a response to a successful implementation of environmental sample analysis in Iraq within the 1$^{\text{st}}$ Gulf War by the International Atomic Energy Agency (IAEA).

In this thesis, which was initiated within a project funded by the the Joint Programme between the Federal Republic of Germany and the IAEA, backtracking methods were applied to assess the localizability of Krypton-85 sources due to clandestine reprocessing activities. However since this noble gas is an ideal tracer substance, the results can be generalized to other tracer substances for mesoscale- to long-range tansport.

1.1 Environmental sample analysis within the NPT

According to the United Nations Office for Disarmament Affairs (UNODA (2012)), currently 190 states, excluding India, Israel, Pakistan and North Korea, joined the NPT and declared not to develop and posses nuclear weapons. Under the responsibility of the IAEA, a safeguard system has been established to monitor the intended non-proliferation

of all State Parties. However, the "most significant gap and biggest challenge for verification of nuclear non-proliferation is the detection of weapons-usable materials production"(Kalinowski, M.B. (2008)).

The introduction of the Additional Protocol (AP) in 1997 permits the agency to use environmental sampling techniques to detect clandestine production of fissile materials (Kalinowski, M.B. et al. (2006)).

Two different approaches are mentioned in the protocol: Article 6 allows the IAEA environmental sampling at specific locations of interest whereas article 9 establishes a legal basis for so-called *wide-area environmental sampling* (WAES). However "the Agency shall not seek such access until the use of wide-area environmental sampling and the procedural arrangements therefore have been approved by the Board" of Governors (IAEA (1997)).

Whereas further research on environmental sampling has to be carried out to be applied for IAEA safeguards purposes, this concept is already set up operationally to support the verification of the CTBT (CTBTO (2012)). The fusion of seismic, hydroacoustic and infrasound explosion signals together with global radionuclide and noble gas monitoring within the International Monitoring System (IMS), helps the Comprehensive Nuclear-Test-Ban Treaty Organisation (CTBTO) to locate explosion centers of clandestine nuclear tests fast and with high accuracy (Wotawa et al. (2003) and Wotawa and Becker (2007)).

1.2 Backtracking of noble gases to detect clandestine nuclear activities

Artificial radioactive *noble gas* isotopes are released into the atmosphere as a by-product of nuclear activities, such as nuclear tests, reprocessing of nuclear elements, or enrichment of uranium.

Kalinowski, M.B. et al. (2006) stated, that due to their special properties, noble gases can be used for atmospheric monitoring to detect and verify clandestine nuclear activities. Noble gases are chemically inert and resistent to dry or wet deposition processes during atmospheric transport. Considering that radioactive decay is the only relevant sink, samples of these isotopes can be taken several hundred kilometers away and can be tracked back to the source using *Atmospheric Transport Models* (ATMs).

Table 1.1 outlines possibilities of detecting different process steps in the production of fissile materials according to in-situ measurements and remote-sensing. Satellite imagery is mainly used for investigation of known facilities where heat generation and the size of

		Satellite Images		Air samples		
		Visible light	Infrared	Stand-off	Regional network	Tracer substance
Plutonium Production	Reactor	Yes	Yes	Yes	Yes	^{85}Kr
	Reprocessing	No	No	Yes	Larger facilities	
Uranium Enrichment	Conversion	No	No	Yes	Larger facilities	reaction products of UF_6 (possibly)
	Calutron/EMIS	No	Yes	Yes	No	
	Gas diffusion	Yes	Yes	Possible	No	
	Centrifuges	No	No	Unlikely	No	

Table 1.1 – Detectability of relevant process steps in production of weapons-usable materials. [Adapted after Kalinowski, M.B. (2008) and iGSE (2006)]

buildings deliver informations of production processes (Kalinowski, M.B. (2008)). Previous studies revealed, that Krypton-85 (^{85}Kr, henceforth Kr-85) is capable of being a tracer substance to detect *clandestine plutonium production*. The reaction products of the highly reactive uranium hexafluoride UF_6 are potential indicators for uranium enrichment during various process steps, which can possibly be traced using different gas sampling techniques and LIDAR-types (Light Detection and Ranging)(iGSE (2006)). Though the signatures are weak, the IAEA considers this approach as a novel technology for verifying IAEA safeguards (IAEA (2010)).

1.3   Suitability of using Kr-85 as a tracer

Spent nuclear fuel elements can be reprocessed to produce weapon-grade plutonium. During the chemical separation of plutonium, other fission products like the radioactive noble gas krypton-85 are co-generated. Due to its properties, Kr-85 is the best atmospheric indicator for detecting clandestine plutonium seperation regarding wide-area atmospheric monitoring (Kalinowski, M.B. (2008)) and has been suggested for use in IAEA safeguard applications.

1.3.1   Properties of Kr-85

Krypton-85 is a chemically inert, radioactive noble gas with a half-life of 10.76 years. The solubility of Kr-85 in water in the equilibrium is specified as $1.85 \cdot 10^{-10}$ g/g (Izrael, Y.A. et al. (1982) after Ahlswede et al. (2013)), thus wet deposition as a concentration sink can be neglected. In the context of environmental tracer studies, Kr-85 is feasable for

evaluation of atmospheric transport models (Zimmermann, P.H. (1989)) and can be used as a groundwater age indicator (Cook, P.G. and Solomon, D.K. (1995) after Ahlswede et al. (2013)). The effective radiation dose on humans of Kr-85 is $4 \cdot 10^{-9}$ Sv per year and Bq m^{-3} (Eckermann and Ryman, J.J. (1993)) and is thus not relevant according to radiation protection aspects.

1.3.2 Sources and background of atmospheric Kr-85

Winger et al. (2005) and Ahlswede et al. (2009) provide an overview to sources and background of atmospheric Kr-85: Anthropogenic sources are at least four orders of magnitude larger of magnitude than natural generation of Kr-85 by cosmic radiation. Far the most of atmospheric Kr-85 originates from nuclear fuel reprocessing facilities for either civilian or military purposes. Small amounts of Kr-85 are released during the operation of nuclear power plants, naval reactors and research reactors. Source terms for different contributors are specified in Tab. 1.2. The global inventory of Kr-85 is estimated to be about 5500 PBq at the end of 2009 (Ahlswede et al. (2013)).

Source	Emission [PBq/a]
La Hague reprocessing facility, France	237
Mayak RT-1 reprocessing facility, Russia	48.63
Rokkasho reprocessing facility, Japan	46
Sellafield reprocessing facility, UK	14.1
Kalpakkam reprocessing facility, India	5.99
Dimona reprocessing facility, Israel	0.41
Nilore reprocessing facility, Pakistan	0.15
Tokai reprocessing facility, Japan	0.1
Power reactors worldwide (cumulative)	0.17
Isotope production facilities worldwide (cumulative)	$0.9\text{-}54 \cdot 10^{-3}$
Power reactor with highest emission	$17.2 \cdot 10^{-3}$
Naval reactors worldwide (cumulative)	$4 \cdot 10^{-3}$

Table 1.2 – Annual contribution of selected Kr-85 sources to the global inventory (for reprocessing facilities: emissions in 2007). [Adapted after Ahlswede et al. (2009)]

The production of 1kg plutonium yields an approximate Kr-85 release of 10 to 35 TBq (Kalinowski, M.B. (2004)) The IAEA assumes 8kg of plutonium containing less than 80-percent Pu-238 is a significant quantity to manufacture a frist-generation explosive device (IPFM (2007)).
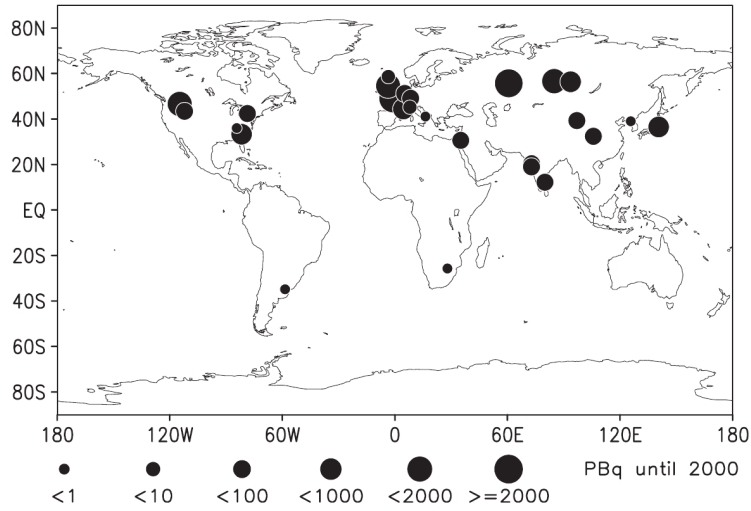
Figure 1.2 – Sites of reprocessing facilities operating between 1945 and 2000. The size of circles indicates the total amount of Kr-85 released until 2000. [Winger et al. (2005)]
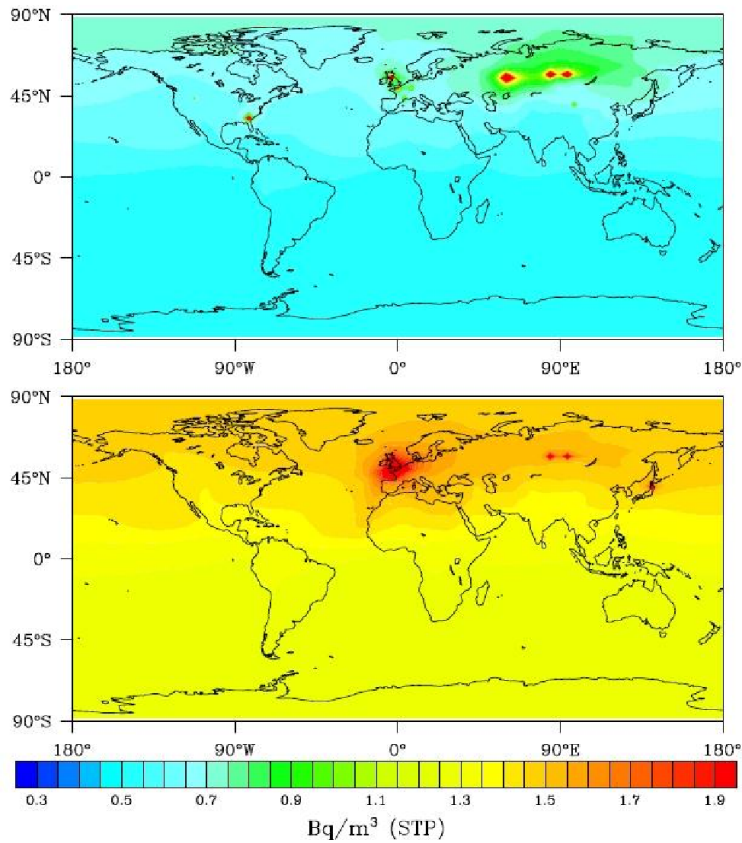
Figure 1.3 – Simulated annual mean concentration of Kr-85 at the surface done with the general circulation model ECHAM5 for 1976 (top) and 2006 (bottom). [Ross et al. (2010)]

Kr-85 can be held back technically from off-gas using physical separation methods such as cryogenic distillation, fluorcarbon adsorption, and adsorption using charcoal or molecular sieves (Jubin (2008) and Schoetter (2010)). However, for economic reasons this has not been accomplished yet on a large scale basis (Winger et al. (2005)). Further countermeasures to a possible Kr-85 detection are summarized by Ross, J.O. (2010).

Another source of Kr-85 are nuclear weapon tests. In 2008, 10 PBq of Kr-85 released from former nuclear weapon tests, remained in the atmosphere, which represent 0.2% of the total Kr-85 background (Ahlswede et al. (2013)). Accidents at nuclear power plants furthermore contribute to the global background of Kr-85. The explosion in Chernobyl in 1986 released about 33 PBq, whereas 44.1 PBq are estimated to have been emmited during the Fukushima accident in 2011 (Ahlswede et al. (2013)).

Simulations done with the global circulation model ECHAM5 (Ross et al. (2010) and Ross, J.O. (2010)) recognized source terms of all known reprocessing facilities and estimated the global background concentration of Kr-85 (Fig. 1.3). As today all operating reprocessing facilities are located on the northern hemisphere (Ahlswede et al. (2013), historical emissions see Fig. 1.2), the concentration of Kr-85 is larger on the northern- than on the southern hemisphere due to weak interhemispheric exchange of airmasses.
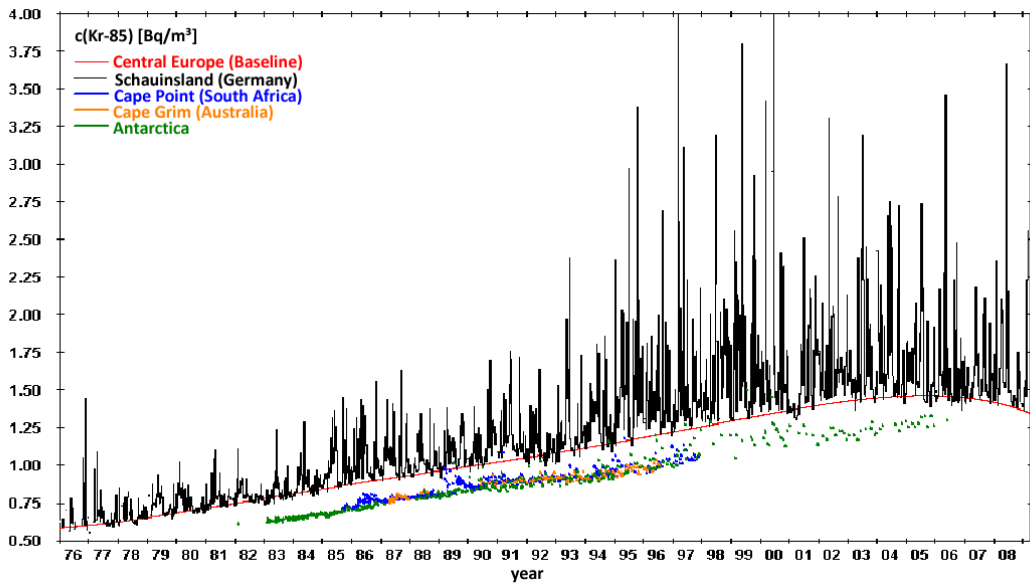
Figure 1.4 – Atmospheric near-surface concentration time-series of Kr-85 of station Schauinsland (weekly samples) and three stations on the Southern Hemisphere (weekly/spot samples). The atmospheric background over Central Europe (red baseline) stagnated after a constant linear growth until 2004. [Adapted after Schlosser et al. (2010)]

Since the largest industrial emittent of Kr-85 in 2007, the reprocessing site La Hague, France, is located near the Sellafield reprocessing facility (UK), the simulated atmospheric background, especially its variability, has its global maximum over Europe.

A time-series of weekly Kr-85 concentration values (Fig. 1.4) measured by the German Federal Office for Radio Protection (BfS) at Schauinsland near Freiburg confirm these results (Schlosser et al. (2010)). The measured concentration at Schauinsland highly depends on the general weather situation, in particular whether a reprocessing facility is located upstream or not. After a constant linear growth, the atmospheric Kr-85 background measured by stations located in Germany showed a stagnating trend after 2004 since an atmospheric equilibrium between radioactive decay and global emission rate was established. Due to a global stagnation of nuclear reprocessing rates, the atmospheric background of Kr-85 in Central Europe stabilized at 1.5 Bqm^{-3}, whereas the lower, less variable levels of Kr-85 concentration on the Southern Hemisphere still converge toward European background values.

A statistic analysis of the sensitivity of a Kr-85 detector in Tsukaba, Japan to the 55km distant Tokai reprocessing plant according to prevailing winds has been done by (Kemp, R.S. and Schlosser (2008)). Geostatistical methods for designing a fixed sampling station network to optimise the detection of radioactive plumes are described in Helle and Pebesma (2013).

1.3.3 Kr-85 emissions of La Hague

The La Hague nuclear reprocessing site is located at the North Cotentin peninsula in Lower Normandy/France, which is a narrow (5km wide) and hilly area with lowgrowing vegetation (moors, hedged farmland) bounded by steep cliffs on the south of the site (Connan et al. (2011)).

According to Ahlswede et al. (2013) and Schoetter (2010), the site was put into operation in 1965 and consists of two reprocessing facilities, UP2 and UP3, which are today operated by AREVA. Having a total capacitiy of 2000 tHM/a (tons of heavy metal per year), it is used for reprocessing spent fuel from European light water reactors. Yearly and monthly Kr-85 emission data are published by AREVA, however the company measures the Kr-85 release with a temporal resoltion of 1h.

Ahlswede et al. (2013) and Ross, J.O. (2010) analysed emission characteristics of La Hague: Due to the reprocessing scheme, Kr-85 is released pulsed. However, disregarding summer holidays, where emissions are halted, no characteristic interval can be found be-

tween the pulses. The emissions of La Hague have daily mean values of several hundred TBq and exceed 1000 TBq occasionally.

The availability of highly refined emission data makes La Hague favourable for potential field campaigns to evaluate Kr-85 measurement techniques and backtracking methods. Temporal and spatial variations of the dispersed Kr-85 plume in the vicinity of La Hague using different in-situ measurement techniques were investigated by Gurriaran et al. (2004). An evaluation of the ability of a number of atmospheric dispersion models (see Chap. 3.2) to reproduce Kr-85 samples collected in the mesoscale vicinity of La Hague using current measurement techniques was done by Connan et al. (2011).

1.3.4 Measuring Kr-85

The β-counting technique

The traditional method to determine Kr-85 concentration values from air-samples is the β-counting technique, which is briefly described in (Ross, J.O. (2010)): First, the noble gases are separated from a 30-200l air sample by filteration through a charcoal adsorption canister. After that, they are extracted from the charcoal by heating and are subsequently separated using gas-chromatography to get a concentrated krypton sample which is then analyzed in a β-counting chamber. The amount of Kr-85 in relation to the total Krypton in the sample is determined and the Kr-85, per air volume at standard temperature and pressure (0°C and 1000 hPa), is calculated for the original air sample.

Observation network

A list published by the Independent Group of Scientific Experts on the detection of clandestine nuclear-weapon-usable materials production (iGSE (2010)) contains all offically operated stations measuring Kr-85 concentration values. Since more than 30 years, the German Federal Office for Radio Protection (BfS) operates a coarse global network of up to 15 Kr-85 stations collecting samples for determining weekly average values of Kr-85 concentration and daily average values in some cases. (Schlosser et al. (2010) and Ross, J.O. (2010)). Seven sites are located in Germany, whereas only few stations are operated on other continents, especially on the Southern Hemisphere. All collected samples are sent to the BfS in Freiburg for subsequent analysis.

Currently, the detection limit for measuring the Kr-85 concentration of samples using the β-counting technique lies at approximately $3 \cdot 10^{-2}$ Bq/m^3, which is about 200 times

below the activity background of Kr-85 in 2002 (Sartorius et al. (2002)).

Earlier measurements were carried out by other countries for limited periods. In the U.S., NOAA (National Oceanic and Atmospheric Administration) collected two historic datasets with high spatial and temporal resolution ("twice daily samples", (iGSE (2010))) which can eventually be used for backtracking purposes based on real measurement data in future.

The IAEA Novel Technologies Program

Ross, J.O. (2010) summarized the further developments of the regularity framework concerning WAES: With the legal basis of the additional protocol, the IAEA General Conference approved a resolution which requests the Secretariat "to examine (...) innovative technological solutions to strengthen the effectiveness and to improve the efficiency of safeguards" (IAEA (2004)). Consequently, in 2005, the IAEA Department of safeguards established the program "Novel Techniques and Instruments for Detection of Undeclared Nuclear Facilities, Material and Activities", abbreviated so-called *Novel Technologies Program*. Within a technical experts meeting on "Noble Gas Monitoring Sampling and Analysis for Safeguards Applications" in September 2005, the suitability of Kr-85 has been considered, however, "the Technical Meeting recommends that the IAEA not pursue long range detection of noble gases" due to "high costs to implement a capability and the low probability of definitive detection" (IAEA (2005) after Ross, J.O. (2010)).

ATTA

Kalinowski, M.B. (2008) stated, that an internal, not officially published study conducted by the IAEA (IAEA (1999)) was responsible for the conclusion that implementing WAES is infeasable. According to Kalinowski, the "simulation methods applied were outdated", "requirements on WAES defined by the study were far too demanding" and new sensor technologies, "in particular the ultra-sensitive trace analysis of krypton-85 (which) allows (...) a radical cost reduction", "were not taken into account".

The adressed novel sensor technology for measuring Kr-85 concentration values, called *atom trap trace analysis* (ATTA), is currently being developed at the Carl Friedrich von Weizäcker Center for Science and Peace Research at the University of Hamburg (ZNF). Besides reducing "the detection tresholds by one order of magnitude" (Kalinowski, M.B. (2008)), the main advantage is the required sample size. Within the traditional beta counting method, more than 100 liters of air have to be taken which need to be pre-processed

using the expensive cryo-adsorption technique, whereas ATTA "can be successfully applied to samples of 1 liter". If this method is applied to random samples collected during routine inspections, the sampling would cause minor additional costs. Mobile devices will enable the inspection agency to conduct "surprise measurements on very short notice". The method of analysis was described in more detail by Daerr et al. (2010). ATTA will be field-tested in 2013 (Kalinowski, M.B. (2012)).

The deterrence criterion

Kemp, R.S. and Schlosser (2008) emphasize, that the *deterrence criterion* according to safeguards means, "that it is not necessary to detect each instance of the proscribed activity [clandestine plutonium separation] with high confidence". It is rather "sufficient to detect the activity only occasionally, as long as the probability of detection is sufficient to create a deterring effect". Therefore, random sampling during routine inspections in combination with the so-called *catch-the-plume scenario* were proposed for safeguard purposes.

1.3.5   The catch-the-plume scenario

If the IAEA has a hint about a possible region of an unreported reprocessing facility, one can predict the dispersion of an fictitious single-point release using an ATM, i.e. Flexpart, in forward mode (Klingberg, F.J. et al. (2010), see Chap. 4.1). Therefore a source term has to be estimated and hypothetically released from the location under suspicion. After calculating the forward dispersion, one can watch the propagation and evolution of a plume by using a post-processing tool (e.g. Web-Grape, a heuristic visualization and localization tool which is operationally used by the CTBTO, see Chap. 4.3.3). Since Kr-85 is diluted quickly in the atmosphere after being released, it is necessary to take air samples as soon as possible to make sure that the obtained measurements are well above the atmospheric background level. By simulating the transport of the noble gas, one can forecast Kr-85 concentration values in the atmosphere and send inspectors to regions of high concentration values to collect air-samples which can thereafter be analyzed either directly in the field or be returned to a laboratory for analysis. This so-called catch-the-plume scenario can be applied outside the legal restrictions of the IAEA safeguard framework "if the country under suspicion is not cooperating and does not permit taking air samples on its territory but the borders are reached by Kr-85 plumes from a suspicious site" (Ross, J.O. (2010)).

1.4 Previous work

1.4.1 The framework project of this thesis

The project "Simulations of atmospheric Noble Gas Concentrations to Assess Sampling Procedures for the Detection of Clandestine Nuclear Reprocessing" (IAEA GER 1643 (C.38)) in the joint programme of IAEA and the Federal Government of Germany was initiated to carry out fundamental research for preparing further IAEA decisions on that matter. In particular, scientific research has to be done according to source strength, atmospheric transport and background to assess the accuracy of localization of Kr-85 sources. Goals of different phases of that project are summarized in Tab. 1.3.

Phase I	Research and development of the technique, including development of appropriate safeguards relevant scenarios, simulation exercises, result assessment, cost-benefit analysis and a Phase I report for Departmental review, followed by a decision to proceed to Phase II.
Phase II	Prototype evaluation, field test exercise and a Phase II report for Departmental review, followed by a decision to proceed to Phase III
Phase III	Appropriate assistance leading to authorization of the technique and systems for inspection use (following the Departmentally approved Equipment Authorization Procedure

Table 1.3 – Phases of the project "Simulations of atmospheric Noble Gas Concentrations to Assess Sampling Procedures for the Detection of Clandestine Nuclear Reprocessing" (IAEA GER 1643). [Klingberg, F.J. et al. (2011)]

Phase I has been subdivided into three parts. The key results presented in this diploma-thesis were achieved during phase I/part III of task IAEA GER 1643 (C.38) carried out by Rainer Kaltenberger and supervised by Prof. Martin B. Kalinowski (ZNF-Hamburg) and Dr. Gerhard Wotawa (ZAMG). Scientific findings of previous parts of phase I are summarized subsequently.

1.4.2 On the detectability of additional Kr-85 sources

Phase I - Part I (Ross et al. (2010))

Ross et al. (2010) used the global general circulation model ECHAM5, which was driven with accessible Kr-85 emission data from all known reprocessing facilities to simulate the long term global background distribution of krypton-85. An evaluation showed, that the simulations fit well with data available from the observation network of the BfS. The capability of detecting additional releases of different source strength was estimated. Therefore the *Lagrangian particle dispersion model* (LPDM) HYSPLIT was driven with hypothetical point releases. The ability of detecting the plumes according to the background variability was analysed subsequently. A plume of Kr-85 was considered to be detectable, if its concentration was at least three sigma of the backgroud concentration of the relevant month.

The outcome showed that, although the background-variability was high over Europe (Fig. 1.5), even the smallest reference case release, which consisted of a total emission of 3.2 TBq in 6 hours, "according to the emission scenario for one dissolution campaign out of fifty campaigns during one year for retrieving one significant quantity of plutonium (8 kg)", stayed detectable within 24 hours after the stop of release (Fig. 1.6). Approximately 25 percent of the 3.2 TBq emissions were still detectable 48 hours after release, whereas an industrial release of 100 TBq/6h remained detectable for more than 2 days under most conditions. The sensitivity of the detectable source strength to the distance of the maximum concentration inside the plume is shown in Fig. 1.6. Under very suitable prevailing weather conditions, a plume stayed detectable more than 1000 km to the source, however for most cases, the detectability was limited to 500 km distance. As the shape of the maximum of a plume was in general occurring as a rather broad peak, small deviations from the plume center affect the detectability only marginally. Due to a less variable background, the chance of detecting a plume was generally much higher on the Southern- than on the Northern Hemisphere.

Though the probability for detecting the smallest reference case were limited (Fig. 1.7), the possibility of detection created a deterrent effect according to the deterrence criterion in the context of safeguards (see Chap. 1.3.4). Even sampling methods providing a detection probability of only 5% of a single plume lead to considerable chances of detection if applied over a long duration, e.g. over one year. In a reference scenario of 51 releases per year, the probabilty of at least one detection is $1 - (1 - p)^{51} = 93\%$. It has to be kept in mind, that this consideration requires a very low false alarm rate.
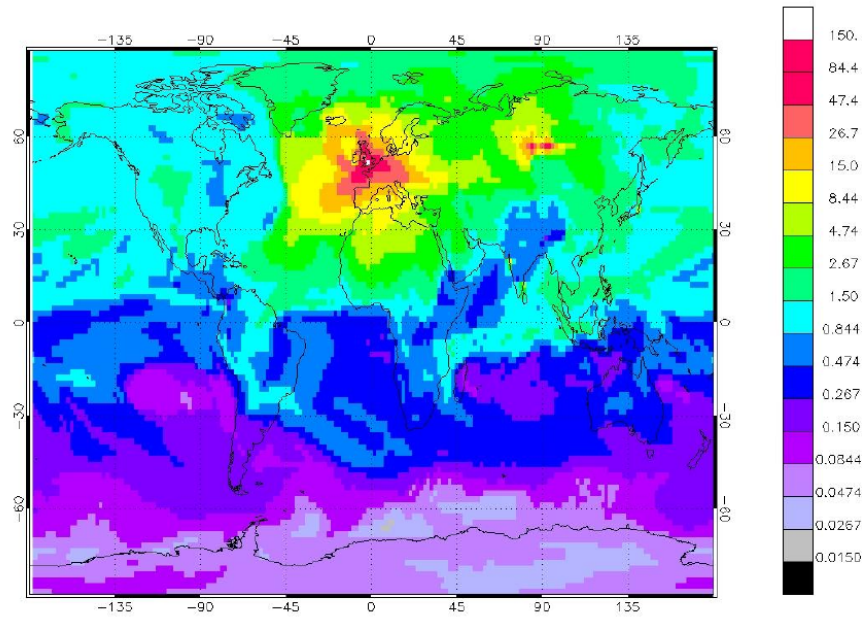
Figure 1.5 – Standard deviation of simulated 6h Kr-85 surface concentration values in percent of the monthly mean concentration value for December 2005. [Ross et al. (2010)]
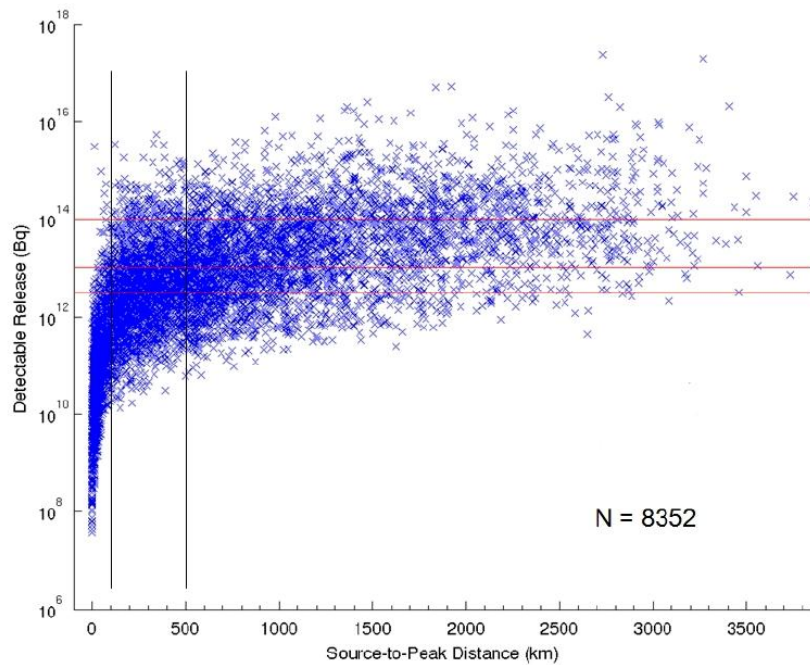
Figure 1.6 – Sensitivity of plume travel distance to minimum detectable release of Kr-85. Horizontal lines denote the three simulated reference cases (3.2, 10 and 100 TBq) whereas vertical lines mark 100 and 500 km distance to the source location. [Ross et al. (2010)]

LON	Time	3.2 TBq	10 TBq	100 TBq
Northern Hemisphere				
70°W	24 h	71 %	93 %	100 %
	48 h	8 %	50 %	90 %
	72 h	3 %	19 %	79 %
20°E	24 h	23 %	55 %	97 %
	48 h	3 %	8 %	77 %
	72 h	1 %	4 %	45 %
70°E	24 h	71 %	94 %	100 %
	48 h	14 %	48 %	94 %
	72 h	5 %	24 %	88 %
120°E	24 h	72 %	93 %	100 %
	48 h	20 %	45 %	95 %
	72 h	10 %	29 %	81 %
Southern Hemisphere				
70°W	24 h	89 %	97 %	100 %
	48 h	54 %	78 %	93 %
	72 h	39 %	62 %	90 %
20°E	24 h	93 %	99 %	100 %
	48 h	51 %	75 %	94 %
	72 h	25 %	54 %	83 %
120°E	24 h	93 %	100 %	100 %
	48 h	49 %	76 %	97 %
	72 h	25 %	54 %	90 %

Figure 1.7 – Percentage of cases fulfilling the detection criterion for the three reference emission quantities 24, 48, and 72 hours after stop of release listed per region (100% corresponds to a sample of 120 plumes on the northern and 72 plumes on the southern hemisphere). [Ross, J.O. (2010)]

1.4.3 Sampling procedures for the detection of unreported reprocessing

Phase I - Part II (Klingberg, F.J. et al. (2011))

If a Member State of the NPT is assumed to undertake unreported reprocessing for the production of plutonium, the simulation of hypothetical Kr-85 releases from the suspected region using ATMs in forward mode can be used to help decide where to send inspectors to collect air samples (Catch-the-plume scenario, see Chap. 1.3.5).

Klingberg, F.J. et al. (2011) (also published in Klingberg, F.J. et al. (2010)) arranged hypothetical emissions of three fictitious release sites in the Northern Hemisphere, each consisting of a 1 PBq/6h release represented by 100.000 particles, and simulated its forward dispersion with the LPDM Flexpart, driven with 0.5° meteorological input data from

ECMWF. The dispersion of the plume in space and time was analysed visually using Web-Grape (see Chap. 4.3.3) and fictitious samples with 3-hour duration on potential receptor points were created in the period close to the emission date at locations with high concentration values. For each release, five different sampling setups (consisting of one to five receptors) were accomplished. After that, Flexpart was started in backward mode to compute the source-receptor sensitivity (SRS) fields for each of the 3h-samples. The potential source region (PSR) was visualized using Web-Grape for the time of emission and evaluated manually using different localization parameters to gain the localizability of unknown point sources.

(a) Dispersion of a Kr-85 plume with 0.5° output grid resolution (Bq/m^3)

(b) Dispersion of a Kr-85 plume with 1° output grid resolution (Bq/m^3)

(c) Display of the PSR with 0.5° output grid resolution (correlation field)

(d) Display of the PSR with 1° output grid resolution (correlation field)
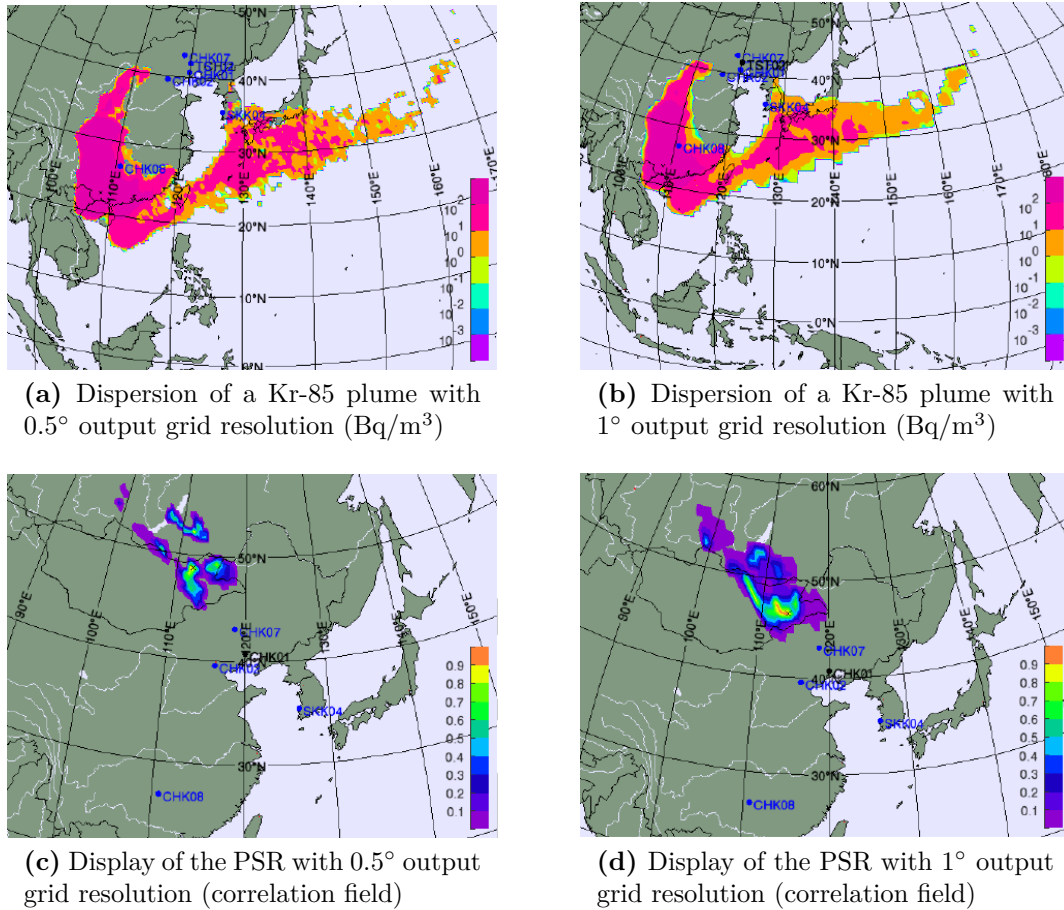
Figure 1.8 – Dispersion of the Kr-85 plume ((a),(b),Bq/m^3) and the PSR ((c),(d), correlation field) for a fictitious release in the Far East Region at 08.January 2008, 09:00 UTC with an output grid resolution of 0.5° ((a),(c)) and 1° ((b),(d)) plotted with Web-Grape. The plume dispersion and the PSR revealed a stronger granularity when using the 0.5° output grid resolution. This results in spotty regions with high correlation values which slightly show another distribution than the simulation done with 1°. [Klingberg, F.J. et al. (2011)]

The receptors were located at a distance of 1088 ± 816 km from one of the three fictitious release points located over Europe. The study revealed, that a sampling scenario consisting of two receptor points achieved the best localizability results over all runs. An average distance of 476 ± 285 km from the location of maximum correlation to the actual release point was found using two receptor points. The average distance from the release points to the so-called area of interest (AOI), an area containing correlation values > 75% of the maximum correlation (maxcor), was determined to be 233 ± 293 km which provides better results than the spatial error of $\triangle_r = 374$ calculated by Becker et al. (2007) based on the same localizability methods applied to the "CTBTO-WMO Experiment on Source Location Estimation", a multi-model ensemble dispersion simulation experiment of several institutions carried out in 2003. Parameters and source estimation results of these studies are listed in Tab. 5.4 and 5.5.

As in the study of Klingberg, F.J. et al. (2011) the shape of PSR appears spotty (Fig. 1.8) when simulating SRS-fields with 0.5° spatial resolution. Considering that the existing software of the CTBTO was optimized for 1°, simulations with 1° resolution have been recommended for further investigations.

1.5 Assessing the detectability of a tracer substance

Fig. 1.1 already provided an overview of aspects, which have to be considered when assessing the detectability of tracer substances. Hence, after discussing the aspects based on the example Kr-85, it is now possible to draw a more detailed version of that chart (Fig. 1.9).

Dependent on the scale, the atmospheric background of a tracer substance can be simulated by Global Circulation Model or Mesoscale Models. This thesis examines aspects of localizability, especially the influence of the temporal sampling resolution, using the Lagrangian particle dispersion model Flexpart. The minimal source strength can also be calculated based on Lagrangian particle dispersion model output which will be briefly described in Chap. 3.4.
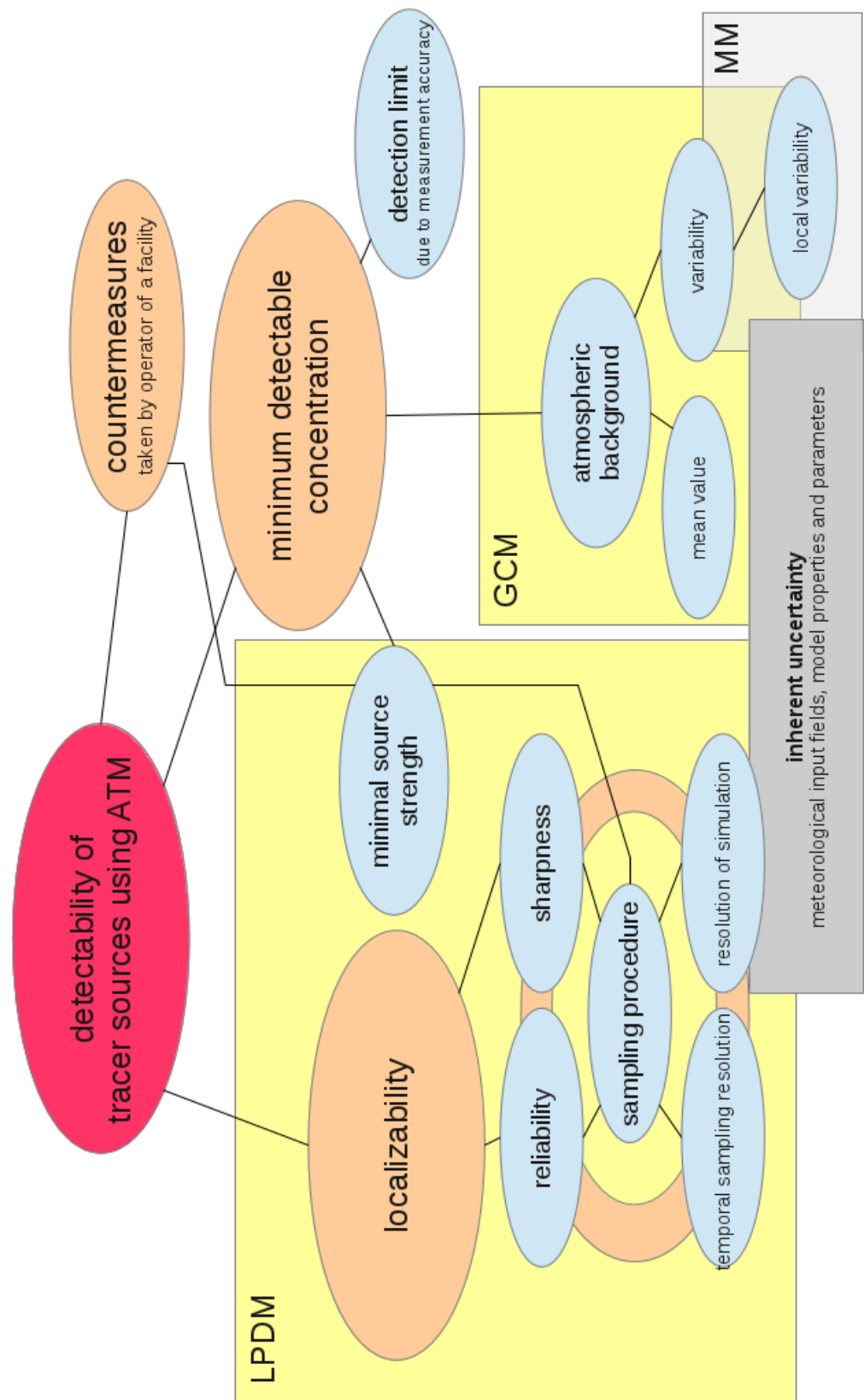
Figure 1.9 – Chart of aspects which have to be considered when assessing the detectability of tracer substances, their dependencies and how Atmospheric Transport Models can be applied. LPDM: Lagrangian Particle Dispersion Model, GCM: Global Circulation Model, MM: Mesoscale Model

Chapter 2

Objectives

Using the catch-the-plume scenario with subsequent backward simulations, Klingberg, F.J. et al. (2010) revealed, that two virtual sampling stations, which are located in medium to long-range distances to the fictitious source, delivered the best results in terms of localizabiliy.

Based upon this finding, the main scope of this thesis is to investigate the effect of different temporal sampling resolutions to the localizability of Kr-85 sources using different localization parameters and to find an optimum temporal resolution in terms of cost-benefit. Furthermore, temporal and spatial localization errors shall be compared to findings in previous studies and qualified statements on the localizability in dependance of prevailing wind-regimes are desired.

Therefore, in agreement with the ZNF-Hamburg (Centre for Science and Peace Research of the University of Hamburg), weekly instantaneous 6h releases of 3.2 TBq Kr-85 each ("according to the emission scenario for one dissolution campaign out of fifty campaigns during one year for retrieving one significant quantity of plutonium (8 kg)", Ross, J.O. (2010)) are hypothetically released in 2009 over the La Hague reprocessing site. After simulating a forward dispersion using the Lagrangian particle dispersion model (LPDM) Flexpart, consequently pseudo-samples at two virtual sampling stations in the center of the plume are created. This has to be done within a time span, for which the simulations of Ross, J.O. (2010) quantified the probability, that the plume stays detectable in respect to the simulated atmospheric background. For each of these samples, the corresponding source-receptor sensitivity (SRS) fields (see Chap. 3.3 for explanation of the concept) are calculated using Flexpart in backward mode and temporally averaged thereafter. In order to quantify the accuracy of the source location estimation, verification parameters

for reliability and sharpness are applied.

The generation of pseudo samples is necessary, since no highly resolved datasets exist for this procedure. To assess, that the 51 simulations over one year yield trustworthy results, the mentioned backtracking method is applied in a case study to real tracer-measurement data from the 1st European Tracer Experiment (ETEX-1).

Chapter 3

Methods

3.1 Two basic approaches

According to Holton (2004) and Bergmann and Schäfer (1998), any meteorological variable Ψ can be written as

$$\Psi = \Psi(x, y, z, t) \tag{3.1}$$

In fluid-dynamics, two basic approaches are used to describe the motion of a fluid. The *Eulerian approach* quantifies the temporal change of Ψ in a fixed Cartesian coordinate frame ($\vec{x} = (x, y, z)$) by its local derivative

$$\frac{\partial \Psi}{\partial t} = \frac{\partial}{\partial t} \Psi(x, y, z, t) \tag{3.2}$$

Within the *Lagrangian approach*, an individual fluid element (e.g. a particle or an air parcel) changes its location with respect to time by keeping its identity. Considering, that $\vec{x} = \vec{x}(t)$, (3.1) transforms into

$$\Psi = \Psi[x(t), y(t), z(t), t] \tag{3.3}$$

Taking the total derivative of (3.3) covers the identity of the two approaches after doing a few transformations:

$$\underbrace{\frac{d\Psi}{dt}}_{Lagrangian\ approach} = \underbrace{\frac{\partial \Psi}{\partial t} + \vec{u} \cdot \nabla \Psi}_{Eulerian\ approach} \tag{3.4}$$

Equation (3.4) is also called *Lagrangian derivative*. The left-hand side describes the Lagrangian approach of an individual fluid element whereas the right-hand side describes

the Eulerian view of a fluid. The Eulerian approach is based on the local derivative of a quantity Ψ, $\frac{\partial \Psi}{\partial t}$, and the advection of this variable, $-\vec{u} \cdot \nabla \Psi$, where $\vec{u} = (u, v, w)$ is the 3-D velocity vector and $\nabla = \left(\frac{\partial}{\partial x}, \frac{\partial}{\partial y}, \frac{\partial}{\partial z} \right)^T$.

3.2 Atmospheric transport modelling

Transport simulations of released particles can be achieved using *Atmospheric Transport Models* (ATMs). Current ATMs are either of Eulerian- or Lagrangian type and can be applied in *forward mode* (positive integration in time) or *backward mode* (negative integration in time, also called *adjoint mode* or *receptor-orientated mode* (Wotawa et al. (2003)).

3.2.1 Eulerian grid models

Eulerian grid models are based on a fixed coordinate system, where fluxes of particles due to advection and diffusion are computed between discrete 3-D grid cells (Wotawa (2010)). Therefore equation (3.4) can be adapted by substituting $\Psi = c$, which represents the concentration of a species:

$$\frac{dc}{dt} = S = P_c - L_c = 0 \tag{3.5}$$

where the source term S is the difference between the production rate of the species concentration (P_c=emission+chemical production) and the loss rate of the species concentration (L_c=deposition+chemical loss) which can be considered as zero for durable tracer substances like Kr-85. Equation (3.5) can be transformed using the continuity equation in Cartesian Coordinates

$$\frac{1}{\rho} \underbrace{\frac{d\rho}{dt}}_{I} + \nabla \cdot \vec{v} = 0 \tag{3.6}$$

through

$$\rho \cdot \underbrace{\frac{dc}{dt}}_{(3.5) \Rightarrow 0} = \frac{d(\rho c)}{dt} - c \cdot \underbrace{\frac{d\rho}{dt}}_{I} = \frac{\partial(\rho c)}{\partial t} + \vec{v} \cdot \nabla(\rho c) + \rho c \nabla \cdot \vec{v} = 0$$

into

$$\frac{\partial \left(\overline{\rho c} \right)}{\partial t} + \nabla \cdot \overline{\rho c \vec{v}} = 0 \tag{3.7}$$

Holding (3.7) under Boussinesq approximation ($\overline{\rho} = const.$, except in buoyancy terms), $\overline{\rho}$ cancels out and the space-time average defined by model grid and the time step can be split into

$$\frac{\partial \bar{c}}{\partial t} + \nabla \cdot \underbrace{\left(\bar{c}\, \vec{v} \right)}_{\vec{F}} + \nabla \cdot \underbrace{\left(\overline{c'\vec{v}'} \right)}_{\vec{J}} = 0 \tag{3.8}$$

with the advective fluxes $\vec{F}$ and the subscale turbulent diffusive fluxes $\vec{J}$. In Eulerian grid models, (3.8) is solved for each chemical species on a discrete 3-D grid in a fixed coordinate system. An advantage of this approach is, that non-linear chemistry can be simulated since inside the grid-box homogenous concentrations are assumed. However, the resolution dependent error occuring due to instantaneous mixing can be counterproductive for tracing particles.

3.2.2 Lagrangian particle dispersion models

Within the Lagrangian approach, each fluid particle keeps its identity during the transport process. The time dependent position of a particle i ($\vec{x}_i\,(t)$) can be calculated by integrating

$$\frac{d\vec{x}_i}{dt} = \vec{u}\,(\vec{x}_i, t) \tag{3.9}$$

with respect to time. The solution of equation (3.9) is called *trajectory* of a particle *i*. Within pure *Lagrangian models*, the trajectory of a single air-parcel is calculated, whereas in a *Lagrangian Particle Dispersion Model* (LPDM) thousands of trajectories of particles from different species are computed.

The principles of forward dispersion of particles using a LPDM are summarized subsequently (Wotawa (2010)): A number of particles (at the order 10^3 - 10^6) is released at a source location specified by a total mass (kg) or activity (Bq), which is called *source term* or *release term*. During dispersion, the mass (activity) of each particle can be reduced by deposition or decay. On a designated timestep, a Cartesian output grid is placed over the domain. Particles and their respective masses are counted in the grid-boxes to calculate respective mass concentrations (activity concentrations). The concentration of a radioactive tracer c is often specified in activity per volume (Bqm^{-3}) which is proportional to particle- or mass concentrations (Ross, J.O. (2010)). As within the present study atmospheric transport of the radioactive noble gas krypton-85 is investigated, the term activity and *activity concentration* will be used henceforth.

LPDMs offer several advantages comparing to Eulerian grid-models (Stohl et al. (2005) and Wotawa (2010)):

1. There is no numerical diffusion or instantaneous mixing.

2. The transport error depends on the resolution of the windfield (both in time and space), but is independent on the choice of the output grid.

3. Diffusion processes can be treated physically exact.

4. In the vicinity of particle source(s), a more exact treatment of transport can be achieved.

Global-scale transport simulations over several timesteps may be computationally demanding as a larger number of particles have to be simulated.

Running a LPDM in backward-mode means, that simulations are done using a negative timestep (Stohl et al. (2005)). Particles are released from a receptor location and are dispersed backward in time. A 4D response function called *source-receptor sensitivity (SRS) field* is then calculated.

3.3 The source-receptor sensitivity (SRS) field concept

According to Seibert and Frank (2004), the source-receptor (s-r) relationship is an important concept in air quality modelling: It describes the sensitivity of a *receptor* element y (e.g. the average concentration c of an certain atmospheric tracer substance in a given grid cell during a given time interval) to a *source* element x and can be basically written as $m = y/x$. This linear formulation of the s-r relationship is valid, if nonlinear chemical reactions are disregarded since all other processes during the atmospheric transport of tracer substances are linear: advection, diffusion, convective mixing, dry- and wet deposition and radioactive decay.

Wotawa et al. (2003) explain this concept as follows: The measured concentration c (Bqm^{-3}) of a specific radionuclide at a sampling site can be split up into a product of a spatio-temporal source field S (Bq) and a corresponding source-receptor sensitivity (SRS) field M (m^{-3}) at discrete locations (i,j) and time intervals t:

$$c = M_{ijt}S_{ijt} \tag{3.10}$$

The values of M can be regarded as the dilution volume, "i.e. the theoretical volume where the source, if evenly dispersed, would give a concentration of c."

LPDMs in backward mode, e.g. Flexpart (section 3.5), calculate an adjoint concentration field C_{ijt} (Bqm^{-3}) which has to be divided by the *total (adjoint) activity* $A^\star$ released in the backward simulation to yield the SRS field M_{ijt} (m^{-3}):

$$M_{ijt} = \frac{C_{ijt}}{A^\star} \tag{3.11}$$

Depending on the sampling setup, it is likely to detect a plume of a tracer at several sampling sites and/or timesteps. For this case, (3.10) can be adapted to a *multiple measurement scenario* based on the vector c_k:

$$c_k = M_{ijtk}S_{ijt} \tag{3.12}$$

M is calculated using ATMs, whereas the transport needs to be simulated fully 4D (including three-dimensional turbulence). SRS fields are 3D in space, but since the assumed sources and sampling sites are located on the ground, a 2D spatial output of the lowest atmospheric layer is sufficient.

(3.12) is an underdetermined linear equation system. Solving this system requires regularization assumptions according to the shape of the source. Considering a single grid cell source acting instantaneously over a time interval $\triangle t$, S has only one none-zero element (Wotawa et al. (2003)). As the sources are unknown, the number of receptor measured concentration values is less, comparing to the number of potential source elements within a week. A simple example: On a $1° \times 1° \times 3h$ geo-temporal grid covering the Earth, there are $180 \times 360 \times 7 \times \frac{24}{3} = 3.6 \times 10^6$ potential source cells. Hence, instead of 3.6 million forward mode computations, it is computationally more efficient to apply the backward method, because the number of required simulations to gain the corresponding SRS-fields M_{ijtk} is equal to the number of receptor elements (Seibert and Frank (2004)).

An efficient method to find a source scenario which is consisent with the observed concentration values is the trial-and-error method.

3.4 Calculating the possible source region (PSR) using the trial-and-error method

According to Becker et al. (2007), equation (3.10) yields a vector of calculated (predicted) concentration values c_k. For each of the discrete geo-temporal source possibilities, the

source strength is calibrated against the vector of the k observed concentration values c_k^{obs} by linear regression analysis:

$$c_k = A \cdot c_k^{obs} + B \tag{3.13}$$

$$R = \frac{cov(c_k; c_k^{obs})}{var(c_k) \cdot var(c_k^{obs})} = \frac{\sum_{i=1}^{k} \left(c_i^{obs} - \overline{c^{obs}}\right)(c_i - \overline{c})}{\sqrt{\sum_{i=1}^{k} \left(c_i^{obs} - \overline{c^{obs}}\right)^2} \sqrt{\sum_{i=1}^{k} (c_i - \overline{c})^2}} \tag{3.14}$$

A denotes the slope of the source calibration. The intercept B of the regression model (3.13), represents a background concentration or noise part of the model error which is usually neglected for backtracking purposes using this method.

The *possible source region PSR(i,j,t)* is defined as times and regions where the Pearson correlation coefficient R (3.14) "related to a hypothetical grid-cell source exceeds a treshold value of 0.1" (Becker et al. (2007)). Determining the geo-temporal maximum value of PSR yields the location, where a single-grid-cell source S_{ijt} would cause computed concentration values c_k being best correlated with the observation vector c_k^{obs}. A discrete single-point location $(\triangle x, \triangle y, t)$ identified to act as an instantaneous source over the time interval $\triangle t$ that way is consistent with a given multiple measurement scenario.

The source-receptor sensitivity (SRS) field concept can also be used to assess the minimal source strength of a measurement scenario (Wotawa et al. (2003)). Therefore, the bias between the calculated- and the observed concentration values may be investigated in further research.

3.5 Flexpart

Stohl et al. (2005) described Flexpart as a LPDM, which was originally designed for calculating dispersion of air pollutants from point sources in the meso- and long-range-scale (e.g. the disperson of radioactive particles released after a nuclear accident). Meanwhile, Flexpart has been developed into a comprehensive tool for atmospheric transport modelling and analysis which is used for a broad field of research and operational applications. Flexpart is able to simulate transport, deposition, diffusion and radioactive decay of particles discharged, using different source geometries (point, line, area, volume) and release intervals. Flexpart supports both forward and backward simulations, making it a suitable model for dispersion and backtracking of radioactive noble gases.

The stochastic part of the wind-vector is parameterized assuming Gaussian turbulence

which is valid only for stable and neutral conditions. However, assuming transport distances longer than particles need to mix up inside the atmospheric boundary layer, the error is minor.

Released under a *GNU* General Public Licence Version 3, the source code of the model can be adjusted individually and compiled for research- or operational purposes for free. Depending on the version, the code is written in Fortran 77 or 95 standard and can be compiled using standard compilers like gfortran in an UNIX/Linux environment. Several versions for different meteorological input data as well as documentations and additional tools can be downloaded at the Flexpart Homepage [1]. Currently, simulations can be carried out using meteorological input data from GFS- or ECMWF- model in netCDF or GRIB format. Apart from global weather models, Flexpart versions for regional models like MM5 or WRF also exist.

Flexpart output has been verified to be reliable by applying several tests with large scale tracer experiments (e.g. the European Tracer Experiment: ETEX, Stohl et al. (1998)) and is operationally used by the Provisional Technical Secretariat (PTS) of the Preparatory Commission of the Comprehensive Nuclear-Test-Ban Treaty Organisation (CTBTO) for analysing the origin of measured tracer concentration values within the radionuclide(RN)-network of the International Monitoring System (IMS) (Wotawa and Becker (2007)).

---

[1]Flexpart-Homepage: `http://transport.nilu.no/flexpart` (Accessed on 6 Jan. 2013), soon: `http://www.flexpart.eu`

Chapter 4

Implementation

Figure 4.1 provides an overview of the procedures which were applied in the present study to gain further expertise about the accuracy of localization, based on the catch-the-plume scenario. Since there are no highly resolved datasets of Kr-85 measurements available because of the high costs and efforts of current sampling- and analyzing procedures (Chap. 1.3.4), a generation of pseudo-samples is required to apply this concept.

In agreement with the ZNF-Hamburg (Centre for Science and Peace Research of the University of Hamburg), fictitious 6h releases of 3.2 TBq Kr-85 were hypothetically released over La Hague (lon. 1.88°, lat, 49.68°) on each Wednesday between 9:00 and 15:00 UTC in the year 2009. The dispersion of the plume was simulated for five consecutive days using the LPDM Flexpart in forward mode. Afterwards, the catch-the-plume scenario was applied for each of the 51 forward runs. The propagation of the plume was plotted and two receptors were chosen which were hit by the centre of the plume beginning from 9h after the release took place. Pseudo-measurements were then generated at two fictitious sampling stations in a sampling window of 48 hours beginning from 0:00 after the release took place using the output of Flexpart. For each of those $2 \cdot 16$ 3h samples, source-receptor sensitivity fields were calculated seven days backward in time using Flexpart in backward mode. Afterwards, the resulting SRS-fields were temporally averaged for each grid point on a global domain to get SRS-fields for 6, 12, 24 and 48h for each of the receptor points. Then, applying the method of Wotawa et al. (2003), the possible source regions (PSR) of the multiple pseudo-measurement scenarios based on different temporal sampling resolutions were calculated. The spatio-temporal correlation fields were subsequently plotted and analyzed to determine localizability parameters for reliability, e.g. the distance between the point of maximum correlation and the release location, and sharpness, i.e. a user-

defined PSR, the so-called *area of interest* (AOI).
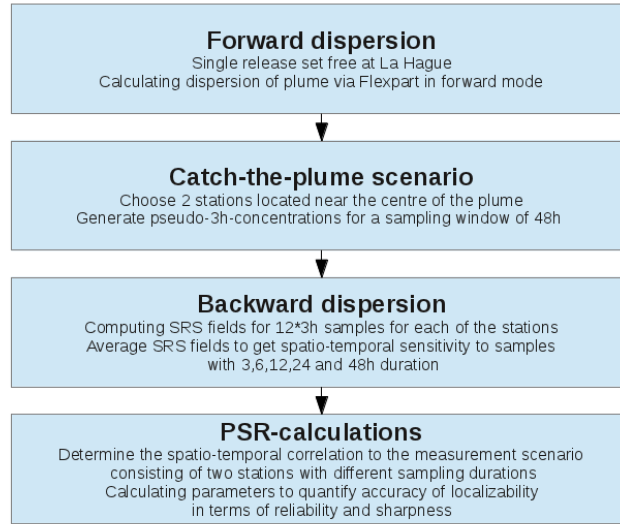
Figure 4.1 – Overview of procedures applied to 51 simulations in the year 2009.

4.1 Forward Simulations

4.1.1 Modelling the forward-dispersion of Kr-85

To account for varying meteorological conditions in determining the accuracy and precision of unknown sources, 51 simulations (henceforth called *runs*) had been carried out throughout each Wednesday of the year 2009 from the fictitious releasepoint La Hague. The forward runs contained fictitious, instantaneous 6h releases, happening on each Wednesday in 2009 from 9 to 15 UTC at 1.88° E and 49.68° N, which marks La Hague reprocessing plant. During that 6 hour interval, a total release of 500.000 particles, possessing a cumulative activity of 3.2TBq, was set free in a height between 8 and 12m above ground and subsequently dispersed five days forward in time. The output grid was set over a global domain with 1° spatial and 3h temporal resolution with 2 vertical layers (0-150 and 150-10000m above surface). All the other parameters and configurations used for these simulations can be looked up in the corresponding *COMMAND*, *RELEASES* and *OUTGRID* files in Appendix C. The technical manual of Flexpart, which was published by Stohl et al. (2005), gives more details on the meaning of the parameters.

ECMWF fields

Flexpart was driven using global ECMWF meteorological analysis fields (henceforth called *wind-fields*) in GRIB1 format with 91 vertical layers, 1° spatial- and 3h temporal resolution. The files can be acquired using a data retrieval routine available at the Flexpart Homepage. Each of these files provide parameters which are needed to perform simulations with Flexpart (compare Stohl et al. (2005)). All wind-fields had to be listed in a so-called *AVAILABLE* file and located in one directory specified by the file *pathnames*.

Postprocessing

The Fortran 77 program *flexout2srsm_forward* (by Gerhard Wotawa/PTS)[1] transcodes the binary Flexpart output of each forward run into a .srm file in ASCII/CTBTO format and changes the output structure from one file per simulated day to one file per release (Seibert, P. (2007)). A .srm file of a forward simulation contains surface level plume concentration values [Bqm^{-3}] of, i.e. of all 1° gridpoints of the global domain specified by file *OUTGRID* in 3h forward steps (see Chap. 4.2.1 for file format).

 After being gunzipped, the dispersion of the plume is then plotted using the routine *srsplot*. Programmed in Fortran 77 by Gerhard Wotawa, srsplot reads in a .srm file and plots the values using ECMWF's MAGICS++ fortran library of an arbitrary domain for *t* timesteps specified in its *CONTROL* file. The graphical output is in postscript (.ps) and animated gif (.gif) format and can be converted into single pngs or jpgs using the *convert* command. The release point is marked and named after information provided in the header of the .srm file, however this can be changed by defining values in the *gard.dat* configuration file (consult Section 4.1.2 for further information).

4.1.2 Applying the catch-the-plume scenario

After obtaining the graphical output, the propagation of the plume is then analyzed visually. Adapting the method of Klingberg, F.J. et al. (2010), two virtual sampling stations had been chosen considering the following points:

- The passing of the plume shall be entirely sampled inside a sampling window of 48h, beginning with 0 UTC (collection start), i.e. 9 hours after the release has been ended.

---

[1]The code of this and the following programs can be requested from Dr. Gerhard Wotawa, MA., currently (as on Jan. 22th, 2013) affiliated to the Central Institute for Meteorology and Geodynamics, Austria (ZAMG, Hohe Warte 38, 1190 Vienna, Austria).

- Position fictious receptor-points at locations featuring high surface concentration values (i.e. near the centre of the plume).

- Locate hypothetical stations on integer gridpoints to avoid grid-errors (as proposed in front of the European Tracer Experiment (ETEX) in 1994, see (JRC (2004)) and Chapter 5.5.1).

- Prefer locations on land rather than on sea.

The propagation of the plume during the first timesteps after the release is recorded for further climatological analysis. Using Google-Maps, the fictitious sampling stations are named after cities or famous places in the vicinity of the integer gridpoint.

The station identifier

Each station is identified by a five-digit ID, headed by a two digit country code in form of its respective internet top-level-domain (i.e. *DE* for Germany). Stations located at sea are identified using a *SP* ("ship"). The third character indicates the tracer substance measured at this station (*K* for krypton-85). Then follows a two-digit running number beginning from *01* for each country.

The stations routine

After choosing two stations, longitude, latitude and station identifiers are written into a configuration file named *station.cnf*. This file is read in by the routine *stations* (coded in Fortran 90 by Rainer Kaltenberger), which generates a *gard.dat* file. In this context, the ASCII file *gard.dat* describes a measurement scenario and contains all collection stop dates of the given stations which are needed to generate *pseudo-samples*. The structure of the the *gard.dat* configuration file can be looked up in Appendix D.2 and CTBTO/IDC (2009).

4.1.3 The generation of a multiple pseudo measurement scenario

Following Becker et al. (2007) and Klingberg, F.J. et al. (2010), time series of hypothetical 3h, 6h, 12h, 24h and 48h samples, so-called *pseudo-samples*, were created for the virtual stations. This was achieved using the Fortran 77 routine *srs2point* (by Gerhard Wotawa, CTBTO/PTS), which expects a .srm - and a *gard.dat* file as input and creates so-called *concentration files* (.con) in ASCII format, listing measurements-values in mBq for the collection stop dates of stations specified by the file *gard.dat*.
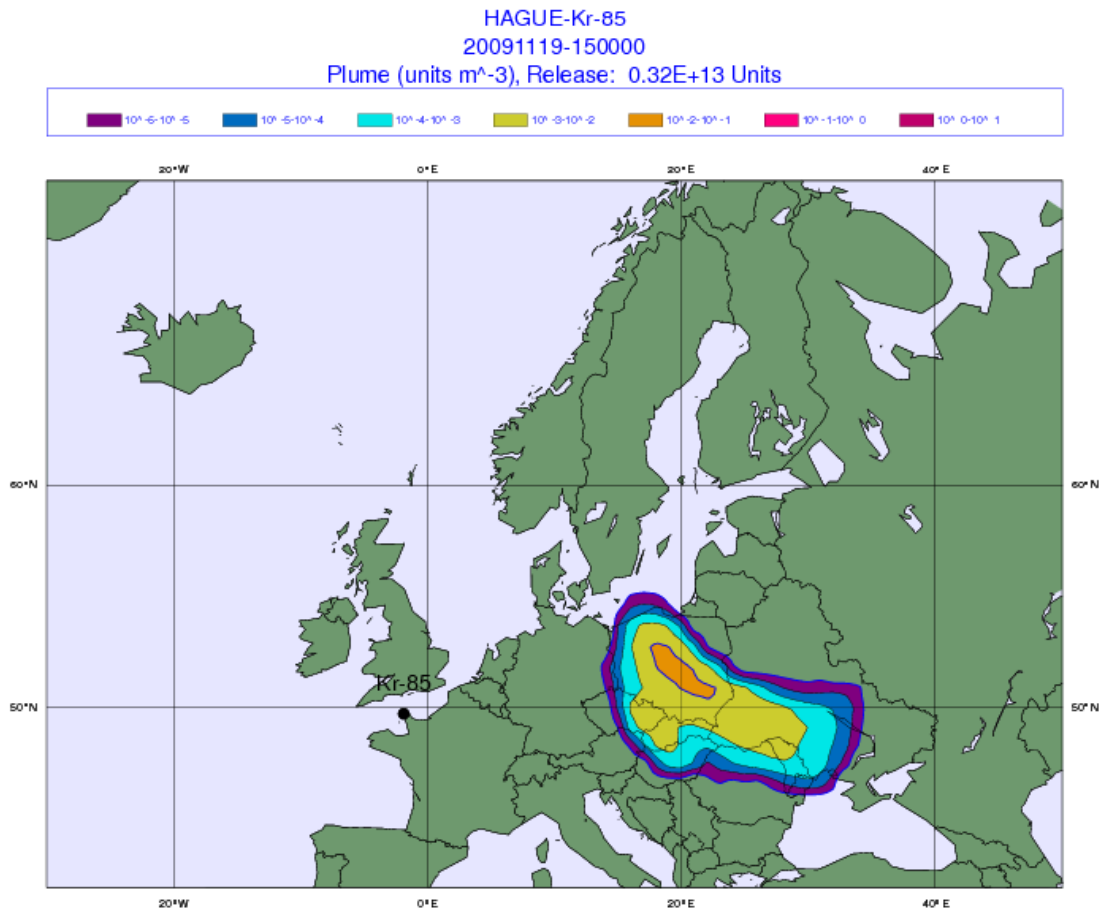
Figure 4.2 – Surface layer Kr-85 concentration values [Bq/m^3] of run 46, 24h after the fictitious release plotted with routine *srsplot*. The plume travelled fast due to brisk westerly winds. Within the catch-the-plume scenario, two hypothetical sampling stations were located on integer grid-points near the centre of the plume in Poland (station PLK01 near Wolsztyn, 52°N, 16°E and station PLK02 in the vicinity of Łódź, 52°N, 20°E. After that, time-series of pseudo-samples have been created at these two locations using the program *srs2point*.

4.2 Backward simulations

4.2.1 Modelling the backward-dispersion of Kr-85

After generating pseudo measurements, the spatio-temporal SRS-fields [m^{-3}] for each of the 3h samples are computed seven days backward in time by running Flexpart in backward mode, making 16 releases per 48h sampling window and station. The backward release of each 3h interval consists of 500.000 particles with a total activity of 10^{12} Bq, however, this value can be chosen arbitrary since it does not affect the calculation of the correlation

coefficient (Equ. 3.14). Other parameter settings remain unchanged in respect to the forward simulations.

Using the output of Flexpart, *flexout2srsm_backward* (likewise *flexout2srsm_forward*) then generates a *.srm*-file in backward format for each release interval which contains the sensitivity values $[\text{m}^{-3}]$ of a global domain for 56 negative 3h timesteps (7 days backward in time). Thus each SRS-field takes into account possible release scenarios (not necessarily point-releases) which affect the station at the sampling time.

The source-receptor sensitivity (SRS) data format

The ASCII formatted *.srm* files contain the 3D values (x,y,t) of the forward/adjoint tracer concentration values (Equ. (3.10)) for one output level. For source-localization, the layer of interest is the surface output level which was specified to be 0-150 m above surface within this study. The structure of SRS-field files differs a bit between forward ("plume") and backward mode which will be described subsequently using CTBTO/IDC (2009) and Seibert, P. (2007).

The *flexout2srsm* routines are written by Gerhard Wotawa (CTBTO/PTS), and follow some conventions used between CTBTO and Regional Specialized Meteorological Centres (RSMCs) of the World Meteorological Organisation (WMO) cooperating with the CTBTO. The structure of output filenames is divided into five sequences of characters. As the model output can become very large, the clear text ASCII files are usually compressed with *gzip* (extension: *.gz*).

`UKK12.fp.2009111203.f8.srm.gz`

- `UKK12`: Station ID as defined in the *RELEASES* cofiguration file.

- `fp`: Code for the model used. `fp` for Flexpart or `hy` for Hysplit (can be changed in *CONTROL* file of routine *flexout2srsm*)

- `2009111203`: The date of collection stop as assumed in the model run (=receptor time interval end) with the syntax `YYYYMMDDhh`

- `f8`: Model version. `f` for Flexpart, `h` for Hysplit, followed by the major version number (can be changed in the *CONTROL* file of routine *flexout2srsm*)

- `srm`: Extension for source-receptor matrices

Each *.srm*-file is radionuclide sample specific (identified by the station ID) and consists of one header line and and a number of data lines as follows:

SRS-data format - backward mode

Header line: CTBTO-format: Longitude of station [degrees] / Latitude of station [degrees] / Measurement (collection) start time in UTC [`YYYYMMDD hh`] / Measurement (collection) stop time in UTC [`YYYYMMDD hh`]/ Total mass (activity) [Bq] released in backward model / Maximum number of hours backward / Output frequency [hours] / Averaging time [hours] / Resolution of output grid in longitude [degrees] / Resolution of output grid in latitude [degrees] / Station identifier.

Optionally, parameters concerning the output grid follow (not CTBTO standard as they assume global $1° \cdot 1°$ grids): Longitude/latitude of the South-Western (SW) corner of the grid element (1,1) [degrees] / Number of grid elements in x and y direction

Data lines: Latitude of grid cell (SW corner of grid cell), [degrees] / Longitude of grid cell, (SW corner of grid cell) [degrees] / Backward time step number (the first one ends with the collection stop) / Value of source-receptor sensitivity [identical to retro-plume concentration, Bq/m^3]

Listing 4.1 – Example of a .srm-file containing backward SRS-data

```
1    -7.00   55.00 20091112 00 20091112 03 0.10E+13  99   3   3 1.00 1.00 "UKK12"
2   -179.00 -90.00 359 180
3    53.00     -9.00     1   0.2572998E-05
4    54.00     -9.00     1   0.4753793E-04
5    55.00     -9.00     1   0.2620561E-09
6    53.00     -8.00     1   0.3145656E-04
7    54.00     -8.00     1   0.2280483E-01
8    55.00     -8.00     1   0.4443888E-04
9    53.00     -7.00     1   0.2248127E-04
10   54.00     -7.00     1   0.5688826E-01
11   55.00     -7.00     1   0.7671008E-01
12   53.00     -6.00     1   0.9668958E-06
13   54.00     -6.00     1   0.1369934E-03
14   55.00     -6.00     1   0.3768251E-08
15   52.00    -10.00     2   0.1643255E-05
16   53.00    -10.00     2   0.2594957E-04
17   54.00    -10.00     2   0.3138570E-05
18  [...]
```

In order to yield source-receptor sensitivities [$1/m^3$], it is necessary to divide the values by the total mass (activity) release (specified by the seventh entry in the header line).

SRS-data format - forward (plume) mode

Header line: CTBTO-format: Longitude of source location [degrees] / Latitude of source location [degrees] /Release start time in UTC [`YYYYMMDD hh`] / Release stop time in UTC [`YYYYMMDD hh`]/ Total mass (activity) [Bq] released in forward model / Maximum number of hours forward / Output frequency [hours] / Averaging time [hours] / Resolution of output grid in longitude [degrees] / Resolution of output grid in latitude [degrees] / Station identifier.

Optionally, parameters concerning the output grid follow (not CTBTO standard as they assume global $1° \cdot 1°$grids): Longitude/latitude of the SW corner of the grid element (1,1) [degrees] / Number of grid elements in x and y direction.

Data lines: Latitude of grid cell (SW corner of grid cell), [degrees] / Longitude of grid cell, (SW corner of grid cell) [degrees] / Forward time step number (the first one ends with the release stop)/ Value of plume concentration [Bq/m³]

Listing 4.2 – Sample of a SRM-file containing forward SRS-data

```
 1    -1.88    49.68 20091111 09 20091111 09 0.32E+13 168   3   3 1.00  1.00 "HAGUE"
 2  -179.00 -90.00 359 180
 3   49.00     -3.00    -1  0.2304476E-02
 4   50.00     -3.00    -1  0.1953120E-01
 5   51.00     -3.00    -1  0.1768459E-05
 6   49.00     -2.00    -1  0.1726483E+00
 7   50.00     -2.00    -1  0.2045984E-01
 8   51.00     -2.00    -1  0.9108082E-06
 9   50.00     -4.00    -2  0.6616995E-04
10   51.00     -4.00    -2  0.1729350E-03
11   52.00     -4.00    -2  0.1016997E-07
12   49.00     -3.00    -2  0.2021094E-03
13   50.00     -3.00    -2  0.7687590E-01
14   51.00     -3.00    -2  0.2354656E-01
15   52.00     -3.00    -2  0.6300851E-07
16   49.00     -2.00    -2  0.1849355E+00
17   50.00     -2.00    -2  0.1383621E+00
18  [...]
```

Again, in order to yield source-receptor sensitivities [1/m³], it is necessary to divide the values by the total mass (activity) release (specified by the seventh entry in the header line).

4.2.2 Averaging SRS-fields

The program *srsavg* (coded in Fortran 90 by Rainer Kaltenberger) temporally averages a sequence of *.srm.gz*-files and writes output to gunzipped *.srm* files in a hierarchic *ATM_SRS_ARCHIVE* folder structure.

Therefore, the routine calls the configuration file *RECEPTORS*, in which the selector for the *.srm.gz*-file read in subroutine has to be typed. *srsavg* next queues all filenames in the directory `$DATPATH` which contains the characters defined by the selector and extracts these files to temporary files (*.tmp*). It is necessary, that these files have a collection duration of 3h each, altogether representing a full sequence of *li* consecutive samples. *li* has to be the common divisor of all denoted sampling resolutions, i.e. 16 consecutive 3h samples are required to be averaged to one 48h sample.

Listing 4.3 – Fortran 90 sequence of the averaging subroutine for the period *avg=12h* called by program *srsavg*

```fortran
open(15,file=file(i),status="new",action="write",iostat=io_error) !Create .srm
    output file
write(15,25) xpoint(i),ypoint(i),ibdate(i+avg/interval-1),ibtime(i+avg/interval
    -1),iedate(i),ietime(i)&
,xmass(i)+xmass(i+2)+xmass(i+3)+xmass(i+4),steps*interval,idhours1(i),idhours2(i),dxout(i
    )&
,dyout(i),trim(species(i)),outlon0(i),outlat0(i),nxout(i),nyout(i) !Write header line
    do kt=1,steps-(avg/interval-1) !Steps-"snippet"
      do ix=1,nx1out-1
        do jy=1,ny1out-1
          avgvalue=(srsgrid(i,ix,jy,kt+3)+srsgrid(i+1,ix,jy,kt+2)+srsgrid(i+2,ix,jy
              ,kt+1)+srsgrid(i+3,ix,jy,kt))/4
          if(avgvalue>srsmin) then
            xlonp=(ix-1)*dxout(i)+outlon0(i)  !Reconvert into real lon
            ylatp=(jy-1)*dyout(i)+outlat0(i)  !Reconvert into real lat
            write(15,26) ylatp,xlonp,t,avgvalue !Write data lines
          end if
        end do
      end do
      t=t+1
    end do
    write(*,27) "Wrote␣File␣"//trim(file(i)) !Console output
```

Listing 4.3 displays a sequence of the averaging subroutine for the averaging argument *avg=12h* called by the program *srsavg*. *i* is the filenumber for accessing information from a total of *li* read in files with temporal resolution of *interval=3h*. As the averaging interval is 12 hours, informations of 4 consecutive 3h samples are required. Line 2 writes the header line of the new output file generated by line 1, which subsequently contains spatio-temporal sensitivities for a sampling period of *avg=12h* using the format described in

section 4.2.1. Beginning with line 4, the averaging of SRS-values follows for the timestep *kt* of the output file. The for-loops starting at lines 6 and 7 cover all grid-coordinates *ix* and *jy* of the given domain. Line 8 contains the core of the sequence: For each dataline written by the sequence in line 12, the averaged SRS-value *avgvalue* is calculated by calling corresponding SRS-values of 4 consecutive files. Lines 10 and 11 transform grid-coordinates back into real coordinates. A data-line is generated, if *avgvalue* is higher than a treshold SRS-value *srsmin* (line 9), which is the default value of array-elements which contain no SRS information (Wotawa, G. (2012)).

The ATM_SRS_ARCHIVE

The hierarchic structure of the subfolders in the output directory *ATM_SRS_ARCHIVE* is required by the *Web-Grape* visualization software (CTBTO/IDC (2008) and CTBTO/IDC (2009), see Chap. 4.3.3). In *Web-Grape*, the path to the SRS-datasets is specified in the configuration file *srs_data_home.txt* by the `$SRSDATAHOME`-variable which has a default value of `$PATH/ATM_SRS_ARCHIVE`. *Web-Grape* expects the subdirectories of `$SRSDATAHOME` to be in the format `YYYYMMDD/$SELECTOR/$FILENAME.srm.gz`. The directory `YYYYMMDD` contains gzipped *.srm*-files with the corresponding collection-stop date, whereas the name of the `$SELECTOR` variable can be modified to meet user defined requirements. In this study, the `$SELECTOR` directory was used as a branch to archive *.srm.gz*-files with different temporal resolutions separately. Thus, the subdirectory `$SELECTOR` was named `flex.XXhrs`, where `XX` stands for the temporal resolution in hours of the containing files (03, 06, 12, 24 and 48 respectively).

4.3 PSR Calculations

Together with the generated pseudo samples, the averaged SRS-fields stored in the hierarchic structure (as described in the previous section) are next used to calculate backward correlation fields to yield and visualize the potential source region (PSR) of the tracer substance.

4.3.1 Calculating the PSR for a multiple measurement scenario

Therefore, the acquired pseudo measurements of 2 hypothetical sampling stations, representing a multiple measurement sceario, which are stored in the concentration (*.con*)
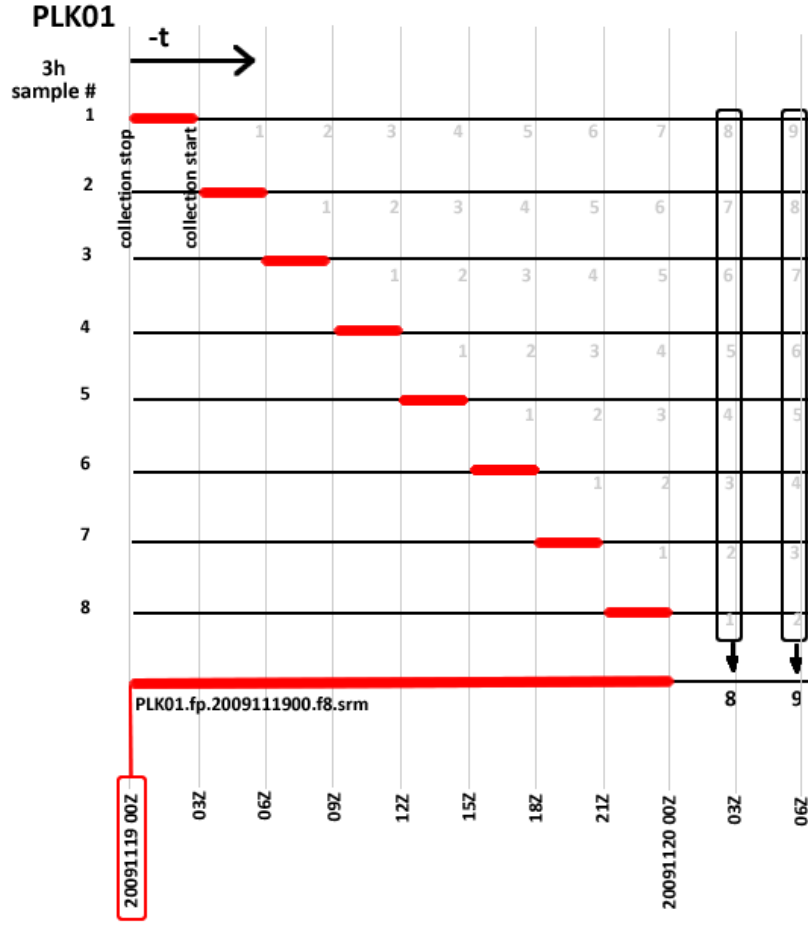
Figure 4.3 – Scheme of the averaging routine *srsavg*. The spatio-temporal SRS-fields for all backward timesteps (grey indices) of 8 consecutive 3h samples (i.e. 8 files, short red lines) for the fictitious sampling station PLK01 are averaged to yield the sensitivities of one 24h sample with collection stop on 19 Nov 2009 at 00Z (long red line) packed in the file `PLK01.fp.2009111900.f8.srm`. The first backward SRS-field of the 24h sample, has the index-value *t=8* and is averaged for each spatial grid-point using the SRS-values of corresponding timesteps of the eight 3h samples (black rectangle pointing to index-value *8*).

files, are typed into the *CONTROL* file of routine *locate_multi* (programmed in Fortran 77 by Gerhard Wotawa (CTBTO/PTS)) for each investigated temporal resolution (see Appendix D.3). Since zero-measurements can also contribute to get a sharper correlation field, it is important to state these samples. Running *locate_multi*, the routine next reads in all .srm files of the corresponding collection stop dates of the pseudo measurements of the two fictitious sampling stations and correlates the spatio-temporal SRS-fields with the multiple-measurement scenario as defined in the *CONTROL* file. The program writes the

time-dependent correlation fields (Chap. 3.4) into a *correlation.txt* file, which has a very similar structure compared to the SRS-data format (see Appendix D.4).

After that, the *correlation.txt* file is used to plot the PSR-fields and to calculate verification parameters, henceforth *localizability parameters* to determine the accuracy of the localization method.

4.3.2 Plotting the PSR

To confine the location where the initial Kr-85 plume, which is responsible for the measurement scenario, has most probably been released, the PSR is visualized by the routine *psrplot*. The routine, which was coded by Gerhard Wotawa (CTBTO/PTS) in Fortran 77, resembles the routine *srsplot* with the exception, that now correlation values provided by the input file *correlation.txt* are plotted. Samples of plots can be found on pages 51 and 71.

4.3.3 Web-Grape

Web-Grape (*Web* connected *grap*hics *e*ngine) is a heuristic post-processing tool, which has been developed by the CTBTO/IDC as a request of the PTS to calculate PSR-fields based on a SRS-database and observations acquired by the radionuclide measurement stations of the IMS (CTBTO (2005)). The SRS-fields stored in the database are pre-computed using different global NWP-models of all RSMCSs of the WMO before the daily measurements are analyzed (Wotawa and Becker (2007)).

In order to determine the PSR of an event, the sampling data has to be entered manually into the GUI of *Web-Grape* for the corresponding collection stop-time of the selected type of nuclide (see Fig. 4.4). *Web-Grape* then computes the PSR by comparing the specified sampling scenario with all possible source assumptions in space and time (Klingberg, F.J. et al. (2010)).

In *Plume*-mode, *Web-Grape* allows to display forward dispersion data. The visualized PSR fields or forward dispersed plumes can be exported as animated *.gif* or as *.kml* file to be displayed in Google-Earth. Further features and specifications of *Web-Grape* can be found in the user-manual (CTBTO/IDC (2008)).

In their study, Klingberg, F.J. et al. (2010) used *Web-Grape* to compute, visualize and analyze the PSR of the investigated pseudo-measurement scenarios. Therefore, parameters regarding the accuracy of source localization have to be determined manually using the ruler

tool in Google Earth. Klingberg et. al. revealed, that *Web-Grape*, which was originally designed for operational purposes, performed quite unstable and crashed sometimes when driven with experimental settings, e.g. different SRS-field resolutions and user-defined station networks (Wotawa, G. (2012)). These facts led the author of the present study carrying out investigations, including the calculation of localizability parameters, using Fortran routines which could be adapted to user-specified requirements. Another advantage of Fortran programs is the ability to easily perform batch-processing, i.e. to carry out calculations for a series of simulations using UNIX shell-scripts.
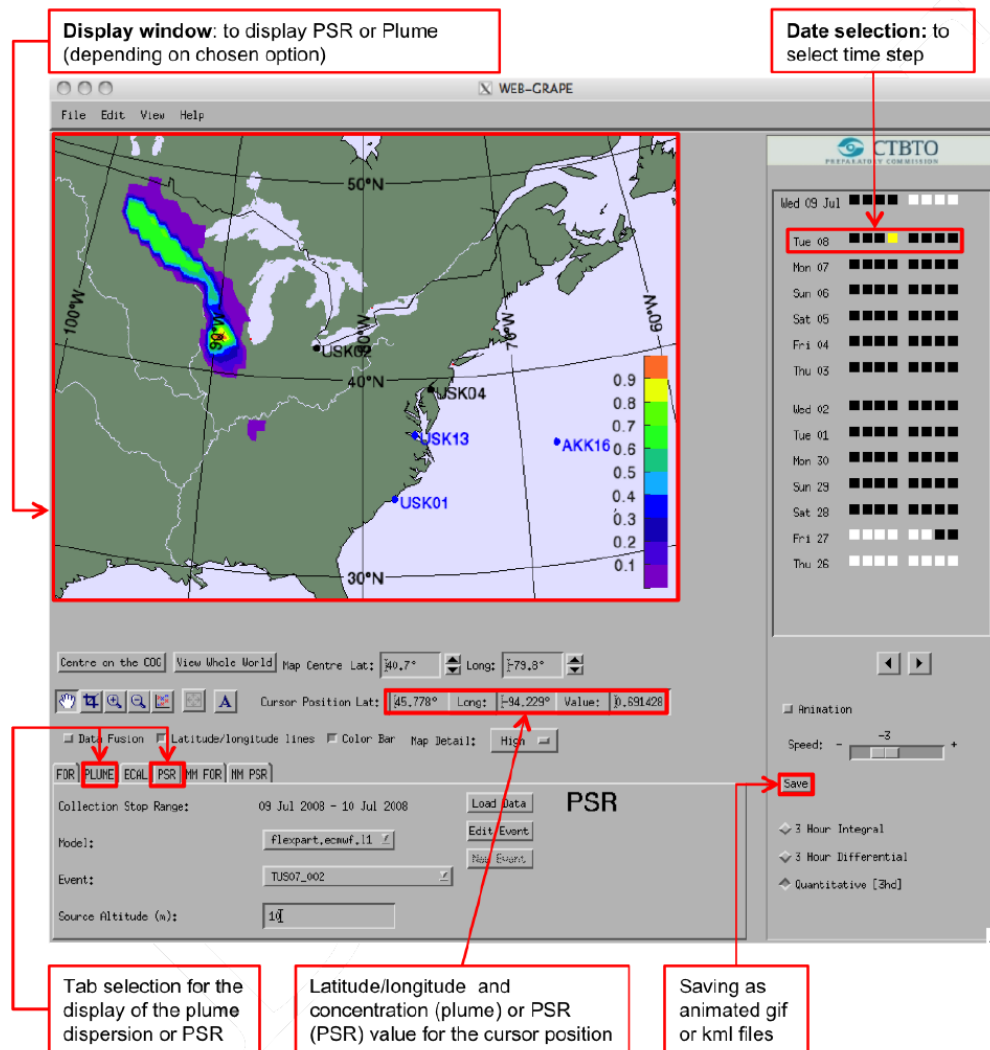
Figure 4.4 – Graphical User Interface (GUI) of the *PSR*-mode of Web-Grape. [Klingberg, F.J. et al. (2011)]

41

4.3.4 Calculating localizability parameters

In order to quantify the accuracy of localization, a number of *localizability parameters* were designed to verify the backtracking results of the investigated measurement scenarios against the initial release points and -times of the forward dispersions. The localizability parameters described in this section were implemented and calculated within the Fortran routine *aoicomp* which post-processes the output of the routine *locate_mult*.

The reliability of localization is represented by the distance from the point of maximum correlation to the source location and the time-series of correlation at the release point. A spatial-temporal investigation of a pseudo-measurement scenario based on backward ensemble dispersion modelling using these parameters was carried out by Becker et al. (2007). Klingberg, F.J. et al. (2011) undertook a number of simulations consisting of several sampling scenarios and found, that the maximum PSR value is sometimes far from the release point, but still located in an area of high PSR-values. Recognizing that, Klingberg et al. introduced a so-called *area of interest* (AOI), which is "a region containing PSR values $\geq 75\%$ of the maximum value". The size of the AOI was computed to quantify the sharpness of accuracy, which is another attribute of source localization. Besides, the minimum distance between the AOI and the source location was calculated.

Calculating a distance on the Great Circle Path

Distances on the earth surface can be calculated by applying methods of spherical trigonometry. All localizability parameters have been computed, based on the standard formula for calculating a distance on a Great Circle arc of a spherical triangle (Kompf, M. (2012)).

$$d = r \cdot arccos\left(sin\varphi_1 \cdot sin\varphi_2 + cos\varphi_1 \cdot cos\varphi_2 \cdot cos\left(\vartheta_2 - \vartheta_1\right)\right) \tag{4.1}$$

where ϑ and φ represent spherical coordinates for longitude and latitude. r is the earth radius ($r = 6378.388$ km).

Computing the correlation value over La Hague

In the present study, the correlation value at La Hague was calculated considering the PSR-values of four surrounding grid-cells. This was achieved by applying the Inverse Distance Weighting (IDW) interpolation method (adapted after Shepard (1968), see Fig. 4.5):

An interpolation value for the unobserved point S is calculated as a linear combination of the observed points P_i

$$S = \frac{\sum_{i=1}^{n} P_i w_i}{\sum_{i=1}^{n} w_i} \tag{4.2}$$

with the weighting functions

$$w_i = \frac{1}{d_i^{\lambda}} \tag{4.3}$$

where the observation values of $n = 4$ surrounding stations are weighted inverse to their distance to the interpolated point. The distances d_i are calculated using equation (4.1). The weighting exponent is choosen with $\lambda = 2$, which is a common value for general surface mapping purposes (Shepard (1968)).
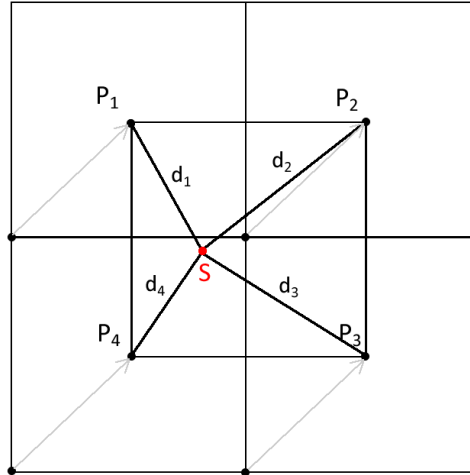
Figure 4.5 – Sketch on the calculation of the PSR-value at La Hague (lon. 1.88°, lat, 49.68° using the *Inverse Distance Weighting* interpolation method. Like the convention on the .srm format, each PSR-value stored in the file *correlation.txt* represents an average value of the grid-cell identified by the coordinates of its SW-corner. Thus the coordinates of the centres of the 4 neighboring grid-cells of the release point La Hague (S) are taken to calculate the distances d_i on the Great Circle Path to La Hague in order to weight the respective correlation values (P_i, grey arrows) inversely.

Determining d(maxcor,Hague) and d(AOI,Hague)

The distance between the location of maximum correlation and La Hague, *d(maxcor,Hague)*, can be directly derived inserting the respective coordinates into formula (4.1). Likewise, in order to compute the distance between the AOI and La Hague, *d(AOI,Hague)*, the coordinates of the centre of the nearest gridcell to the source having PSR-values which meet the AOI criterion, are determined and inserted into (4.1).

Since the grid distance for $\triangle\lambda, \triangle\varphi = 1°$ is approximately 111km in mid-latitudes, the grid-induced localization error can be up to $\sqrt{2} \cdot \frac{1}{2} \cdot 111\text{km} = 79\text{km}$.
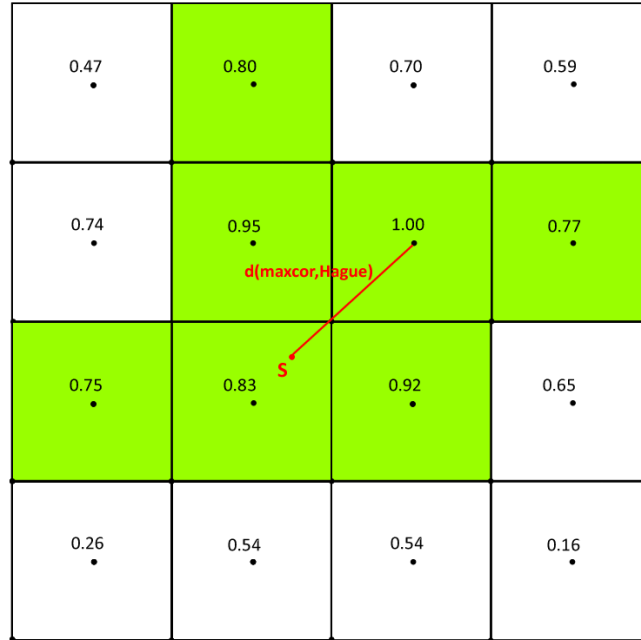
Figure 4.6 – For each timestep, the maximum value of PSR is determined and the distance between La Hague (S) and the centre of the grid-cell possessing the maximum correlation is calculated. All area elements at t_0 containing $\geq 75\%$ of the cell holding the maximum correlation value are subsequently summed up to gain the area of interest (AOI).

Calculating the Area of Interest (AOI)

An area increment on a sphere can be calculated using

$$dA = r^2 sin\vartheta d\vartheta d\varphi \tag{4.4}$$

Thus, a surface area segment of a longitude/latitude gridcell on earth (radius r) can be obtained by

$$\Delta A = r^2 \left[(sin\varphi_2 - sin\varphi_1) (\vartheta_2 - \vartheta_1) \right] \tag{4.5}$$

Substituting $\triangle\varphi = \vartheta_2 - \vartheta_1 = \frac{\pi}{180}$, which is the zonal resolution of the grid-cells, yields

$$\Delta A = r^2 \cdot \frac{\pi}{180} \left(sin\varphi_2 - sin\varphi_1 \right) \tag{4.6}$$

For a series of i,j grid coordinates this area can be computed using

$$A = \Delta A_{ij} = r^2 \frac{\pi}{180} \sum_i \sum_j sin\varphi_{j+1} - sin\varphi_j \tag{4.7}$$

Introducing the area of interest, which is "a region containing PSR values $\geq 75\%$ of the maximum value" (Klingberg, F.J. et al. (2011)) of the corresponding time t_0, only grid-cells which meet this criterion are summed up (see also Fig. 4.6):

$$AOI = r^2 \frac{\pi}{180} \sum_i \sum_j sin\varphi_{j+1} - sin\varphi_j \bigg|_{t_0, PSR(i,j,t_0) \geq 0.75 \cdot max(PSR(i,j,t_0))} \tag{4.8}$$

4.4 Flowchart

Figure 4.7 represents a detailed flowchart of the whole process which was applied for each of the 51 runs to assess the accuracy of localization of single-point sources of Kr-85 using a receptor-orientated (backward) approach. All programs were coded in Fortran and several process steps were automatized by Korn-Shell scripts (blue boxes) which saved time and offered more flexibility compared to Web-Grape.
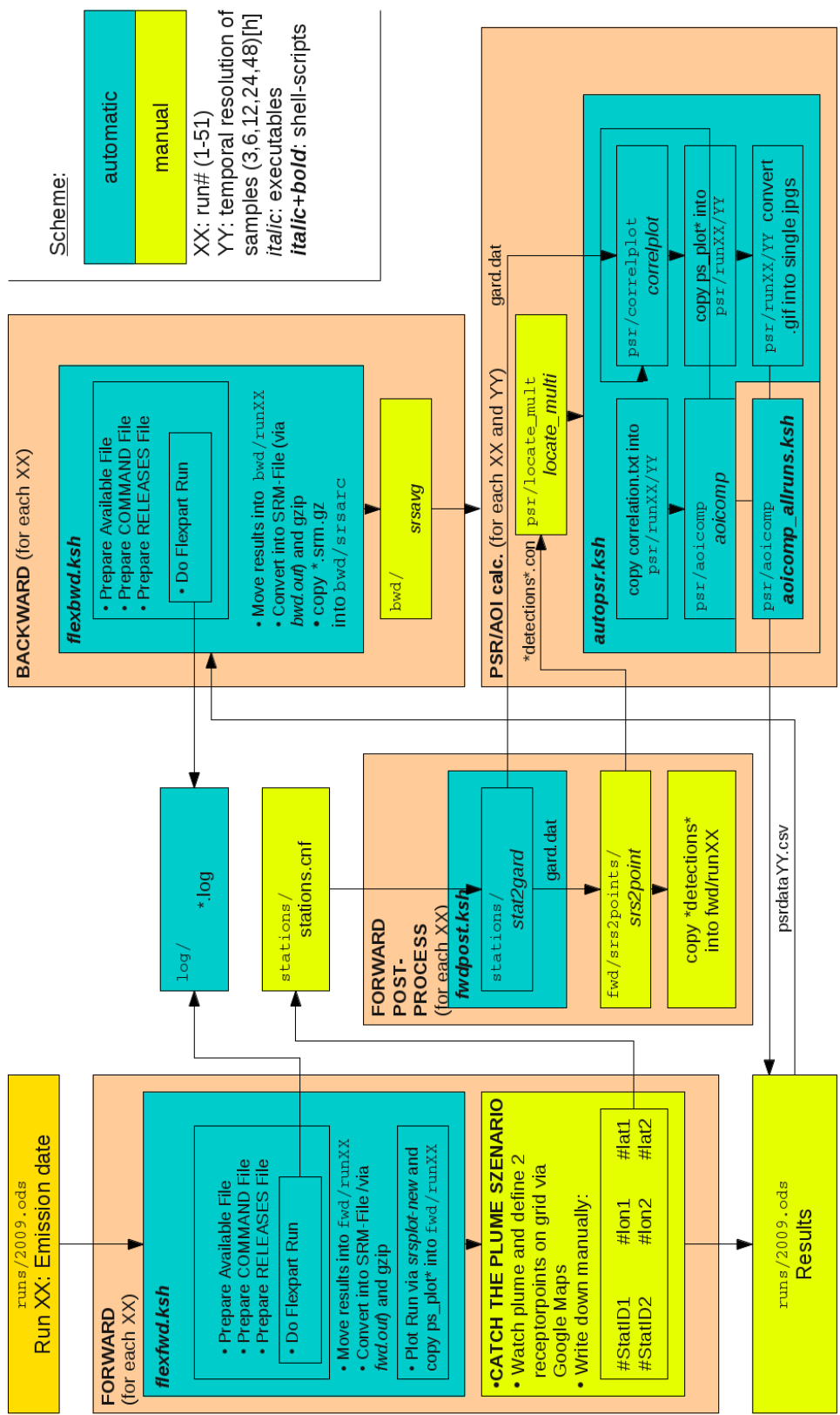
Figure 4.7 – Flowchart of the whole process which was applied for each of the 51 simulations in 2009.

Chapter 5

Results

5.1 Sampling stations
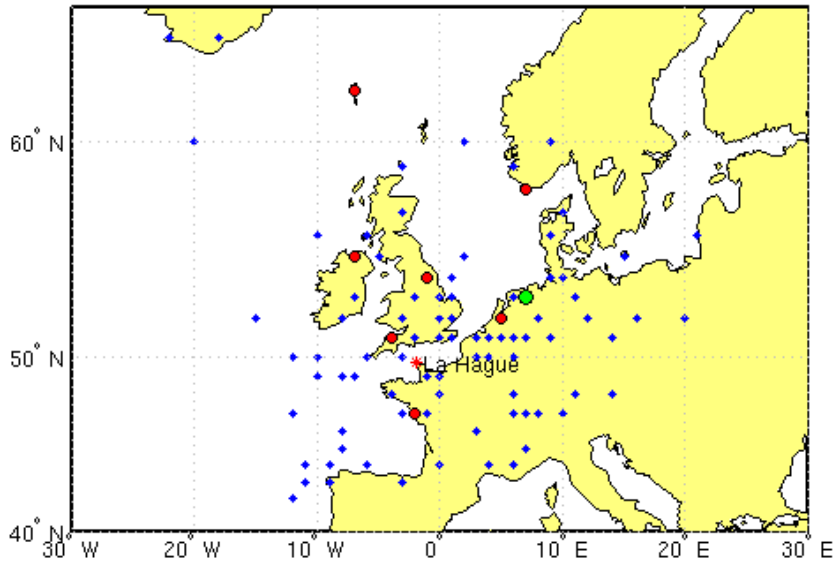
Figure 5.1 – Receptor points of all runs after applying the catch-the-plume scenario. To avoid grid induced errors, all virtual sampling stations were located on integer grid points. The red star marks the release point La Hague. Blue dots denote sampling stations used once. Red circles mark receptor points used twice and the green circle marks a station which was used three times (station NLK03, The Netherlands, Staadskanaal, lat. 53°, lon. 7°).

Fig. 5.1 illustrates the chosen receptor points for all 51 runs after applying the catch-the-plume scenario. A complete list of all 93 sampling stations is printed in Appendix B.1.

The frequency of the chosen sampling stations per country is plotted in Fig. 5.2.
21 stations were necessarily located on the ocean to meet the catch-the-plume scenario
requirements. France and United Kingdom follow with 16 stations each whereas 10 stations
are located on the territory of Germany. Due to the increasing distance to the release point,
locations in other countries represent the minority of all chosen receptor points. The great-
circle distances (Eq. 4.1) between the stations and the fictitious realease point La Hague
are analysed subsequently.

On average, the stations are located 722 km away from La Hague reprocessing facility.
The most distant station is ISK02 (Reykjavik, Iceland), with a distance of 1992 km. Ship
SPK09 is the nearest receptor point to the source (88 km distant). Station NLK03, lo-
cated near Staadskanaal in the Netherlands, has been used three times which denotes the
maximum of usage regarding all chosen stations within the catch-the-plume scenario (Fig.
5.1). The distance from NLK03 to La Hague is 719 km.
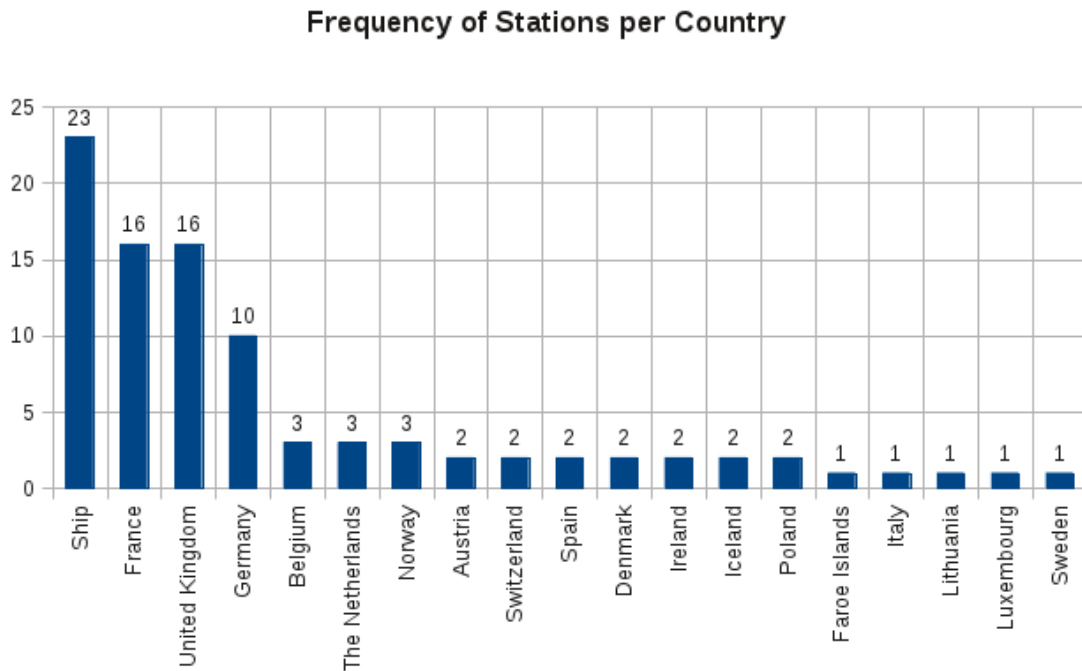
Figure 5.2 – Frequency of chosen sampling stations per country.

5.2 Spatial localizability of point sources using different temporal resolutions

Within this study, five different temporal sampling resolutions based on fictitious releases were tested.

The potential source region (PSR) at the middle of the release (12 UTC) of run 12 is plotted in Fig. 5.4 to visualize the effect of all tested sampling durations.

Initially, the fictitious release at La Hague has taken place at the backside of a deep trough reaching from Great Britain to Eastern Europe. Prevailing Northwesterlies over La Hague (Fig. 5.3) are advecting cold air westwards of the Alpine Arc into the Mediterrenean region, forcing cyclogenesis over the Gulf of Genua. The chosen receptors ITK01 and FRK16 are located at the inflow region of the developing low.

It is obvious, that the area of PSR increases with the temporal length of the samples (Fig. 5.4). As the collection time increases, more and more 3h SRS-fields are aggregated (compare Fig. 4.3), resulting in the depiction of a superset of PSR-shapes based on shorter sampling intervals. The correlation field for the 48h samples is extending to the middle of the Atlantic ocean, having a total AOI of 1.144.541 km² and tends to become a "plateau-pattern" of PSR (term introduced by Becker et al. (2007)) with a bimodal spatial distribution of the correlation values 0 and 1. This circumstance implicates, that with a longer collection interval an increasing amount of potential localizability information gets lost, as fewer measurements are available for backtracking purposes.
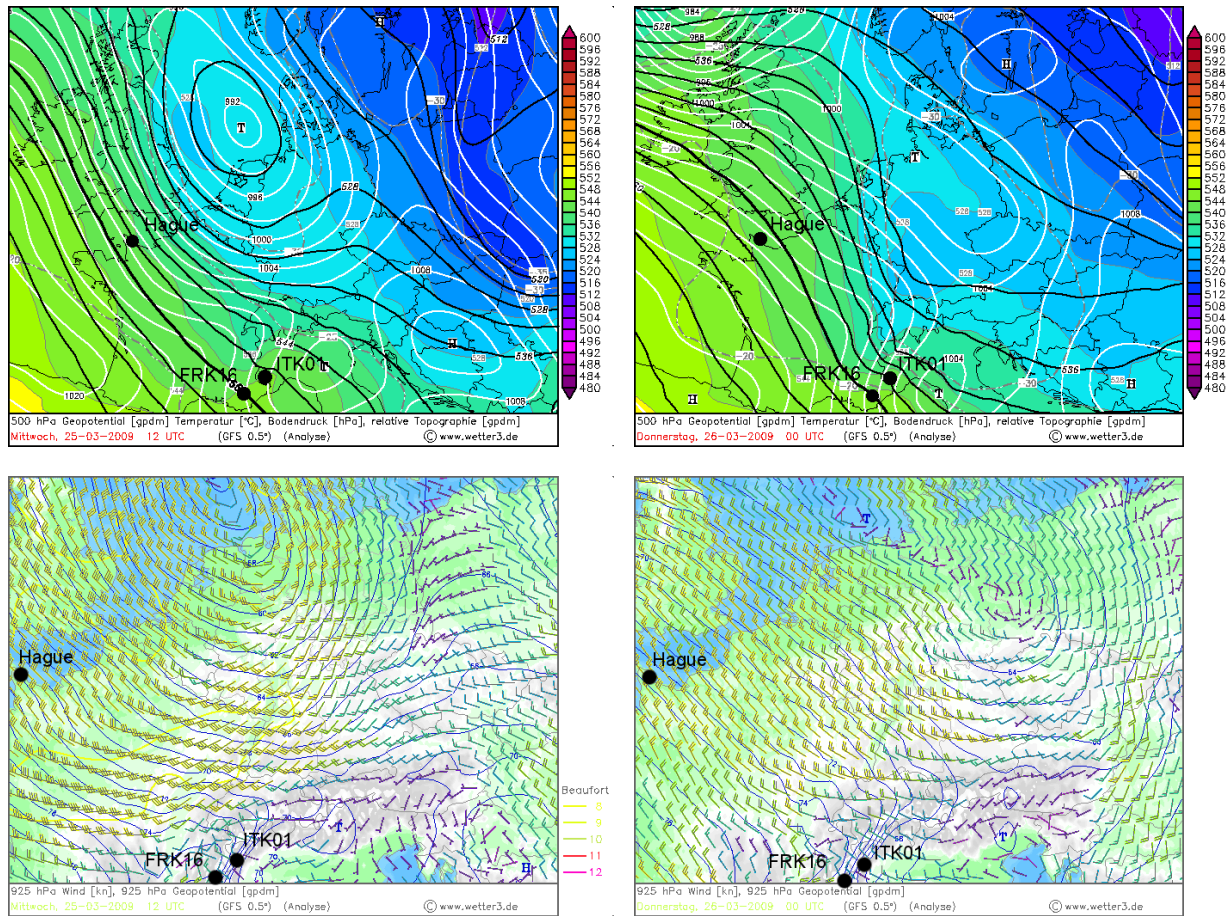
Figure 5.3 – Synoptic situation for the fictitious Kr-85 release at La Hague (site marked with "Hague") on March 25th 2009 12 UTC (left) and close to the sampling date on March 26th 2009 00 UTC (right, black dots "ITK01" and "FRK16" denote fictitious sampling stations). Plotted above are 500hPa isolines of geopotential (black, [gpdm]) and 500hPa isolines of temperature (grey, [°C]), surface pressure field (white, [hPa]), and H500-H1000 relative topography (contours, [gpdm]). Plotted below are 925hPa isolines of geopotential (blue, [gpdm]) and wind barbs in 925hPa. Geostrophic streamlines of the atmospheric boundary layer can be assumed to be parallel to the blue geopotential isolines in 925hPa, which corresponds to a height of about 800m above mean sea level. [Charts adapted after http://www.wetter3.de/Archiv/]
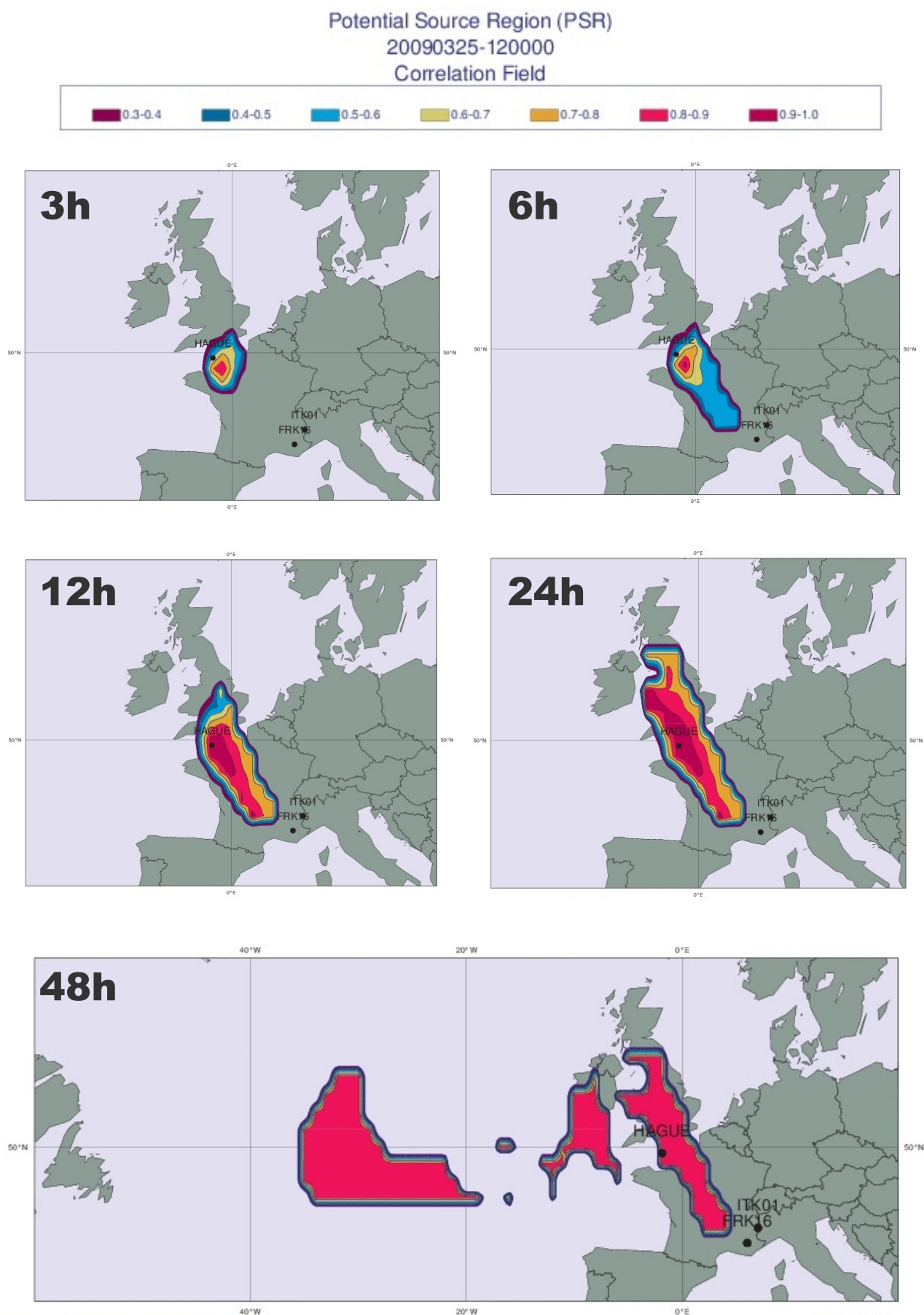
Figure 5.4 – Visualization of the potential source region (PSR) for different temporal sampling durations at the release time of run 12.
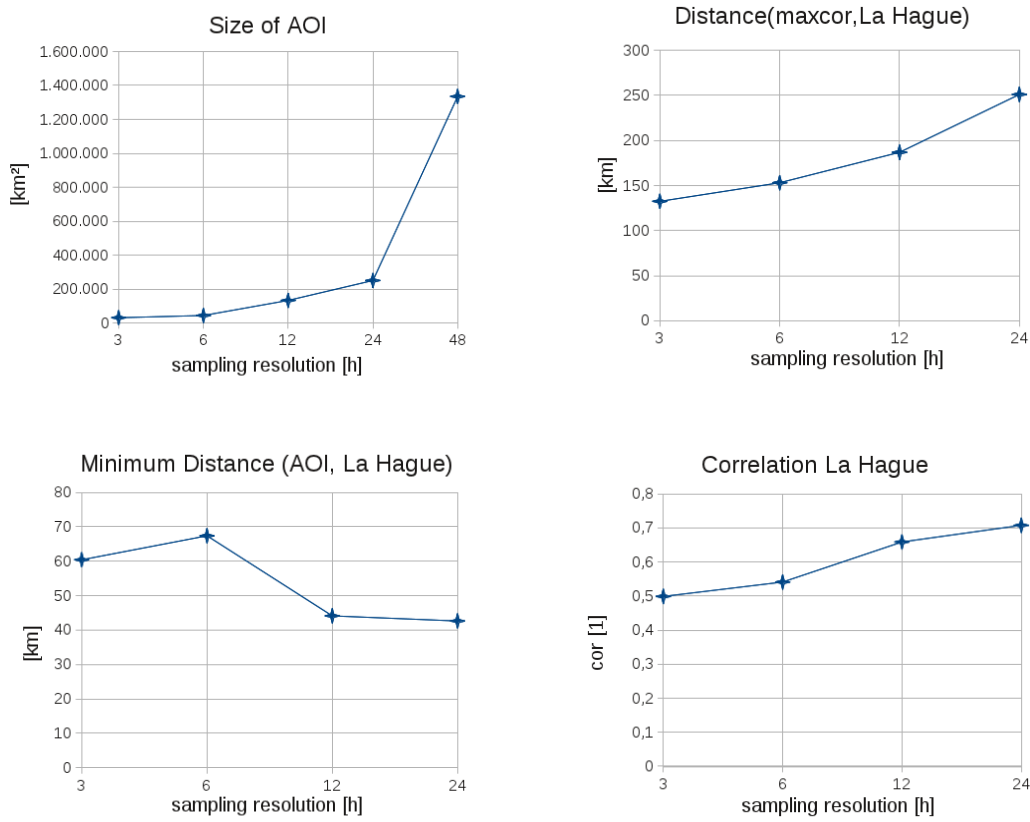
Figure 5.5 – Spatial localizability parameters as a function of temporal sampling resolution. The diagrams above illustrate mean values of localizability parameters over all 51 runs in 2009 at the time, where a fictitious 6h-release over La Hague took place. Parameters explained in Chap 4.3.4.

Single releases of Kr-85 with a duration of 6 hours were entirely sampled within a 48h interval in all 51 runs using the present sampling setup. 48h samples of two receptor points at the same time did not contain much signal information. This leads to the question whether grid points are sensitive to the two samples at the same time or not, resulting in areas possessing full correlation or with no correlation. Using 48h samples, it is not possible to acquire more refined statements. Because of the resulting huge AOI, a temporal sampling resolution of $\geq$48h cannot be recommended and is thus not investigated further in the following chapters.

The mean values for the localizability parameters over all 51 runs at the time of release for all sampling durations are plotted in Fig. 5.5. The AOI increases exponentially with the investigated temporal sampling resolutions, however, considering that the x-axis is

scaled exponentially itself, the size of AOI grows quadratically with the temporal sampling resolution (Fig. 5.5a). The mean distance between the location of maximum correlation (maxcor) and La Hague ranges from 130 to 250km (Fig. 5.5b). Figure 5.5c illustrates the mean minimum distance between the AOI and La Hague, which drops below 50km for 12h and 24h. The localization error of 1° gridded output in mid-latitudes can be up to 79km (Chap. 4.3.4).

The positive trend of the correlation over La Hague (Fig. 5.5d) with the sampling duration is mainly caused by three reasons:

- As the AOI increases with the duration of collection, it is more likely that La Hague is located inside a field of higher correlation.

- With longer duration of the samples, the PSR tends to have only perfect- (value 1) or no correlation (value 0).

- An effect which is related to the "double penalty problem" from verification science (Goeber, M. and Wilson, C. (2012)): The better the spatial-temporal resolution of the model-output (i.e. shorter sampling intervals), the poorer the verification results get, i.e. the retroplume can more easily miss the release point when it gets sharper. This effect is manifested by the relative frequency of misses (cor. value at La Hague < 0.2) in Tab. 5.2.

$\triangle_t$	d(maxcor,Hague) [km]	d(AOI,Hague) [km]	cor(Hague)	AOI [km^2]
3h	132.5±114.7	60.4±86.9	0.50±0.29	30.698±31.561
6h	153.2±134.4	67.4±86.4	0.54±0.29	43.870±46.097
12h	186.9±154.0	44.1±71.1	0.66±0.30	132.979±292.011
24h	251.1±209.2	42.6±73.3	0.71±0.30	250.159±361.473
48h	*	*	*	1.334.974±949.131

Table 5.1 – Mean value and standard deviation of localizability parameters for all simulations (n=51) and investigated temporal sampling resolutions.

Table 5.1 contains the average values of all parameters plotted in Fig. 5.5 in detail. The high standard deviation values imply a large variability of most values. The sensitivity of detectability to different synoptic flow regimes will be investigated within the following section. Table 5.2 shows the relative frequency of certain treshold values of all runs and

n = 51	$\triangle_t$= 3h	$\triangle_t$= 6h	$\triangle_t$= 12h	$\triangle_t$= 24h
distance(maxcor,La Hague)				
<55 km	37%	33%	25%	18%
<111 km	55%	49%	35%	29%
<350 km	92%	86%	86%	75%
Minimum distance (AOI, La Hague)				
<55 km	71%	65%	75%	75%
<111 km	76%	78%	84%	82%
<350 km	100%	100%	100%	100%
Correlation La Hague				
$\geq$0.9	2%	8%	22%	29%
$\geq$0.7	29%	39%	61%	69%
$\geq$0.5	57%	57%	71%	100%
$\leq$0.2(misses)	24%	16%	10%	12%
=0	4%	6%	6%	4%
AOI				
<1.000 km^2 [1]	0%	0%	0%	0%
<10.000 km^2	24%	16%	4%	2%
<100.000 km^2	96%	92%	67%	31%
<1.000.000 km^2	100%	100%	98%	96%

Table 5.2 – Relative frequency of reached treshold values of localizability parameter values for all runs (n=51) and temporal sampling resolutions. [1]) 1.000km^2 mark the maximum size of an area for carrying out on-site inspections in terms of the CTBT.

temporal sampling resolutions which confirm the effects listed above. In 86% of all events, based on a 12h sampling interval, the error of the estimated release point location was < 350km and correlation values at La Hague ranged $\geq$ 0.7 in 61% of all cases. The treshold-value of 1000km^2, which marks the maximum extent of an area for carrying out on-site inspections, the ultimate measure for verifying nuclear explosions in terms of the CTBT (CTBTO (2009)), has never been undermatched. However, the CTBTO additionally uses seismic ellipses for source localization and the idea of a catch-the-plume scenario in terms of the NPT is to verify clandestine reprocessing at nuclear facilities, whose locations are already known.

In 4 to 6 % of all cases, the method was not applicable due to complex synoptic situations mostly because of splitting points or deformation bands, which led to a large delay of the surpassing retroplume (see also Fig. 5.7). Detailed spatial localizability results for the individual runs are listed in Appendix A.

5.2.1 The influence of synoptic flow-regimes over La Hague

Once released, the general weather situation heavily influences the propagation and dispersion of the Kr-85 plume. High values of standard deviation of localizability parameters values as depicted in chapter 5.2 suggest a strong dependency on whether advection or diffusion processes dominate, which is manifested by synoptic flow patterns. One approach to investigate this problem is to analyse the localizability according to prevailing synoptic flow regimes over the release point La Hague at the time of the hypothetical releases.
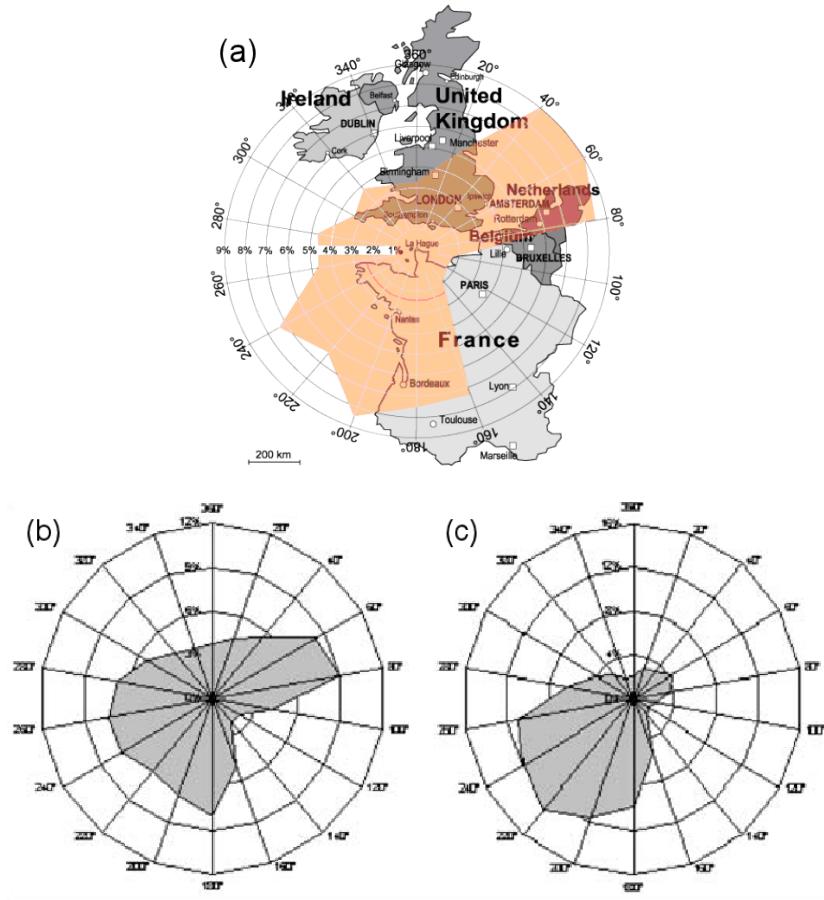
Figure 5.6 – Wind rose for all (a), dry (b) and rainy (c) weather conditions measured at the La Hague reprocessing plant effluents exhaust stack (height 100m). [Adapted after WISE (2002) and Fréchou and Calmet (2003)]

Fig. 5.6 shows the wind direction frequency in % of time for different weather conditions measured at the 100m high La Hague reprocessing plant effluents exhaust stack. The data was collected by the former reprocessing facility operator COGEMA and published by the World Information Service on Energy in Paris WISE (2002) (a) and Fréchou and

Calmet (2003)] (b,c), unfortunately without providing detailed information on the sampling interval and on the period when the measurements took place.

Wind-rose (a) shows a maximum of measured winds from the east to northeast sector. This peak originates from winds blowing at dry conditions (b), which are strongly related to anticyclonic flow regimes. However, at most of the time, the winds blow from the southwesterly quadrant (a), indicating a strong maritime influence of prevailing westerlies. At rainy conditions, southwestern flows dominate (c), which is connected to maritime cyclonic influence of lows located northwest of Cotentin Peninsula. All wind-roses indicate a minimum frequency of winds blowing from north and southeast-direction.

$\triangle_t$=12h,n=51	N	E	S	W
rel. frequency	12%	22%	24%	43%
$cor(Hague)$	0.74	0.43	0.72	0.72
$\sigma(cor(Hague))$	0.26	0.32	0.26	0.29
AOI [km^2]	79.423	236.810	155.640	83.309
$\sigma(AOI)$ [km^2]	77.950	599.504	184.104	57.746

Table 5.3 – Localizability results for 51 simulations in 2009, consisting of two stations with a sampling interval of 12h for different synoptic flow regimes over La Hague. Mean values and standard deviations of the correlation value over La Hague (cor(Hague)) and the AOI are tabulated against classified flow directions. The prevailing flows were estimated and clustered into 4 classes, after analysing the propagation of the Kr-85 plumes within the first time-steps after the releases took place.

In general, the climatology of prevailing flows over La Hague, investigated at the release dates of undertaken simulations in 2009 (Tab. 5.3), is similar to the measurements at the La Hague reprocessing plant effluents exhaust stack (Fig. 5.6a). The backward simulations for a temporal sampling resolution of 12h deliver the best results in terms of localizability (PSR(Hague)). If the releases at La Hague take place at conditions with wind-directions from the west, south and north, the mean correlation values can be expected to be about 0.7. Table 5.3 thus indicates the chance of localizing the source maximizes at times, when the wind over La Hague originates from maritime, cyclonic flow-regimes, i.e. during western- and southern wind mostly during rainy conditions (Fig. 5.6c) or maritime, backside trough northerlies. This statistical correlation is conclusive, as cyclonic flows as well as cold-air advection through northerlies on the backside of a trough are favoured by strong atmospheric gradients resulting in higher wind speeds, which strengthens the role of advection and weakens the influence of diffusion during the Kr-85 transport pro-

cess. The stratification of AOI to different flow regimes shows, that within backside trough northerlies, the role of diffusion is minor, resulting in a rather low mean AOI of 79.423 km^2 compared to continental flows from the east, where diffusive processes are more dominant, leading to a greater extent of AOI (236.810km^2). However, the sharpness of localization heavily differs from case to case as the standard deviation of AOI remains high considering all flow-directions.

5.3 Temporal localizability of point sources using different temporal resolutions

After analyzing the spatial localizability, this section focuses on the temporal localizability of a Kr-85 single point release using the present sampling setup. If the location of a reprocessing facility is known and suspicious concentration values of surrounding Kr-85 sampling stations are detected, one can investigate the time series of the correlation values at this reprocessing facility. The most likely time of release at this point can be reconstructed as the time when the correlation value at the fixed point reaches its maximum.

The time lag between the reconstructed release time and the initial release time of the simulations is plotted in Fig. 5.7. In most of the runs, the release time could be reconstructed correctly within ±3h. There is no significant trend of temporal localizability as the duration of the samples increases.

The accuracy of temporal localization is shown in Fig 5.8. Fig. 5.8a shows the localizability at the release time whereas Fig. 5.8b includes a tolerance of ±6h. Allowing a tolerance of ±6h for detecting the initial 6h release time, there is no significant difference in the hit rate as a function of the sampling resolution. Temporal localization within ±6h can be achieved in 70% to 80% of all cases almost independent of the underlying temporal sampling resolution. Detailed temporal localizability results for the individual runs are listed in Appendix A.
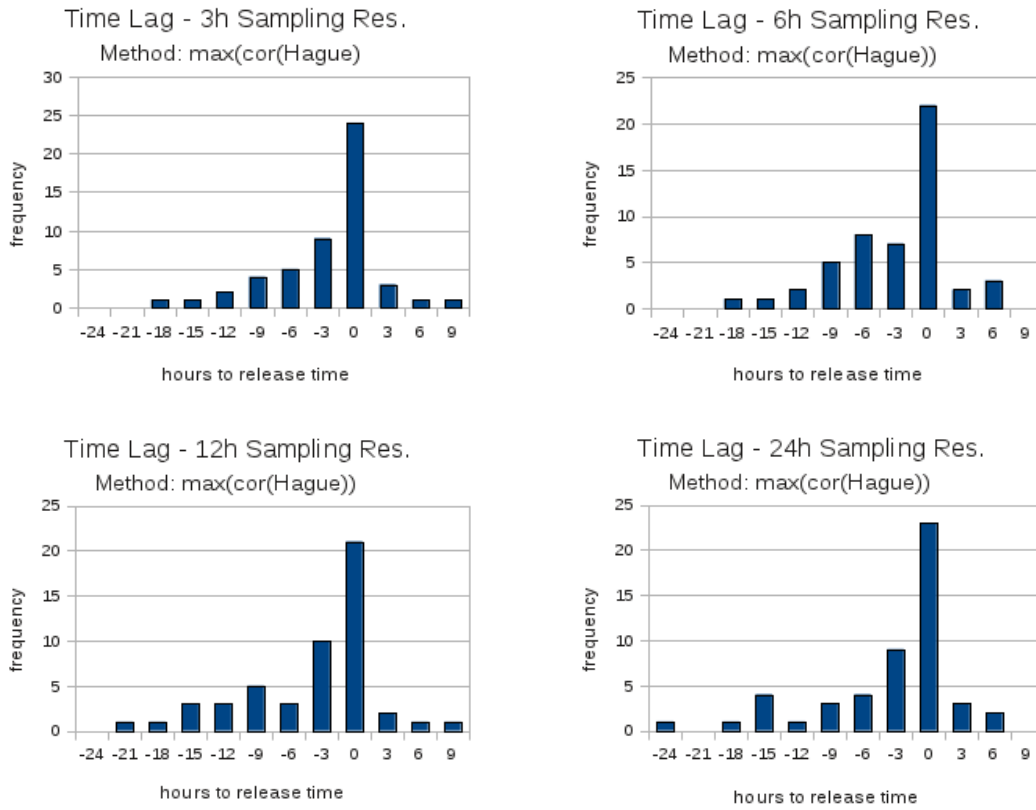
Figure 5.7 – Accuracy of temporal localization. Plotted is the frequency of temporal lags between the release times predicted by the model (maximum of correlation value over fixed point La Hague) and the original times of fictitious releases (12 and 15 UTC resp.) for all simulations.

5.4 Comparison of results with previous studies

Tab. 5.4 compares simulation parameters and settings for the localizability studies of Klingberg, F.J. et al. (2011), Becker et al. (2007) and this thesis. In particular, different sampling scenarios, simulation durations, the number of runs and the model settings heavily affect the localizability results, which are printed in Tab. 5.5.

As the studies of Klingberg and Kaltenberger are both based on the catch-the-plume scenario with similar transportation times, the results of these studies are relatively easy to compare. However, it has to be considered, that the smoothing sampling window in the study of Klingberg is generally chosen a bit later than in the present study which is noticeable as receptor points are located more distant from the source (1080 km and 722 km resp.) resulting in higher values of AOI. Besides, in contrast to the study of Klingberg,
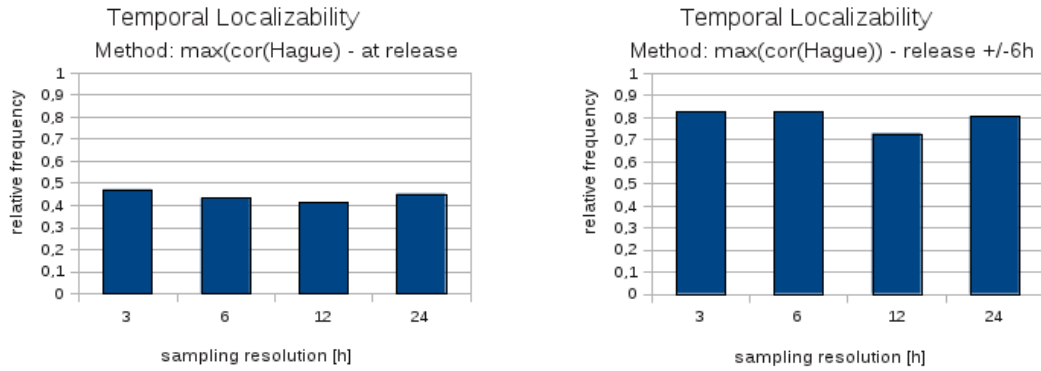
Figure 5.8 – Temporal localizability of all runs. Explanations see text.

the receptor points are located on integer grid points within the present study to minimize grid-induced errors. This ideal placement of receptor points may not be applicable in practice. However, existing software can be adapted to place receptor points anywhere in the domain.

	Kaltenberger	**Klingberg et al (2011)**	**Becker et al (2007)**
Simulation parameters			
Simulated substance	inert tracer (Kr-85)	inert tracer (Kr-85)	inert tracer
LPDM	Flexpart	Flexpart	multi model ensemble consisting of 12 different LPDMs/settings
Output horizontal resolution	1.0°	0.5°	1.0°
Output temporal resolution	3h	3h	3h
Determination of localizability parameters	automatic (Fortran routines)	manual (gauging via Web-Grape)	x
Meteorological input data			
NWP system	ECMWF 4DVAR	ECMWF 4DVAR	ECMWF 4DVAR, NCEP GFS, DWD GEM and others
Vertical layers	91	91	ECMWF:60
Horizontal resolution	1.0°	0.5°	1.25°-1.0°
Temporal resolution	3h	3h	1h-6h
Simulations			
Number of events	51	11 [1]	1
In year	2009	2008	2005
Release			
Fictitious release point(s)	1	3	1
Source term	1.3TBq	1PBq	1.3PBq
Release duration	6h	6h	3h
Thousands of particles released forward	500	100	x
Thousands of particles released backward per sample	500	100	0.5-500
Sampling scenario			
Sampling network	variable, receptor points chosen within catch-the-plume scenario	variable, receptor points chosen within catch-the-plume scenario	fixed network of 79 [2] radionuclide stations (CTBTO IMS)
Receptor points	2	up to 5	15
Receptor points located on	integer grid points	near nuclear facilities if possible	optimized network in terms of global detectability of events
Concentration samples	pseudo	pseudo	pseudo
Sampling window	fixed, 9 – 57h after release	smooting, 24h inside 24-72h after release	9 days
Temporal sampling resolution	3/6/12/24/48h	3h	3h

Table 5.4 – Comparison of model settings, methods and data used in denoted localizability studies. "x": Information not available. [1] 11 forward simulations consisting of 5 sampling scenarios each (1-5 receptor points). [2] Source: Wotawa (2010)

	Kaltenberger	Klingberg et al (2011)	Becker et al (2007)
Receptor points			
Average distance of receptor points to source	722km±398km	1080km	x
Nearest station	88km	69km	x
Most distant station	1992km	2854km	x
Accuracy of localization			
Situation A: Release time not known			
Distance(maxcor,releasepoint)	*	*	378km
Distance(AOI, releasepoint)	*	*	*
Temporal deviation	70%-80% inside of 6h [1]	*	14h
Situation B: Release time known			
Distance(maxcor,releasepoint)	$\triangle_t$ / [km] 3h / 132.5±114.7 [2] 6h / 153.2±134.4 [2] 12h / 186.9±154.0 [2] 24h / 251.1±209.2 [2]	$\triangle_t$ / [km] 3h / 476±285 [3]	$\triangle_t$ / [km] 3h / 663 (ensemble average) 3h / 74 (best centered single model)
Distance(AOI, releasepoint)	$\triangle_t$ / [km] 3h / 60.4±86.9 [2] 6h / 67.4±86.4 [2] 12h / 44.1±71.1 [2] 24h / 42.6±73.3 [2]	$\triangle_t$ / [km] 3h / 233±293 [3]	*
Correlation at release point	$\triangle_t$ / [km] 3h / 0.50±0.29 [2] 6h / 0.54±0.29 [2] 12h / 0.66±0.30 [2] 24h / 0.71±0.30 [2]	$\triangle_t$ / [1] 3h / 0.24±0.37 [3]	*
Sharpness of localizability			
AOI	$\triangle_t$ / [km^2] 3h / 30.698±31.561 [2] 6h / 43.870±46.097 [2] 12h / 132.979±292.011 [2] 24h / 250.159±361.473 [2] 48h / 1.334.974±949.131 [2]	$\triangle_t$ / [km^2] 3h / 129.657±256.107 [4]	*

Table 5.5 – Comparison of localizability results of denoted studies. "x": Information not available. "*": Not investigated. [1]) Average of 70% of all runs and sampling resolutions. [2]) Average over all 51 runs with 2 receptor points each (best localization result for analysed steps at 12/15 UTC of release day). [3]) Average of all 11 runs with 2 receptor points each (best localization result for analysed steps at 9/12/15 UTC of release day). [4]) Average over all 11 runs with 3 receptor points each (best localization result for analysed steps at 9/12/15 UTC of release day).

The appearance of spotty regions adressed by Klingberg (Chap. 1.4.3) when using a horizontal output resolution of 0.5° is most likely due to the relatively low number of released particles which led to poorer localizability results in some cases. Regarding the results for the correlation value over the release points, the present study performed much better which can be explained through minimizing grid-induced errors by

- locating hypothetical sampling stations on integer grid-points (Chap. 4.1.2)

- implementation of the objective inverse distance weighting interpolation method (Chap. 4.3.4)

- lack of complex topography in the vicinity of La Hague where the hypothetical releases took place (Chap. 1.3.3)

Taking into account the study of Becker et al., one has to consider, that this study is based on a multi-model ensemble consisting of 12 models driven in different ways using diverse settings and meteorological input data. Although the inert tracer released by Becker et. al experienced a relatively long transportation time of 9 days, the results regarding accuracy of localizability are comparable to those by Klingberg (663 km and 476 km resp.). This is the reason for the fact that pseudo samples were generated at 15 optimum-located receptor points inside the CTBTO International Monitoring System (IMS) consisting of 79 already fixed radionuclide stations worldwide (Wotawa (2010)), which maintains a satisfactory backtracking result over a large distance. However, the present study achieved better localizability results according to the distance between the location of maximum correlation and the release point (distance for all tested temporal sampling resolutions $\leq$ 250 km). Regarding a situation, where the release time is not known, between 70% and 80% of all runs and temporal sampling resolutions of all simulations lie inside a 6h interval. The results for the multi model ensemble and its associated longer plume propagation time delivered a temporal deviation of 12h.

5.5 Validation of localization technique against the ETEX dataset

The generation of pseudo-samples within this study was required as there are no highly resolved datasets of Kr-85 measurements available because of high costs of current sampling- and analyzing procedures (see Chap. 1.3.4). Real measurements of atmospheric tracers are

acquired during tracer experiments which are then used to validate and verify atmospheric transport models.

In 1994, several international institutions affiliated to arrange the experimental part of the ETEX (European Tracer EXperiment) project (JRC (2004)). A temporary, homogenous sampling network consisting of 168 ground-level sampling stations had been set up across Europe to measure two initial tracer releases in northwestern France. The released perfluorcarbon compounds (PFCs) "are environmentally safe, non-toxic, not washed out by rain, and allow extremely high detection sensitivity, due to the very low atmospheric background levels (...)." Additional concentration measurements had been carried out by three aircrafts. Moreover, in-situ meteorological measurements and upper air observations using SODAR (Sound Detection and Ranging) and constant volume ballons had been done to investigate the early stage of development of the plume in the vicinity of the release site. After the experiment, the concentration measurements and additional meteorological measurements were gathered in a database, which is available for free on the ETEX project homepage (JRC (2004)) for any further model evaluation by the scientific community. Since then, the high-resoluted ETEX dataset has been used by several institutions to test their trajectory models using real measurements. A validation of Flexpart against the ETEX dataset has been carried out by Stohl et al. (1998). A post-factum evaluation of the performance of long-range dispersion models based on the first release (ETEX-1) has been carried out in 1996 (ATMES-II). Based upon this dataset, the localization technique used in this study will be validated and analyzed in this chapter.

5.5.1   Setup of ETEX

During the two experiments, perfluorcarbon tracers (PFCs), i.e. "hydrocarbons in which all hydrogen atoms are replaced by fluorine atoms", were released. Being stable in air ("non-depositing, non-scavenged, non-reactive" with a chemical half-life times of around 100 years) with low, relatively constant atmospheric background (in the order of 10^{-15}l per liter of air) and chemically detectable even at very low concentration values (10-16 v/v (volume to volume)), PFCs meet the tracer method requirements in a very similar way Kr-85 does.

The tracer was released in form of a homogeneous air stream at the 4m heigh experimental exhaust stack of a release unit located at Monterfil in Northwestern France (48°3′30″N, 2°0′30″W), See figures 5.9 and 5.11d), which was chosen based on a climatological study, enabling the plume to pass as many stations as possible of the ground-based sampling

network consisting of 168 stations spread over large parts of Europe (Fig. 5.9). "Initially, the proposal was to place samplers at 0.5° to 1° intervals of longitude and latitude across Europe", however "the costs and effort (according to electrial supplies, communication systems and the need to be operated by personnel with a scientific background round the clock for 7 consecutive days) would have been totally prohibitive." Hence, almost all of the 168 sampling stations had been chosen to be located at existing WMO stations to meet these practical requirements. The sampling technique of the ground-level stations used in ETEX is similar as of current, operational Kr-85 samplers. In active samplers, "a known-air volume is passed through and adsorbed in a column of activated charcoal packed into a tube that quantitatively removes all PFC material from the air."
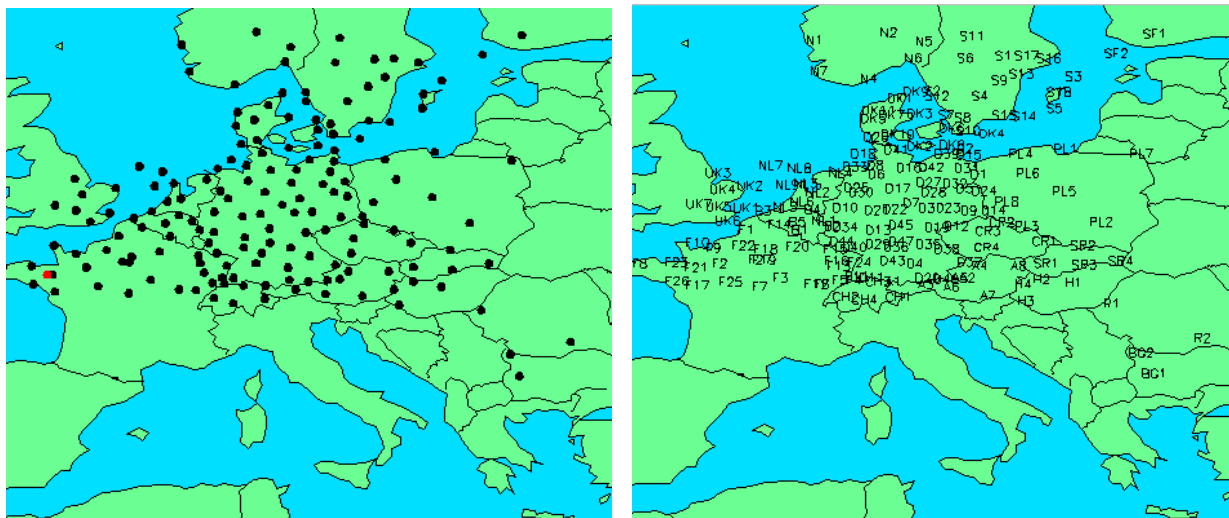
Figure 5.9 – Stations of the ETEX sampling network. The release point at Monterfil (48°3′30″N, 2°0′30″W) is marked red. [JRC (2004)]

The stations collected samples over a period of 3 consecutive days (24 three-hour samples) each, which started progressively delayed from West to East. After the last sample had been collected 90 hours after the release start, all samples were sent to JRC Ispra for chemical analyses. An ambient background level of each station was estimated by determining a baseline value when analysing measured concentration values before and after the passage of the plume. After that, this value has been substracted from the concentration measurements.

5.5.2 The first experiment

Within the first experiment, ETEX-1, the release of 340 kg of perfluoromethylcyclohexane (PMCH) started at 23 October 1994 at 1600 UTC and ended at 24 October, 0350 UTC with in an average flow rate of PMCH of 7.98 g/s. After the passage of a cold-front, unstable air mass with showers was advected by a rather strong West to South-Westerly flow. During the release, neither centres of high- or low-pressure nor extending ridges or throughs had passed close to the release site. Additionally, no frontal systems passed Monterfil during or shortly before or after the period of release. The dispersion of the plume according to synoptic situations is discussed subsequently and is illustrated in Fig. 5.11 and Fig. 5.10.

The synoptic chart of October 24, 00 UTC (Fig. 5.11a), which describes the surface pressure field and in-situ measurements at WMO stations, valid 8 hours after the release had been started at Monterfil, illustrates an unstable flow over the release site and the advection area. Because of a northerly movement of the controlling low westwards of the Norwegian coast, the surface pressure gradient weakened, resulting in decreasing winds over the advection area. Under the influence of a blocking high-pressure cell over West-Siberia, the meanwhile occluded cold front in its dissipation stage, which initially passed Monterfil before the start of the release time, showed only little eastward propagation. At October 24, 04UTC, 12 hours after the start of release, the plume had been already extended (Fig. 5.10a). However, "the splitting into two parts may be due to a real effect or an artefact of the mapping procedures due to the lack of observations between France and Belgium." The centre of the plume had travelled substantially and was observed near the border between Belgium and Germany. 12 hours later on October 24, 16 UTC (Fig. 5.10b), the plume was extending from Northern France across the Netherlands, Belgium and Central Germany to the West of Poland possessing concentration maxima in the Southern Netherlands.

On October 25th at 00UTC, the mentioned cold front almost dissipated North of around 48° (Fig. 5.11b). This figure also shows a secondary low at 52° N and 5°E and its belonging cold-front identified by the cyclonic curvature of the surface pressure field over the British Isels. With the approach of the front, the wind was backing more to the south during this day. The diffluent flow due to a saddle point in the surface pressure field over Eastern Europe caused the tracer cloud to split (Fig. 5.10c, valid for October 25, 04UTC). Following the Southwestern surface flow of the dipole shaped low-pressure complex over the North Sea and holding the maximum of measured concentration values, the western branch of the plume continued extending North via Denmark (Fig. 5.10d) while the eastern part remained stationary in Poland with a local maxima in Slovakia. After the passage of

the front had been taken place, (Fig. 5.11c) suggests a veering of the wind over Western Europe towards west-south-west.
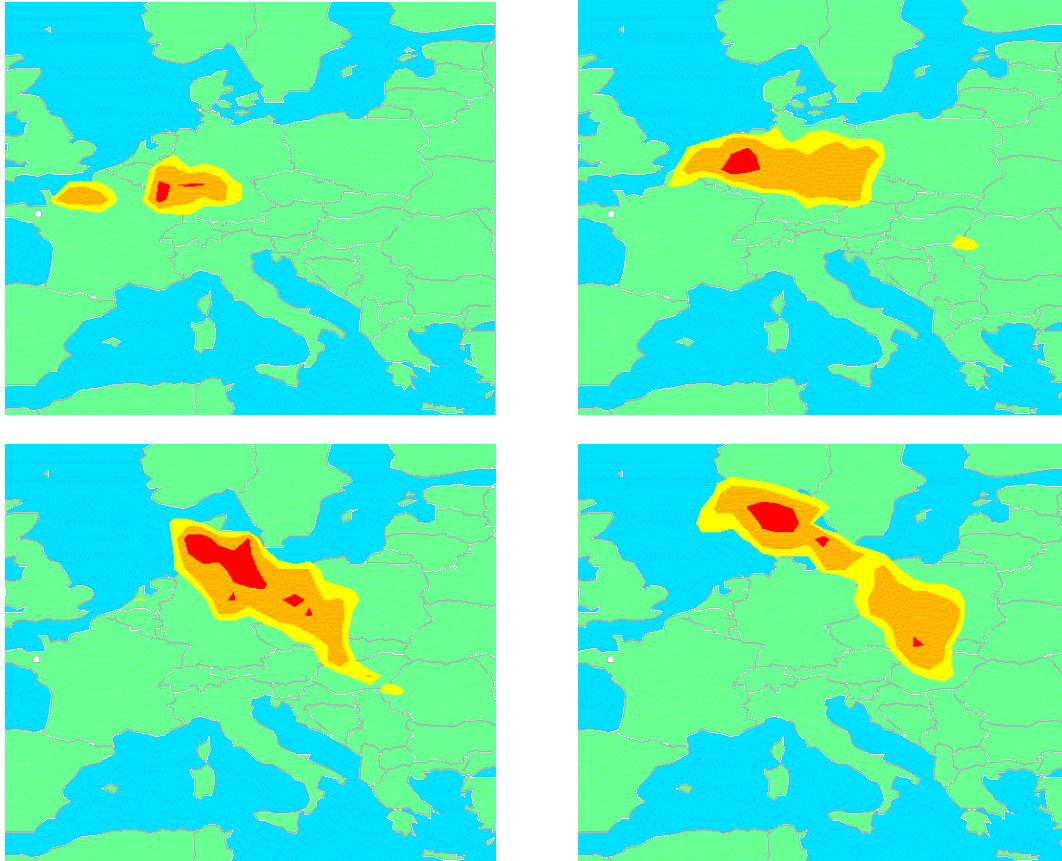
Figure 5.10 – Position of the measured tracer cloud at T+12, T+24, T+36 and T+48 (from above left). "T" is the time of the start of release (23 October 1994 at 1600 UTC). 0.01, 0.1 and 0.5 ng/m^3 contours are shown, respectively, in yellow, orange and red. [JRC (2004)]
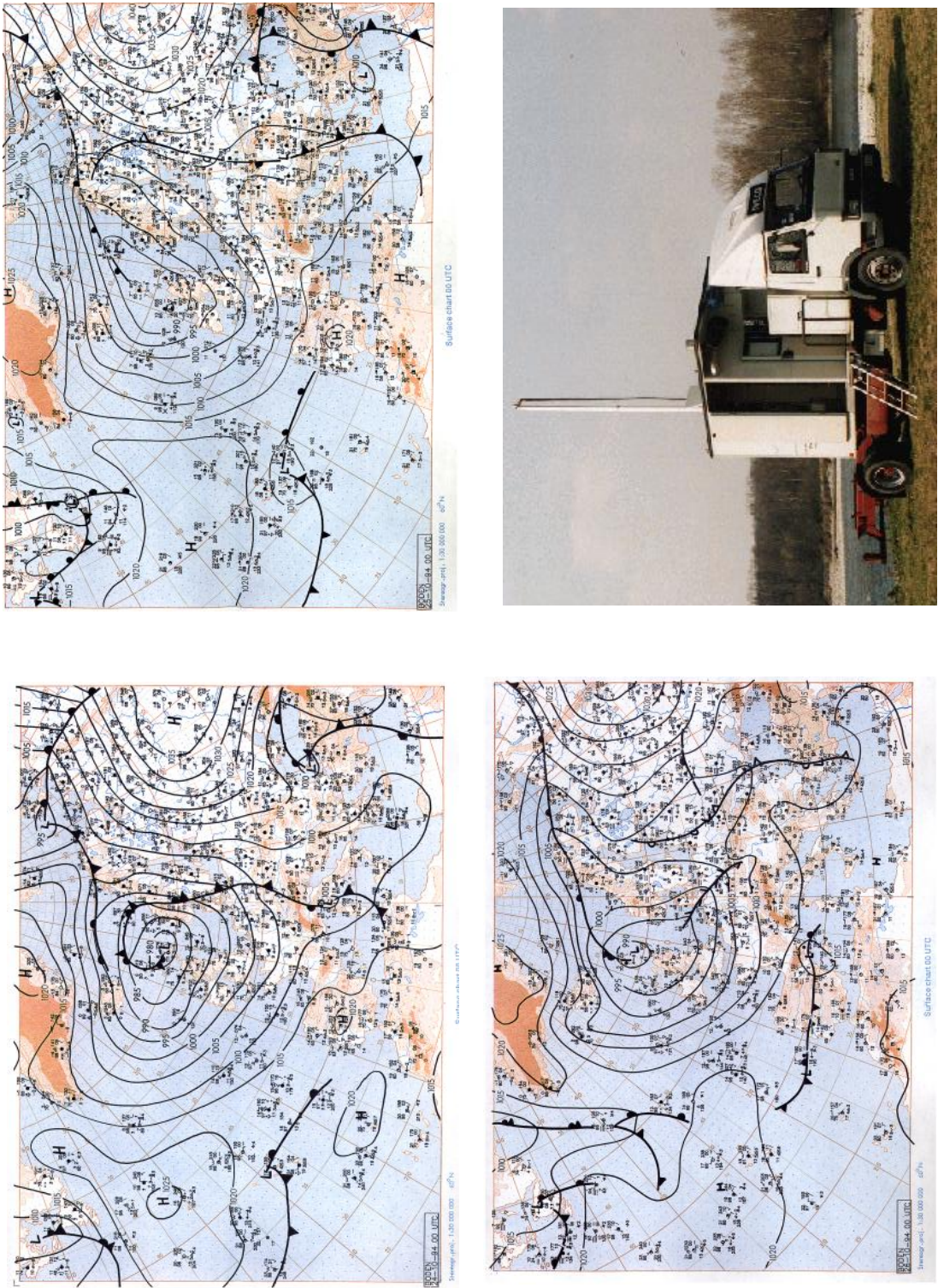
Figure 5.11 – Synoptic charts for the first ETEX release valid for 24, 25 and 26 October 1994 at 00 UTC each (from above left). The release unit is shown by the picture in the bottom right. [JRC (2004)]

5.5.3 Catch-the-plume scenario and backward simulations

The decision for the chosen sampling stations as input-data for the backward simulations was made by applying the catch-the-plume scenario. Fig. 5.9 and Fig. 5.10 have therefore to be compared to determine appropriate sampling stations which are sited at locations featuring high tracer concentration values over a period as long as possible close to the emission date. Likewise, for the sampling window of undertaken simulations using pseudo-measurements in the present study, the stations were chosen which allowed to entirely sample the collection peak inside a 48h period of 11 to 59 hours after the stop of release while being hit by the center of the plume.

	51RUNS	ETEX
start of release [UTC]	2009MMDD09	1994102316
end of release [UTC]	2009MMDD15	1994102404[1]
duration of release [h]	6	12
collection start of sampling window [UTC]	2009MM(DD+01)00	1994102418
collection stop of sampling window [UTC]	2009MM(DD+01)03	1994102615
travelling time between end of release and collection start of sampling window [h]	9	11
concentration peaks entirely sampled within sampling window	yes	yes
investigated backward timesteps for PSR analysis[2]	19,20	20,21,22,23
release site [°N;°E]	La Hague [49.68;-1.88]	Monterfil [48.03;-2.01]
4 surrounding points SW-corners of gridcells used for inverse distance weighting [°N;°E]	[50;-2],[50,-1], [49;-1],[49;-2]	[49;-3],[49,-2], [48;-2],[48;-3]
distance to nearest grid point [km]		

Table 5.6 – Differences of settings between the ETEX-1 simulations and the 51 simulations in 2009. [1]) Exact ending at 03:50 UTC. [2]) Timestep 1 is valid for the collection start of the last 3h sample in the 24h sampling window.

A total of three stations were chosen which met all these requirements. Afterwards, the backward correlation routine *locate_mult* was driven by two different measurement scenarios, consisting of two or three sampling stations respectively. Therefore, one station in Germany (D42), one station in Poland (PL08) and a third station in Denmark (DK05, additionally used as input for the scenario based on three receptor points) were selected.

In order, that the later averaged files could be written in the *ATM_SRS_ARCHIVE*, CTBTO standards had to be used, i.e. the station names had to consist of five characters. Thus, the stations were renamed to DET42, PLT08 and DKT05 in which the T stands for a general tracer substance. The spatio-temporal backward sensitivity of each of the stations was determined by starting Flexpart in backward mode via the Korn Shell script *flexbwd.ksh*. A total release of 500.000 particles during 24 October 1994 15 UTC (collection start) and 26 October 1994 15 UTC (collection stop) was dispersed 5 days backward in time from each receptor point using the Kr-85 tracer-scheme in the *RELEASES* file which was generated by the shellscript. After that, the resulting three .srm files were averaged over the sampling time using the program *srsavg* to gain receptor sensitivities for 6, 12, 24 and 48h. Next, the 3h concentration values, which had been measured by these stations, were extracted and converted from the ETEX-dataset and were manually averaged over 6, 12, 24 and 48h. The routine *locate_mult* was then driven by two multiple measurement scenarios consisting of the averaged concentration values of two and three stations respectively. Subsequently, *autopsr.ksh* was run twice (one time for each scenario) to determine localizability parameters and to plot the PSR. Since the release lasted 12h, the investigated timesteps of *aoicomp* had to be adapted. Table 5.6 lists the minor differences between the simulations of the ETEX dataset and the 51 simulations in 2009 based on pseudo-measurement scenarios. The localizability results are discussed in the following section. Model parameters and exact locations of the three stations can be found in Appendix B.2.

5.5.4 Results and Discussion

After evaluating this backtracking case-scenario based on different temporal resolutions of real measurement data, the results show that all localizability parameter values (Tab. 5.7) range in the same order of magnitude as the 51 simulations in 2009 (Tab. 5.1).

Compared to Tab. 5.1, there is an inverse trend of the distance between the AOI and the relaease point along with the temporal resolution. However it has to be remarked, that the standard deviation of the values of the 51 runs was large, which underlines the

dependence of localizability based on long-range tracer transport to the synoptic weather situation. The time-lag of the peak of correlation on the release site to the real relase time based on backward simulations shows reasonable results for sampling resolutions $\leq$ 12h.

The investigated catch-the-plume scenario consisting of two stations delivers similar localizability results as those with three stations making two stations sufficient for back-tracking a source within a weather situation, where advection rules over diffusion processes which is consistent with the conclusions of Klingberg, F.J. et al. (2011). Plots of the PSR for two and three stations for a temporal sampling resolution of 12h underline that con-clusion: The relase-point is hit by the retro-plume during the release time in both cases, whereas the PSR based on 3 stations is a bit larger than the 2 stations sampling-scenario. However, the size of AOI is almost the same in both sampling scenarios. Overall, the 12h temporal sampling resolution again shows reasonable results in terms of cost-benefit.
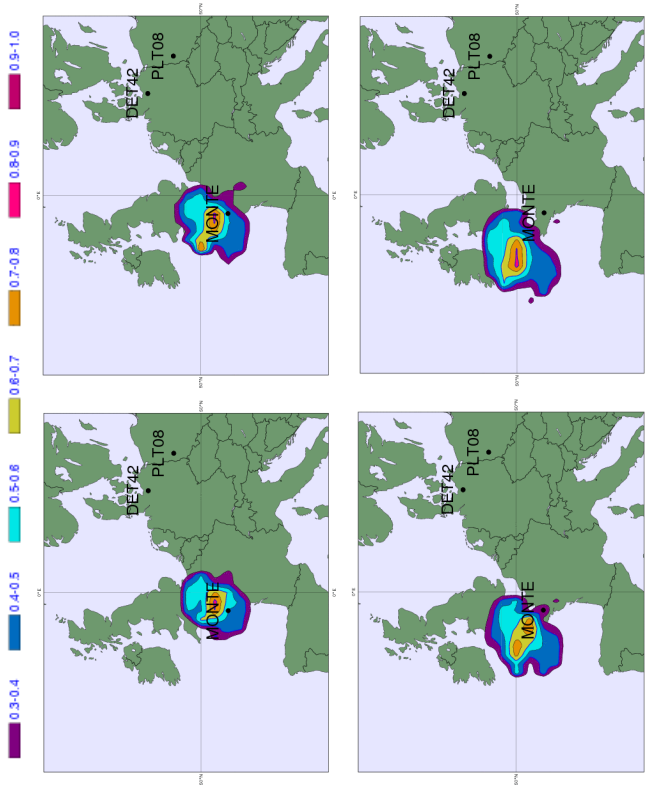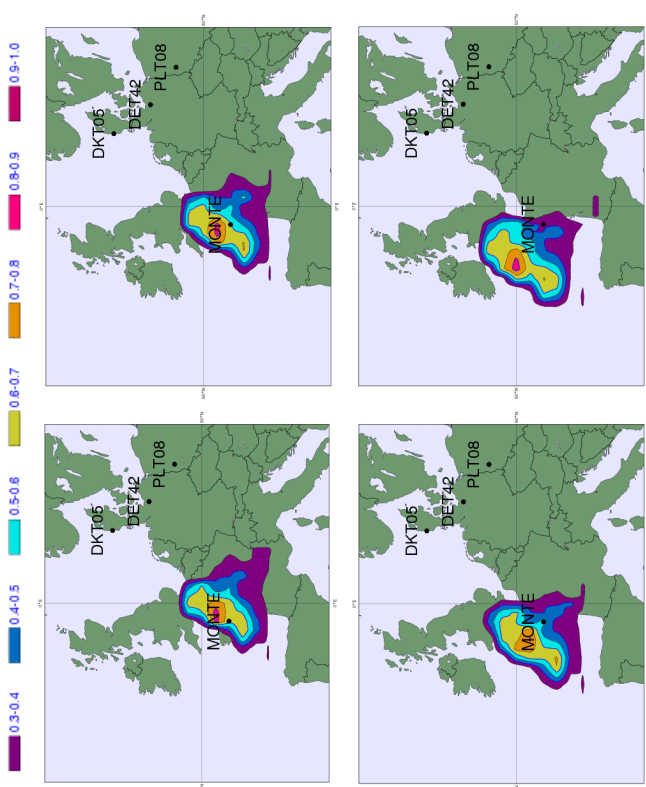
	2 stations (DET42,PLT08)						3 stations (DET42,PLT08, DKT05)				
$\triangle_t$	dist(maxcor,source)	dist(AOI,source)	cor(source)	AOI	time lag		dist(maxcor,source)	mindist(AOI,source)	cor(source)	AOI	time lag
3h	64 km	0 km	0.41	24.090 km2	-3 h		65 km	0 km	0.32	24.739 km2	-3 h
6h	168 km	0 km	0.55	40.475 km2	-3 h		65 km	0 km	0.43	65.374 km2	-3 h
12h	197 km	168 km	0.55	31.954 km2	-3 h		168 km	69 km	0.44	31.786 km2	-3 h
24h	168 km	168 km	0.44	39.488 km2	-9 h		168 km	124 km	0.44	55.713 km2	-9 h
48h	1358 km	0 km	1.00	1.820.480 km2	-6 h		304 km	0 km	0.96	1.637.342 km2	-9 h
12h	Correlation field						Correlation field				

Table 5.7 – Results on the localizability of the source localization in Monterfil using 2 (left column) resp. 3 sampling stations (right column) of the ETEX-1 dataset after applying the catch-the-plume scenario. The images represent the correlation field for a sampling duration of 12h on 1994/10/24 03 UTC, 1994/10/24 00 UTC, 1994/10/23 21 UTC and 1994/10/23 18 UTC, where MONTE is the source location and DET42, PLT08 and DKT05 mark the corresponding sampling stations.

Chapter 6

Discussion and Conclusions

Within this study, the effect of different temporal sampling resolutions on the localizability of fictitious 6h releases of the tracer substance Krypton-85 at La Hague reprocessing facility was investigated. A catch-the-plume scenario based on two sampling stations was applied about 10h after each release. The results can be generalized for any other atmospheric inert tracer substance since the radioactive noble gas Kr-85 is chemically inert, resistant to dry- and wet deposition and has a half-life of 10.76 years. The following key statements could be made:

Spatial localizability:

- samples with durations ≥48h cannot be recommended since the size of the area of Interest (AOI) gets very large and the "plateau-kind" of correlation field contains poor localization information

- 24h collection durations yield reasonable reliability results, but the AOI is still large

- a temporal sampling of 12h delivers the best localizability results in terms of cost-benefit for 1° atmospheric transport simulations

- 3h and 6h samples overall yield sharp correlation fields with minor distances between the simulated and the real tracer source, but as the sampling duration decreases, the simulated retro-plume misses the source location in some cases.

Temporal localizability:

- The temporal localizability decreases with the duration of the samples.

- In most of the runs, the release time could be reconstructed correctly within ±3h.

- Temporal localization within $\pm$6h can be achieved in around 70% of all cases almost independent of the underlying temporal sampling resolution.

Regarding 3h and 6h sampling resolution, further investigations have to be made whether increasing the spatial resolution of the model leads to improved simulation results. Therefore, the problem of "spotty" correlation fields, adressed by Klingberg, F.J. et al. (2011) when carrying out 0.5° simulations, can probably be attenuated by increasing the order of released particles by the factor 10 or more.

The validation of the method against the European Tracer Experiment(ETEX)-dataset as well as the simulations based upon 51 different synoptic situations revealed, that two sampling stations are sufficient for backtracking purposes even at great distances up to 2000km within weather situations, where advection processes dominate over diffusion, yielding sharp concentration peaks at the sampling stations. It has to be investigated further, if the use of more sampling stations can improve the results of localizability for weak-gradient flows, where diffusion rules over advection.

Within the present study, the La Hague reprocessing facility, which is situated on smoothed topography, has been chosen as the location of the fictitious emission scenarios. Nesting-methods which are featured by Flexpart, i.e. a finer output grid in the vicinity of the source, can be applied, if a tracer source is located in complex topography.

The minimum detectable source strength, which is a second criterion for the detectability of atmospheric tracer sources, was not investigated within this thesis. Herein especially for 3h and 6h temporal sampling resolutions local short-term background variability have to be considered.

Until now, traditional Kr-85 analysis methods require expensive pre-processing techniques and large sample sizes. The German Federal Office for Radio Protection (BfS) routinely collects samples to determine weekly average concentration values of Kr-85, which is far too long for obtaining reasonable localizability. The novel technology ATTA (atomic trap trace analysis), which is currently developed at the Center for Science and Peace Research at the University of Hamburg, will soon allow a radical cost reduction and simplification of sampling procedures. Shorter sampling intervals, e.g. of 6h or 12h, are expected to reduce the detection thresholds by one order of magnitude and mobile air samplers could be used (Kalinowski, M.B. (2008)). In states, which ratified the Additional Protocol of the NPT, several catch-the-plume scenarios could be applied by inspectors of the IAEA where correlation fields could be combined to yield comprehensive information of whether at a location under suspicion or even at an unknown location clandestine plu-

tonium separation has been undertaken. Since Klingberg, F.J. et al. (2011), Ross, J.O. (2010) and this thesis revealed, that depending on the synoptic situation a localization of a clandestine reprocessing activity is possible up to 2000km away from the source, this scenario can be applied outside the legal restrictions within the IAEA safeguards framework if the Kr-85 plumes of a non-cooperating country reach the borders of its territory.

There are several conventions, where environmental sample analysis of atmospheric tracer substances generally may be applied to verify compliance. Within the proposed Fissile Material Cutoff Treaty (FMCT), the investigated method might be applied to verify the ban of the production of fissile material for nuclear weapons or other nuclear explosive devices in future. Non-radioactive tracers might be sampled as well to verify compliance within the following treaties (Kalinowski, M.B. et al. (2006)):

- Convention on the Prohibition of the Development, Production, Stockpiling and Use of Chemical Weapons and on their Destruction (CWC)[1]

- Vienna Convention for the Protection of the Ozone Layer[2]

- Montreal Protocol on Substances that Deplete the Ozone Layer[3]

- Stockholm Convention on Persistent Organic Pollutants (POPs)[4]

- Basel Convention on Transboundary Movement of Hazardous Wastes[5]

The open-source LPDM Flexpart, which is already set up operationally to contribute to the verification of the CTBT, is being developed and used by an increasing number of scientific groups and can be adapted for the verification of other treaties or specific purposes. NGOs can operate Flexpart to confirm the independence of statements published by international organizations in divisive issues.

---

[1]http://www.opcw.org/chemical-weapons-convention/
[2]http://ozone.unep.org/new_site/en/vienna_convention.php
[3]http://ozone.unep.org/pdfs/Montreal-Protocol2000.pdf
[4]http://chm.pops.int/Convention/tabid/54/Default.aspx
[5]http://www.basel.int/Portals/4/Basel%20Convention/docs/text/BaselConventionText-e.pdf
Links to the respective treaties accessed on 6 Feb. 2013

Appendix A

Localizability parameter values of all runs

Run	RelStart [UTC]	RelEnd [UTC]	Flow	Stat#1	Stat#2	3h d(mcor,H) [km]	3h d(AOI,H) [km]	3h cor(Hague) [1]	3h AreaAOI [km²]	3h max(cor(Hague)) deltat [h]	3h cor [1]	6h d(mcor,H) [km]	6h d(AOI,H) [km]	6h cor(Hague) [1]	6h AreaAOI [km²]	6h max(cor(Hague)) deltat [h]	6h cor [1]
1	20090107 090000	20090107 150000	N	SPK01	SPK02	34	0	0,64	8.193	-3	0,69	34	0	0,83	16.385	0	0,83
2	20090114 090000	20090114 150000	S	UKK01	FOK01	295	139	0,31	33.092	0	0,31	190	101	0,60	40.310	0	0,60
3	20090121 090000	20090121 150000	S	UKK02	ISK01	49	49	0,32	23.426	0	0,32	49	49	0,33	38.987	0	0,33
4	20090128 090000	20090128 150000	E	UKK03	FOK01	34	0	0,80	15.895	0	0,80	34	49	0,87	47.684	0	0,87
5	20090204 090000	20090204 150000	E	ESK01	FRK01	101	49	0,27	38.815	-9	0,52	361	0	0,45	71.421	-9	0,60
6	20090211 090000	20090211 150000	N	FRK02	FRK03	134	0	0,80	40.798	0	0,80	134	0	0,80	66.659	-3	0,84
7	20090218 090000	20090218 150000	N	FRK04	FRK05	102	0	0,27	8.030	6	0,50	102	102	0,33	8.030	6	0,54
8	20090225 090000	20090225 150000	W	FRK06	ATK01	34	0	0,60	23.759	0	0,60	493	0	0,48	38.473	0	0,48
9	20090304 090000	20090304 150000	W	UKK04	FRK07	49	34	0,49	8.030	3	0,59	49	34	0,53	23.759	3	0,72
10	20090311 090000	20090311 150000	W	NLK01	DEK01	34	0	0,87	78.804	0	0,87	34	0	0,87	101.897	0	0,87
11	20090318 090000	20090318 150000	E	SPK03	ISK02	310	49	0,47	108.239	-3	0,77	310	49	0,50	124.457	-6	0,84
12	20090325 090000	20090325 150000	W	ITK01	FRK16	102	0	0,76	16.385	0	0,76	102	0	0,74	23.924	0	0,74
13	20090401 090000	20090401 150000	E	SPK04	SPK05	295	232	0,00	16.385	-9	0,57	295	232	0,00	16.385	-9	0,58
14	20090408 090000	20090408 150000	W	UKK05	SPK06	139	34	0,48	16.385	3	0,74	139	139	0,49	16.385	3	0,72
15	20090415 090000	20090415 150000	E	SPK07	SPK08	34	0	0,85	32.280	0	0,85	95	34	0,67	31.456	-3	0,70
16	20090422 090000	20090422 150000	S	UKK06	UKK07	34	0	0,85	32.280	0	0,85	34	0	0,89	32.280	0	0,89
17	20090429 090000	20090429 150000	S	UKK08	UKK09	34	0	0,71	8.030	0	0,71	34	0	0,90	15.895	0	0,90
18	20090506 090000	20090506 150000	W	DEK02	DEK03	102	0	0,67	15.895	0	0,67	102	0	0,63	23.924	0	0,63
19	20090513 090000	20090513 150000	W	SPK09	UKK10	34	0	0,81	23.924	-18	0,85	34	0	0,82	31.789	-18	0,87
20	20090520 090000	20090520 150000	W	BEK01	LUK01	95	0	0,77	48.335	-3	0,79	34	0	0,88	55.871	-3	0,90
21	20090527 090000	20090527 150000	W	DEK04	DEK05	34	0	0,89	48.340	0	0,89	34	0	0,90	39.654	0	0,90
22	20090603 090000	20090603 150000	E	SPK10	SPK11	119	49	0,02	8.030	-12	0,58	119	49	0,15	8.030	-12	0,77
23	20090610 090000	20090610 150000	W	FRK08	DEK06	95	95	0,60	15.729	-6	0,70	173	102	0,30	72.262	-9	0,67
24	20090617 090000	20090617 150000	W	NLK01	NLK02	134	0	0,91	31.458	0	0,91	173	0	0,92	47.020	0	0,92
25	20090624 090000	20090624 150000	E	SPK12	SPK13	418	310	0,00	25.059	-9	0,00	418	295	0,00	25.059	-9	0,00
26	20090701 090000	20090701 150000	E	IRK01	IRK02	361	190	0,14	49.309	0	0,14	190	190	0,37	16.060	0	0,37
27	20090708 090000	20090708 150000	W	CHK01	ATK02	165	134	0,23	50.269	-3	0,41	355	134	0,25	41.916	-3	0,48
28	20090715 090000	20090715 150000	W	NLK03	DEK07	102	102	0,51	7.865	0	0,51	102	102	0,52	15.729	0	0,68
29	20090722 090000	20090722 150000	W	NLK03	DEK08	34	0	0,78	16.223	0	0,78	34	0	0,85	32.445	0	0,85
30	20090729 090000	20090729 150000	S	DKK01	NOK01	134	0	0,55	91.321	-3	0,71	134	95	0,49	192.026	-6	0,80
31	20090805 090000	20090805 150000	N	FRK09	FRK10	34	0	0,63	8.030	0	0,63	34	0	0,66	16.223	0	0,66
32	20090812 090000	20090812 150000	W	FRK11	CHK02	134	134	0,42	16.385	0	0,42	165	165	0,30	8.193	-3	0,43
33	20090819 090000	20090819 150000	W	UKK16	NOK02	49	0	0,71	48.828	3	0,75	49	0	0,76	90.431	0	0,90
34	20090826 090000	20090826 150000	S	NOK02	NOK03	207	49	0,22	30.105	0	0,22	101	49	0,68	37.802	0	0,68
35	20090902 090000	20090902 150000	S	UKK11	DKK02	538	317	0,06	28.366	-6	0,16	538	317	0,06	86.146	-6	0,07
36	20090909 090000	20090909 150000	E	SPK14	SPK15	177	177	0,06	8.193	-9	0,70	177	177	0,37	8.193	-6	0,66
37	20090916 090000	20090916 150000	E	SPK16	SPK17	232	139	0,16	16.706	-3	0,68	360	247	0,00	58.945	-6	0,95
38	20090923 090000	20090923 150000	W	FRK12	FRK13	173	173	0,16	8.030	-15	0,64	193	173	0,25	7.865	-15	0,75
39	20090930 090000	20090930 150000	N	SPK18	ESK02	34	0	0,70	16.060	-6	0,74	34	0	0,73	16.060	-6	0,76
40	20091007 090000	20091007 150000	E	FRK09	FRK14	134	0	0,55	55.543	9	0,59	177	0	0,74	72.089	6	0,74
41	20091014 090000	20091014 150000	E	SPK19	SPK20	34	0	0,64	8.030	0	0,64	34	0	0,62	8.030	0	0,62
42	20091021 090000	20091021 150000	S	UKK12	SPK21	49	49	0,10	16.060	-3	0,38	119	49	0,02	23.924	-6	0,46
43	20091028 090000	20091028 150000	S	UKK13	UKK14	95	0	0,59	15.895	-3	0,74	95	0	0,67	15.895	-3	0,79
44	20091104 090000	20091104 150000	W	NLK03	DEK09	49	0	0,69	16.060	0	0,69	34	101	0,76	31.954	0	0,76
45	20091111 090000	20091111 150000	W	UKK12	UKK15	384	208	0,16	189.850	-6	0,17	510	101	0,15	258.094	-9	0,59
46	20091118 090000	20091118 150000	W	PLK01	PLK02	173	0	0,70	24.090	0	0,70	173	34	0,73	23.594	6	0,73
47	20091125 090000	20091125 150000	W	SEK01	LTK01	134	95	0,64	55.713	-3	0,73	134	95	0,73	62.581	0	0,73
48	20091202 090000	20091202 150000	S	SPK22	SPK23	225	225	0,05	7.527	-6	0,45	225	225	0,07	7.527	-6	0,53
49	20091209 090000	20091209 150000	W	BEK02	DEK10	95	0	0,87	15.895	0	0,87	101	0	0,91	55.713	0	0,91
50	20091216 090000	20091216 150000	W	BEK03	FRK15	134	49	0,19	8.193	-12	0,38	134	49	0,21	8.193	-12	0,42
51	20091223 090000	20091223 150000	S	UKK11	UKK03	34	0	0,76	31.456	0	0,76	34	0	0,81	23.759	0	0,81

Localizability results per run. Three evaluation windows (12h, 24h, 48h), each reporting Spatial Localizability (d(mcor,H), d(AOI,H), cor(Hague), AreaAOI) and Temporal Localizability (max(cor(Hague)): deltat, cor). Columns are given in the order they appear in the source sheet.

Run	12h d(mcor,H) [km]	12h d(AOI,H) [km]	12h cor(Hague) [1]	12h AreaAOI [km²]	12h deltat [h]	12h cor [1]	24h d(mcor,H) [km]	24h deltat [h]	24h cor [1]	24h AreaAOI [km²]	24h cor(Hague) [1]	24h d(AOI,H) [km]	48h cor(Hague) [1]	48h d(mcor,H) [km]	48h d(AOI,H) [km]	48h cor(Hague) [1] (2)	48h AreaAOI [km²]	48h deltat [h]	48h cor [1]
1	33,98	0	0,84	32.931	0	0,84	34	0	0,84	41.124	0,85	0	0,85	1076	0	0,90	734.417	-24	1,00
2	231,79	34	0,63	87.492	0	0,63	232	0	0,63	87.492	0,63	34	0,63	4703	34	0,62	3.739.171	3	0,91
3	538,25	0	0,86	636.522	0	0,86	538	0	0,86	841.744	0,85	0	0,85	606	34	0,73	3.148.487	3	0,73
4	33,98	0	0,90	88.968	0	0,90	34	0	0,90	139.720	0,87	0	0,87	2732	95	0,00	5.062.928	-9	1,00
5	713	49	0,39	55.859	-9	0,51	877	-9	0,51	54.379	0,52	165	0,78	1600	49	0,00	3.205.324	6	1,00
6	134,25	0	0,90	155.622	0	0,90	134	0	0,90	245.959	0,96	0	0,96	530	134	0,00	1.587.204	-6	1,00
7	101,59	102	0,22	8.030	9	0,53	403	9	0,53	239.409	0,83	0	0,83	262	0	0,83	356.014	6	0,83
8	118,6	0	0,76	109.745	0	0,76	384	0	0,76	137.477	0,75	0	0,75	481	119	0,00	1.452.902	9	0,90
9	33,98	0	0,80	71.771	0	0,80	95	0	0,80	151.381	0,86	0	0,86	270	0	0,83	947.689	3	1,00
10	326,28	0	0,95	117.456	-15	0,95	263	-15	0,95	140.714	0,93	0	0,95	1102	0	0,00	1.018.400	-9	1,00
11	360,41	49	0,54	2.039.967	-6	0,95	796	-6	0,95	2.164.839	0,33	49	0,96	1420	49	0,00	2.741.074	-9	1,00
12	101,59	0	0,94	156.729	-3	0,96	102	-3	0,96	292.177	0,94	0	0,98	570	0	1,00	1.028.114	-6	1,00
13	294,75	190	0,00	32.445	-9	0,65	493	-9	0,65	8.511	0,00	262	0,25	3349	190	0,00	2.006.630	-21	1,00
14	176,63	0	0,84	92.185	0	0,84	177	0	0,84	91.706	0,82	0	0,82	1689	49	0,00	1.807.010	-6	1,00
15	95,23	95	0,56	95.525	-21	0,68	622	-21	0,68	39.323	0,38	95	0,65	737	95	0,00	479.425	-21	1,00
16	33,98	0	0,89	32.280	0	0,89	34	0	0,89	96.998	0,96	0	0,96	360	0	1,00	810.606	-6	1,00
17	33,98	0	0,97	39.819	0	0,97	34	0	0,97	140.525	0,96	0	0,96	2866	0	0,80	2.246.489	-12	0,90
18	134,32	0	0,78	39.654	-3	0,85	173	-3	0,85	112.734	0,86	0	0,97	2014	0	0,80	2.847.212	-3	1,00
19	33,98	0	0,88	31.789	-18	0,91	49	-18	0,91	63.906	0,98	0	0,99	2789	0	0,00	1.905.552	3	1,00
20	134,25	0	0,96	129.726	-3	0,97	134	-3	0,97	114.020	0,93	0	0,95	628	49	1,00	807.635	-9	1,00
21	172,91	0	0,96	253.252	0	0,96	328	0	0,96	549.205	0,94	0	0,94	139	0	1,00	1.561.886	0	1,00
22	190,12	119	0,00	47.679	-12	0,59	119	-12	0,59	39.819	0,11	49	0,82	49	0	0,00	479.146	-3	1,00
23	33,98	0	0,92	31.624	0	0,92	173	0	0,92	264.146	0,97	0	0,97	481	0	1,00	434.792	0	1,00
24	274,44	0	0,91	76.952	0	0,91	317	0	0,91	107.400	0,87	0	0,87	134	0	1,00	1.071.344	-9	1,00
25	417,76	310	0,00	25.059	-9	0,00	295	-9	0,00	83.836	0,00	295	0,00	1199	295	0,00	461.936	-9	0,00
26	33,98	0	0,67	15.729	-3	0,74	361	-3	0,74	128.935	0,19	147	0,19	1841	95	0,00	978.397	-9	0,00
27	165,45	134	0,13	41.916	-3	0,52	165	-3	0,52	108.896	0,07	134	0,48	1841	95	0,00	978.397	0	0,00
28	258,07	102	0,17	31.123	-9	0,54	247	-9	0,54	23.915	0,56	193	0,88	1337	0	1,00	894.949	3	1,00
29	33,98	0	0,84	40.961	0	0,84	370	0	0,84	132.162	0,88	0	0,91	1872	34	0,71	845.806	9	1,00
30	313,17	95	0,72	275.304	-3	0,98	393	-3	0,98	398.263	0,22	134	0,94	165	95	0,00	1.843.248	-6	1,00
31	33,98	0	0,82	48.991	-12	0,82	218	-12	0,82	219.508	0,91	0	0,91	1246	0	1,00	961.713	-6	1,00
32	165,45	34	0,62	24.415	-3	0,67	134	-3	0,67	41.445	0,52	134	0,52	348	0	1,00	552.685	6	1,00
33	270,4	0	0,90	173.777	6	0,99	270	6	0,99	774.971	0,89	0	0,99	1507	0	0,83	1.466.243	-9	1,00
34	134,25	0	0,97	116.613	0	0,97	134	0	0,97	211.339	0,95	0	0,95	1994	0	1,00	1.254.070	-9	1,00
35	538,25	0	0,87	177.961	0	0,87	538	0	0,87	375.306	0,92	0	0,92	190	0	1,00	1.326.408	0	1,00
36	231,79	49	0,44	25.057	-3	0,56	139	-3	0,56	100.861	0,42	134	0,82	690	134	0,00	723.579	-12	1,00
37	190,12	119	0,46	154.531	-12	0,91	101	-12	0,91	129.909	0,94	0	0,96	445	0	1,00	726.317	-3	1,00
38	192,93	173	0,22	23.924	-15	0,79	173	-15	0,79	47.684	0,85	0	0,98	34	0	0,80	365.562	-9	1,00
39	138,9	0	0,78	32.445	-12	0,97	49	-12	0,97	139.850	0,80	0	0,97	139	34	0,73	604.320	-12	1,00
40	176,63	0	0,88	198.516	-9	0,89	34	-9	0,89	1.164.083	0,87	0	0,89	2651	0	1,00	1.504.333	-9	1,00
41	33,98	0	0,79	24.090	0	0,79	49	0	0,79	88.324	0,78	0	0,78	119	0	0,80	452.059	-9	1,00
42	101,45	49	0,40	31.118	-6	0,56	247	-6	0,56	150.608	0,87	0	0,95	606	49	0,00	769.298	-21	1,00
43	49	0	0,75	16.060	3	0,82	95	3	0,82	47.185	0,64	95	0,81	2220	0	1,00	615.979	-6	1,00
44	33,98	0	0,85	63.077	0	0,85	262	0	0,85	223.619	0,83	0	0,96	262	0	1,00	1.229.646	6	1,00
45	509,61	101	0,24	337.233	-15	0,92	805	-15	0,92	871.382	0,13	101	0,89	1246	101	0,00	1.509.015	-15	0,73
46	388,69	173	0,35	39.155	-3	0,47	245	-3	0,47	168.418	0,72	102	0,72	801	134	0,00	556.264	-9	0,00
47	134,32	0	0,84	93.704	-3	0,89	101	-3	0,89	349.111	0,99	0	0,99	1773	95	0,71	1.900.684	-9	0,00
48	224,84	225	0,38	7.697	-6	0,71	34	-6	0,71	31.617	0,83	0	0,87	369	34	0,00	918.274	-9	1,00
49	190,12	0	0,90	87.668	0	0,90	510	0	0,90	110.584	0,86	0	0,86	263	101	0,00	1.075.220	-12	1,00
50	134,25	49	0,21	102.201	3	0,60	101	3	0,60	162.683	0,40	49	0,84	357	49	0,00	1.232.640	6	1,00
51	101,45	0	0,98	109.587	0	0,98	190	0	0,98	308.916	0,98	0	0,98	539	0	1,00	857.178	-9	1,00

Appendix B

Receptor points

B.1   List of receptor points used in the 51 simulations

Name	Lon[°]	Lat[°]	Country	Location	Usage	Distance to source [km]
ATK01	14	48	Austria	Vorchdorf	1	1176
ATK02	10	47	Austria	Gaschurn	1	927
BEK01	5	51	Belgium	Diest	1	510
BEK02	4	51	Belgium	Dendermonde	1	443
BEK03	3	51	Belgium	Roeselare	1	376
CHK01	7	47	Switzerland	Neuchâtel	1	721
CHK02	8	47	Switzerland	Luzern	1	789
DEK01	11	53	Germany	Dannenberg	1	967
DEK02	6	51	Germany	Heinsberg	1	579
DEK03	12	52	Germany	Zerbst	1	1008
DEK04	9	51	Germany	Marburg	1	786
DEK05	14	51	Germany	Dresden	1	1136
DEK06	11	48	Germany	Landsberg	1	961
DEK07	8	52	Germany	Münster	1	740
DEK08	10	54	Germany	Neumünster	1	946
DEK09	9	54	Germany	Trennewurth	1	888
DEK10	7	51	Germany	Köln	1	647

DKK01	9	56	Denmark	Herning	1	1013
DKK02	10	57	Denmark	Aalborg	1	1132
ESK01	-9	43	Spain	Lake Fervenza	1	922
ESK02	-3	43	Spain	Bilbao	1	749
FOK01	-7	62	Faroe Islands	Koltur	2	1407
FRK01	-4	48	France	Quimper	1	243
FRK02	3	46	France	Alès	1	548
FRK03	4	44	France	Clermont-Ferrand	1	774
FRK04	-1	49	France	Torigni-sur-Vire	1	99
FRK05	0	49	France	Saint-Pierre-Sur-Dives	1	156
FRK06	4	50	France	Hirson	1	424
FRK07	3	50	France	Péronne	1	352
FRK08	6	48	France	Êpinal	1	607
FRK09	-2	47	France	Bouin	2	298
FRK10	0	44	France	Gabarret	1	648
FRK11	6	47	France	Besançon	1	655
FRK12	0	48	France	Le Mans	1	232
FRK13	-1	47	France	Cholet	1	305
FRK14	-4	48	France	Quimper	1	243
FRK15	3	50	France	Combles	1	352
FRK16	6	44	France	Château-Amoux-Saint-Auban	1	871
IRK01	-8	52	Ireland	Midleton	1	502
IRK02	-7	53	Ireland	Athy	1	513
ISK01	-18	64	Iceland	Kalfafell	1	1860
ISK02	-22	64	Iceland	Reykjavik	1	1992
ITK01	7	45	Italy	Torino	1	848
LTK01	21	56	Lithuania	Klaipėda	1	1681
LUK01	6	50	Luxembourg	Enscherange	1	567
NLK01	5	52	The Netherlands	Utrecht	2	548
NLK02	6	53	The Netherlands	Heerenveen	1	660
NLK03	7	53	The Netherlands	Stadskanaal	3	719

NOK01	6	59	Norway	Stavanger	1	1155
NOK02	7	58	Norway	Kristiansand	2	1093
NOK03	9	60	Norway	Veggli	1	1340
PLK01	16	52	Poland	Wolsztyn	1	1280
PLK02	20	52	Poland	Łódź	1	1554
SEK01	15	55	Sweden	Bornholm	1	1287
SPK01	-8	46	Ship	Ship1	1	614
SPK02	-12	47	Ship	Ship 2	1	805
SPK03	-20	60	Ship	Ship 3	1	1624
SPK04	-8	45	Ship	Ship 4	1	696
SPK05	-6	44	Ship	Ship 5	1	706
SPK06	2	60	Ship	Ship 6	1	1175
SPK07	-6	50	Ship	Ship 7	1	298
SPK08	-10	50	Ship	Ship 8	1	584
SPK09	-3	50	Ship	Ship 9	1	88
SPK10	-7	49	Ship	Ship 10	1	379
SPK11	-10	49	Ship	Ship 11	1	594
SPK12	-12	50	Ship	Ship 12	1	727
SPK13	-15	52	Ship	Ship13	1	956
SPK14	-9	44	Ship	Ship 14	1	832
SPK15	-11	44	Ship	Ship 15	1	938
SPK16	-11	43	Ship	Ship 16	1	1020
SPK17	-12	42	Ship	Ship 17	1	1159
SPK18	-3	47	Ship	Ship 18	1	310
SPK19	-8	49	Ship	Ship 19	1	450
SPK20	-10	49	Ship	Ship 20	1	594
SPK21	-10	56	Ship	Ship 21	1	889
SPK22	1	54	Ship	Ship 22	1	520
SPK23	2	55	Ship	Ship 23	1	648
UKK01	-3	57	United Kingdom	Ballater	1	818
UKK02	-3	59	United Kingdom	Kirkwall	1	1040
UKK03	-4	51	United Kingdom	Barnstaple	2	210
UKK04	1	51	United Kingdom	St. Mary's Bay	1	252

UKK05	1	52	United Kingdom	Ipswich	1	328
UKK06	-2	51	United Kingdom	Salisbury	1	147
UKK07	-2	53	United Kingdom	Stoke-on-Trent	1	370
UKK08	0	52	United Kingdom	Cambridge	1	290
UKK09	0	53	United Kingdom	Boston	1	392
UKK10	0	51	United Kingdom	Newik	1	199
UKK11	-1	54	United Kingdom	York	2	485
UKK12	-7	55	United Kingdom	Limavady	2	687
UKK13	-3	52	United Kingdom	Hereford	1	270
UKK14	-5	55	United Kingdom	Loch Ryan	1	629
UKK15	-6	56	United Kingdom	Jura	1	756
UKK16	1	53	United Kingdom	Norwich	1	420

B.2 List of receptor points used for the validation against the ETEX-1 dataset

Name	Lon[°]	Lat[°]	Country	Location	Usage	Distance to source [km]
DET42	11.34	53.65	Germany	-	1	1123
PLK08	15.53	51.93	Poland	-	1	1323
DKT05	8.13	65.00	Denmark	-	1	1122

Appendix C

Model settings

In this chapter, settings used for the Flexpart simulations are listed. Please consult Stohl et al. (2005) to get the meaning of the parameters.

Listing C.1 – Flexpart OUTGRID file of forward and backward-simulations for all simulations.

```
1  *******************************************************************************
2  *                                                                             *
3  *       Input file for the Lagrangian particle dispersion model FLEXPART      *
4  *                       Please specify your output grid                       *
5  *                                                                             *
6  *******************************************************************************
7
8  1.    ------.----        4X,F11.4
9          -179.0000        GEOGRAFICAL LONGITUDE OF LOWER LEFT CORNER OF OUTPUT GRID
10     OUTLONLEFT          (left boundary of the first grid cell - not its centre)
11
12 2.    ------.----        4X,F11.4
13          -90.0000        GEOGRAFICAL LATITUDE OF LOWER LEFT CORNER OF OUTPUT GRID
14     OUTLATLOWER         (lower boundary of the first grid cell - not its centre)
15
16 3.    -----              4X,I5
17          359            NUMBER OF GRID CELLS IN X DIRECTION
18     NUMXGRID
19
20 4.    -----              4X,I5
21          180            NUMBER OF GRID CELLS IN Y DIRECTION
22     NUMYGRID
23
24 5.    ------.---         4X,F10.3
25          1.000          GRID DISTANCE IN X DIRECTION
26     DXOUTLON
27
28 6.    ------.---         4X,F10.3
29          1.000          GRID DISTANCE IN Y DIRECTION
```

```
30      DYOUTLAT
31
32  8.   -----.-              4X, F7.1
33       150.0
34      LEVEL 2              HEIGHT OF LEVEL (UPPER BOUNDARY)
35
36  9.   -----.-              4X, F7.1
37      10000.0
38      LEVEL 3              HEIGHT OF LEVEL (UPPER BOUNDARY)
```

C.1 Flexpart forward simulations

Listing C.2 – COMMAND file of forward simulation #46 (run46).

```
1  +++++++++++++ HEADER ++++++++++++++++
2  +++++++++++++ HEADER ++++++++++++++++
3  +++++++++++++ HEADER ++++++++++++++++
4  +++++++++++++ HEADER ++++++++++++++++
5  +++++++++++++ HEADER ++++++++++++++++
6  +++++++++++++ HEADER ++++++++++++++++
7  +++++++++++++ HEADER ++++++++++++++++
8  1
9  20091118 090000
10 20091125 090000
11 10800
12 10800
13     900
14  99999999
15 900    SYNC
16 -5.0   CTL
17 4      IFINE
18 1      IOUT
19 2      IPOUT
20 1      LSUBGRID
21 1      LCONVECTION
22 0      LAGESPECTRA
23 0      IPIN
24 1      IOFR
25 0      IFLUX
26 0      MDOMAINFILL
27 1      IND_SOURCE
28 1      IND_RECEPTOR
29 0      MQUASILAG
30 0      NESTED_OUTPUT
31 0      LINIT_COND         INITIAL COND. FOR BW RUNS: 0=NO,1=MASS UNIT,2=MASS MIXING RATIO
        UNIT
```

Listing C.3 – RELEASES file of forward simulation #46 (run46).

```
 1  *
 2  *
 3  *
 4  *
 5  *
 6  *
 7  *
 8  *
 9  *
10  ***************************************************************************
11  +++++++++++++++++++++++++++++++++++++++++++++++++++++++++++++++++++++++++++
12  1                          Total number of species emitted
13  19                         Index of species in file SPECIES
14  ==========================================================================
15  20091118 090000
16  20091118 150000
17     -1.8800
18     49.6800
19     -1.8800
20     49.6800
21   1
22       8.0
23      12.0
24  500000
25  3.20000e+12
26  HAGUE
27  +++++++++++++++++++++++++++++++++++++++++++++++++++++++++++++++++++++++++++
```

C.2   Flexpart backward simulations

Listing C.4 – COMMAND file of a backward simulation within run 46 (yielding the SRS-fields for 8 of 16 samples for the station PLK01).

```
 1  +++++++++++++ HEADER ++++++++++++++++
 2  +++++++++++++ HEADER ++++++++++++++++
 3  +++++++++++++ HEADER ++++++++++++++++
 4  +++++++++++++ HEADER ++++++++++++++++
 5  +++++++++++++ HEADER ++++++++++++++++
 6  +++++++++++++ HEADER ++++++++++++++++
 7  +++++++++++++ HEADER ++++++++++++++++
 8  -1
 9  20091116 000000
10  20091121 000000
11  10800
12  10800
13     900
14   99999999
15  900    SYNC
```

```
16  -5.0   CTL
17  4       IFINE
18  1       IOUT
19  2       IPOUT
20  1       LSUBGRID
21  1       LCONVECTION
22  0       LAGESPECTRA
23  0       IPIN
24  1       IOFR
25  0       IFLUX
26  0       MDOMAINFILL
27  1       IND_SOURCE
28  1       IND_RECEPTOR
29  0       MQUASILAG
30  0       NESTED_OUTPUT
31  0       LINIT_COND          INITIAL COND. FOR BW RUNS: 0=NO,1=MASS UNIT,2=MASS MIXING RATIO
            UNIT
```

Listing C.5 – RELEASES file of a backward simulation within run 46 (yielding the SRS-fields for 8 of 16 samples for the station PLK02).

```
1   *
2   *
3   *
4   *
5   *
6   *
7   *
8   *
9   *
10  ************************************************************************
11  ++++++++++++++++++++++++++++++++++++++++++++++++++++++++++++++++++++++++
12  1                        Total number of species emitted
13  19                       Index of species in file SPECIES
14  ======================================================================
15  20091120 000000
16  20091120 030000
17     20.00
18     52.00
19     20.00
20     52.00
21   1
22      8.0
23     12.0
24  500000
25  1.00000e+12
26  PLK02
27  ++++++++++++++++++++++++++++++++++++++++++++++++++++++++++++++++++++++++
28  20091120 030000
29  20091120 060000
30     20.00
31     52.00
```

```
32      20.00
33      52.00
34   1
35        8.0
36      12.0
37  500000
38  1.00000e+12
39  PLK02
40  +++++++++++++++++++++++++++++++++++++++++++++++++++++++++++++++++++++++
41  20091120 060000
42  20091120 090000
43      20.00
44      52.00
45      20.00
46      52.00
47   1
48        8.0
49      12.0
50  500000
51  1.00000e+12
52  PLK02
53  +++++++++++++++++++++++++++++++++++++++++++++++++++++++++++++++++++++++
54  20091120 090000
55  20091120 120000
56      20.00
57      52.00
58      20.00
59      52.00
60   1
61        8.0
62      12.0
63  500000
64  1.00000e+12
65  PLK02
66  +++++++++++++++++++++++++++++++++++++++++++++++++++++++++++++++++++++++
67  20091120 120000
68  20091120 150000
69      20.00
70      52.00
71      20.00
72      52.00
73   1
74        8.0
75      12.0
76  500000
77  1.00000e+12
78  PLK02
79  +++++++++++++++++++++++++++++++++++++++++++++++++++++++++++++++++++++++
80  20091120 150000
81  20091120 180000
82      20.00
83      52.00
```

```
 84      20.00
 85      52.00
 86   1
 87       8.0
 88      12.0
 89  500000
 90  1.00000e+12
 91  PLK02
 92  +++++++++++++++++++++++++++++++++++++++++++++++++++++++++++++++++++++++
 93  20091120  180000
 94  20091120  210000
 95      20.00
 96      52.00
 97      20.00
 98      52.00
 99   1
100       8.0
101      12.0
102  500000
103  1.00000e+12
104  PLK02
105  +++++++++++++++++++++++++++++++++++++++++++++++++++++++++++++++++++++++
106  20091120  210000
107  20091121  000000
108      20.00
109      52.00
110      20.00
111      52.00
112   1
113       8.0
114      12.0
115  500000
116  1.00000e+12
117  PLK02
118  +++++++++++++++++++++++++++++++++++++++++++++++++++++++++++++++++++++++
```

Appendix D

File formats and configuration files

D.1 Format of concentration (.con) file

Listing D.1 – First 27 lines of a concentration (.con) file. See CTBTO/IDC (2009) for further explanations.

```
 1  STAT |COL START    | COL STOP     | Kr -85
 2  aaaaa -------- ------ -------- ------
 3  Collection stop Day: 20091118
 4  Collection stop Day: 20091119
 5  PLK01 20091118 120000 20091119 000000 .586E+02
 6  PLK01 20091119 000000 20091119 120000 .119E+05
 7  PLK01 20091118 120000 20091119 000000 .586E+02
 8  PLK01 20091119 000000 20091119 120000 .119E+05
 9  PLK01 20091118 180000 20091119 000000 .117E+03
10  PLK01 20091119 000000 20091119 060000 .806E+04
11  PLK01 20091119 060000 20091119 120000 .157E+05
12  PLK01 20091119 120000 20091119 180000 .222E+03
13  PLK01 20091118 180000 20091119 000000 .117E+03
14  PLK01 20091119 000000 20091119 060000 .806E+04
15  PLK01 20091119 060000 20091119 120000 .157E+05
16  PLK01 20091119 120000 20091119 180000 .222E+03
17  PLK01 20091118 180000 20091119 000000 .117E+03
18  PLK01 20091119 000000 20091119 060000 .806E+04
19  PLK01 20091119 060000 20091119 120000 .157E+05
20  PLK01 20091119 120000 20091119 180000 .222E+03
21  PLK01 20091118 180000 20091119 000000 .117E+03
22  PLK01 20091119 000000 20091119 060000 .806E+04
23  PLK01 20091119 060000 20091119 120000 .157E+05
24  PLK01 20091119 120000 20091119 180000 .222E+03
25  PLK01 20091118 210000 20091119 000000 .234E+03
26  PLK01 20091119 000000 20091119 030000 .568E+04
27  PLK01 20091119 030000 20091119 060000 .104E+05
```

D.2 Format of gard.dat file

Listing D.2 – A gard.dat file generated by routine stations. See CTBTO/IDC (2009) for further explanations.

```
 1     3
 2    16.0000  52.0000 PLK01 0000           -999.9 -9.9E+09 -9.99  48.0 PLK01
 3    20.0000  52.0000 PLK02 0000           -999.9 -9.9E+09 -9.99  48.0 PLK02
 4    -1.8800  49.6800 HAGUE 0000           -999.9 -9.9E+09 -9.99  48.0 La Hague
```

D.3 Control file of routine locate_multi

Listing D.3 – CONTROL file of routine locate_multi

```
 1 # SRS File archive
 2 /daten3/gewot_data/hamburg_projekt/flex/flexpart82-3-Std_1010bwd/output2/ATM_SRS_ARCHIVE
 3 flex.06hrs
 4 #
 5 # Species measured
 6 #
 7 1                     !  Number of species
 8 TRACER     -1.0       !Ideal tracer substance, no decay + no deposition
 9 #
10 # Scenario/Measurements
11 #
12 16                    ! Number of measurements
13 PLK01 20091119 06    .806E+04
14 PLK01 20091119 12    .157E+05
15 PLK01 20091119 18    .222E+03
16 PLK01 20091120 00    .000E+00
17 PLK01 20091120 06    .000E+00
18 PLK01 20091120 12    .000E+00
19 PLK01 20091120 18    .000E+00
20 PLK01 20091121 00    .000E+00
21 PLK02 20091119 06    .729E+03
22 PLK02 20091119 12    .511E+04
23 PLK02 20091119 18    .125E+05
24 PLK02 20091120 00    .122E+03
25 PLK02 20091120 06    .805E+01
26 PLK02 20091120 12    .000E+00
27 PLK02 20091120 18    .000E+00
28 PLK02 20091121 00    .000E+00
29
30 +++++++++++++++++++++++++++
```

D.4   File format of correlation.txt file

Listing D.4 – First 30 lines of correlation.txt output file of routine locate_multi for run 46.

```
 1   -99.90 -99.90 20091121 00 20091112 03 0.20E+13   213   3   3 1.00 1.00 "CORRELATION␣MAP"
 2    2
 3    16.00   52.00
 4    20.00   52.00
 5   50.00    13.00     2 -0.1966762E-01
 6   51.00    13.00     2 -0.1966761E-01
 7   52.00    13.00     2 -0.1966761E-01
 8   50.00    14.00     2 -0.1966761E-01
 9   51.00    14.00     2 -0.1966762E-01
10   52.00    14.00     2 -0.1966762E-01
11   50.00    15.00     2 -0.1966762E-01
12   51.00    15.00     2 -0.1966761E-01
13   52.00    15.00     2 -0.1966762E-01
14   52.00    16.00     2 -0.1966762E-01
15   50.00    17.00     2 -0.1966762E-01
16   51.00    17.00     2 -0.1966762E-01
17   50.00    18.00     2 -0.1966762E-01
18   51.00    18.00     2 -0.1966762E-01
19   52.00    18.00     2 -0.1966762E-01
20   50.00    19.00     2 -0.1966762E-01
21   51.00    19.00     2 -0.1966762E-01
22   52.00    19.00     2 -0.1966762E-01
23   50.00    20.00     2 -0.1966762E-01
24   51.00    20.00     2 -0.1966762E-01
25   52.00    20.00     2 -0.1966762E-01
26   50.00    11.00     3 -0.1966760E-01
27   51.00    11.00     3 -0.1966762E-01
28   49.00    12.00     3 -0.1966762E-01
29   50.00    12.00     3 -0.1966762E-01
30   51.00    12.00     3 -0.1966762E-01
```

Bibliography

Ahlswede, J., Hebel, S., Kalinowski, M.B., and Ross, O. (2009). Update of the global krypton-85 emission inventory. *Occasional paper*, 9.

Ahlswede, J., Hebel, S., Ross, J.O., Schoetter, R., and Kalinowski, M.B. (2013). Update and improvement of the global krypton-85 emission inventory. *Journal of Environmental Radioactivity*, 115:34–42.

Becker, A., Wotawa, G., De Geer, L.E., Seibert, P., Draxler, R.R., Sloan, C., D'Amours, R., Hort, M., Glaab, H., Heinrich, P., Grillon, Y., Shershakov, V., Katayama, K., Zhang, Y., Stewart, P., Hirtl, M., Jean, M., and Chen, P. (2007). Global backtracking of anthropogenic radionuclides by means of a receptor oriented ensemble dispersion modelling system in support of Nuclear-Test-Ban Treaty verification. *Atmospheric Environment*, 41(21):4520–4534.

Bergmann, L. and Schäfer, C. (1998). *Lehrbuch der Experimentalphysik: Erde und Planeten*, volume 7. Walter de Gruyter.

Connan, O., Smith, K., Solier, L., Maro, D., Hébert, D., and Bacon, G. (2011). Mesoscale dispersion of 85Kr in the vicinity of the AREVA La Hague reprocessing plant. *Radioprotection*, 46(6):423–429.

Cook, P.G. and Solomon, D.K. (1995). Transport of Atmospheric Trace Gases to the Water Table: Implications for Groundwater Dating with Chlorofluorocarbons and Krypton 85. *Water Resources Research*, 31(2):263–270.

CTBTO (2005). Verification science: A new tool for NDC analysis of atmospheric transport calculations. *CTBTO Spectrum Newsletter*, 7:19 & 24. URL: `http://www.ctbto.org/fileadmin/content/reference/outreach/spectrum_issues_singles/ctbto_spectrum_7/p19.pdf` (Accessed on 10 Dec.2012).

CTBTO (2009). On-site inspections the ultimate verification measure. Comprehensive Nuclear-Test-Ban Treaty Organization. URL: http://www.ctbto.org/fileadmin/user_upload/public_information/2009/osi_the_ultimate_verification_measure-web.pdf (Accessed on 3 Jan.2013).

CTBTO (2012). Verification Regime. Comprehensive Nuclear-Test-Ban Treaty Organization. URL: http://www.ctbto.org/verification-regime (Accessed on 30 Oct.2012).

CTBTO/IDC (2008). WEB-Grape 1.3 Software User Tutorial. Technical report, International Data Centre of the Comprehensive Nuclear-Test-Ban Treaty Organization.

CTBTO/IDC (2009). CTBTO_WMO_SEA Software Requirements Specification. Technical report, International Data Centre of the Comprehensive Nuclear-Test-Ban Treaty Organization.

Daerr, H., Kalinowski, M., Kohler, M., and Sahling, P. (2010). Ultra-Trace Analysis of Krypton-85. Report IAEA-CN-184/37.

Eckermann, K. and Ryman, J.J. (1993). Federal Guidance Report No. 12: External exposure to radionuclides in air, water, and soil. Technical report, Oak Ridge National Laboratory and US Environmental Protection Agency. URL: http://www.epa.gov/rpdweb00/docs/federal/402-r-93-081.pdf (Accessed on 30 Oct.2012).

Fréchou, C. and Calmet, D. (2003). 129I in the environment of the La Hague nuclear fuel reprocessing plant - from sea to land. *Journal of Environmental Radioactivity*, 70(1-2):43–59.

Goeber, M. and Wilson, C. (2012). Why, when a model resolution is improved, do the forecasts often verify worse?
URL: http://cawcr.gov.au/bmrc/wefor/staff/eee/verif/Goeber_Wilson/Double_penalty_combined.html (Accessed on 27 Nov.2012).

Gurriaran, R., Maro, D., Bouisset, P., Hebert, D., Leclerc, G., Mekhlouche, D., Rozet, M., and Solier, L. (2004). In situ metrology of 85Kr plumes released by the COGEMA La Hague nuclear reprocessing plant. *Journal of Environmental Radioactivity*, 72:137–144.

Helle, K. B. and Pebesma, E. (2013). Stationary sampling designs based on plume simulations. In Mateu, J. and Müller W.G., editors, *Spatio-Temporal Design: Advances in Efficient Data Acquisition*, pages 319–344. John Wiley & Sons.

Holton, J. (2004). *An Introduction to Dynamic Meteorology*, volume 88 of *International geophysics series*. Elsevier Academic Press.

IAEA (1997). INFCIRC/540: Model Protocol Additional to the Agreement(s) and State(s) and the International Atomic Energy Agency for the Application of Safeguards. Vienna, Austria, September 1997. URL: `http://www.iaea.org/Publications/Documents/Infcircs/1997/infcirc540c.pdf` (Accessed on 30 Oct.2012).

IAEA (1999). Use of Wide Area Environmental Sampling in the Detection of Undeclared Nuclear Activities. Member State Supports Program to the IAEA. Report STR-321.

IAEA (2004). Strengthening the Effectiveness and Improving the Efficiency of the Safeguards System and Application of the Model Additional Protocol. Resolution GC(48)/RES/14.

IAEA (2005). Technical Meeting on Noble Gas Monitoring Sampling And Analysis for Safeguards Applications. Tech. Rep. STR-351.

IAEA (2010). Novel Technologies for IAEA Safeguards. Report IAEA-CN-184/326.

iGSE (2006). iGSE - Detection of Clandestine Production of Nuclear-Weapons-Usable Materials. *INESAP Information Bulletin*, 27:4–8. URL: `http://www.inesap.org/bulletins/bulletin-27` (Accessed on 10 Dec.2012).

iGSE (2010). Measurements of Krypton-85. Independent Group of Scientific Experts on the detection of clandestine nuclear-weapons-usable materials production. URL: `http://www.igse.net/index.php?id=125` (Accessed on 12 Dec.2012).

IPFM (2007). Global Fissile Material Report 2007. International Panel on Fissile Materials. URL: `http://fissilematerials.org/library/gfmr07.pdf` (Accessed on 30 Oct.2012).

Izrael, Y.A., Nazarov, I.M., and Riabosapko (1982). Kr-85 anthropogenic emissions into the atmosphere. *Soviet Meteorology and Hydrology*, 6:1–9.

JRC (2004). Homepage of the European Tracer EXperiment (ETEX). Joint Research Centre of the European Commission, Ispra, Italy. URL: `http://rem.jrc.ec.europa.eu/etex/` (Accessed on 4 Dec.2012).

Jubin, R. (2008). Spent fuel reprocessing. Introduction to Nuclear Chemistry and Fuel Cycle Separations Course. Consortium for Risk Evaluation with Stakeholder Participation (CRESP).

Kalinowski, M.B. (2008). Remote environmental sampling for the detection of clandestine nuclear weapons production and testing. In Janssens-Meanhout, G., editor, *Nuclear Safeguards and Non-Proliferation Course Syllabus*, pages 269–278. European Safeguards Research and Development Association (ESARDA), Dec. 2008, European Communities, Luxembourg.

Kalinowski, M.B. (2012). personal communication.

Kalinowski, M.B., Feichter, J., Nikkinen, M., and Schlosser, C. (2006). Environmental Sample Analysis. In Avenhaus, R., Kyriakopoulos, N., Richard, M., and Stein, G., editors, *Verifying Treaty Compliance: Limiting weapons of mass destruction and monitoring Kyoto protocol provisions*, pages 367–387. Springer.

Kalinowski, M.B., H. Sartorius, S. U. W. W. (2004). Conclusions on plutonium seperation from atmospheric krypton-85 measured at various distances from the Karlsruhe reprocessing plant. *Journal of Environmental Radioactivity*, 73:203–222.

Kemp, R.S. and Schlosser, C. (2008). A performance estimate for the detection of undeclared nuclear-fuel reprocessing by atmospheric krypton-85. *Journal of Environmental Radioactivity*, 99:1341–1348. Erratum Journal of Environmental Radioactivity, Vol 100(2009), 99.

Klingberg, F.J., Hebel, S., and Kalinowski, M.B. (2011). Simulation of atmospheric noble gas transport to determine the accuracy of locating unreported reprocessing. Phase I, 2nd Year Status Report for Task C.38/A1643. *Report JOPAG/01.09-PRG-373.*

Klingberg, F.J., Hebel, S., Kilian, M., Wotawa, G., and Kalinowski, M.B. (2010). Simulation of atmospheric noble gas transport to assess sampling procedures for locating unreported reprocessing. Paper to a poster presented at the IAEA Symposium on International safeguards, 1-5 November 2010, IAEA-CN-184/36.

Kompf, M. (2012). Entfernungsberechnung.
URL: `http://www.kompf.de/gps/distcalc.html` (Accessed on 12 Dec.2012).

Ross, O., Ahlswede, J., Annewandter, R., Schlünzen, K.H., and Kalinowski, M.B. (2010). Simulations of atmospheric krypton-85 to assess the detectability of clandestine nuclear reprocessing. Paper to a poster presented at the IAEA Symposium on International Safeguards, 1-5 November 2010, IAEA-CN-184/034.

Ross, J.O. (2010). Simulation of atmospheric krypton-85 transport to assess the detectability of clandestine nuclear reprocessing. Dissertation, Max Planck Institute for Meteorology, Reports on Earth System Science, 2010-82.

Sartorius, H., Schlosser, C., Schmid, S., and Weiss, W. (2002). Verfahren zur Bestimmung der Aktivitätskonzentration der atmosphärischen Edelgase Krypton-85 und Xenon-133. *Loseblattsammlung FS-78-15-AKU Empfehlungen zur Überwachung der Umweltradioaktivität*, Blatt 3.4.9.

Schlosser, C., Auer, M., Sartorius, H., and Kumberg, T. (2010). Edelgasmessungen des BfS für IMIS und CTBTO. In *Fachgespräch zur Überwachung der Umweltradioaktivität, Freiburg, 23.-26.03.2009, Tagungsband*, pages 111–119. Bundesministerium für Umwelt, Naturschutz und Reaktorsicherheit (BMU).

Schoetter, R. (2010). Noble gas treatment and emission characteristics of point sources with relevance to undeclared nuclear activities, Diploma thesis, Department of Physics, University of Hamburg.

Seibert, P. and Frank, A. (2004). Source-receptor matrix calculation with a Lagrangian particle dispersion model in backward mode. *Atmospheric Chemistry and Physics*, 4:51–63.

Seibert, P. (2007). Flex_to_srm Software, Version 2 2007-04-13. README file. URL: `http://www.wau.boku.ac.at/11748.html?&L=0` (Accessed on 12 Dec.2012).

Shepard, D. (1968). A two-dimensional interpolation function for irregularly-spaced data. In *Proceedings of the 1968 23rd ACM national conference*, pages 517–524. ACM.

Stohl, A., Forster, C., Frank, A., Seibert, P., and Wotawa, G. (2005). Technical note: The lagrangian particle dispersion model FLEXPART version 6.2. *Atmospheric Chemistry and Physics*, 5:2461–2474.

Stohl, A., Hittenberger, M., and Wotawa, G. (1998). Validation of the lagrangian particle dispersion model FLEXPART against large-scale tracer experiment data. *Atmospheric Environment*, 32(24):4245–4264.

UNODA (2012). Treaty on the Non-Proliferation of Nuclear Weapons (NPT). United Nations Office for Disarmament Affairs. URL: `http://www.un.org/disarmament/WMD/Nuclear/NPT.shtml` (Accessed on 30 Oct.2012).

Winger, K., Feichter, J., Kalinowski, M.B., Sartorius, H., and Schlosser, C. (2005). A new compilation of the atmospheric krypton-85 inventories from 1945 to 2000 and its evaluation in a global transport model. *Journal of environmental radioactivity*, 80(2):183–215.

WISE (2002). Graphs prepared by WISE-Paris for the presentation of the Scientific and Technological Options Assessment report at the Public Hearing of the Committee of Petitions European Parliament, Bruxelles, 17-18 April 2002. World Information Service on Energy. URL: `http://www.wise-paris.org/index.html?/english/ourgraphs/stoa/` `stoa_graphs.html&/english/frame/menu.html&/english/frame/band.html` (Accessed on 27 Nov.2012).

Wotawa, G. (2010). Meteorological applications for environment and emission control. Script of lecture held at the University of Vienna from March to June 2010.

Wotawa, G. and Becker, A. (2007). Atmospheric transport modelling and data fusion in support of Comprehensive Nuclear-Test-Ban Treaty verification. In *29th Monitoring Research Review: Ground-Based Nuclear Explosion Monitoring Technologies*, pages 806–812.

Wotawa, G., De Geer, L.E., Denier, P., Kalinowski, M.B., Toivonen, H., D'Amours, R., Desiato, F., Issartel, J.P., Langer, M., Seibert, P., Frank, A., Sloan, C., and Yamazawa, H. (2003). Atmospheric transport modelling in support of CTBT verification - overview and basic concepts. *Atmospheric Environment*, 37:2529–2537.

Wotawa, G. (2012). personal communication.

Zimmermann, P.H., Feichter, J. R. C. W. W. (1989). A global three-dimensional source-receptor model investigation using 85Kr. *Atmospheric Environment*, 23(1):25–35.

Acknowledgements

First of all, I'd like to thank Prof. Leopold Haimberger (Department of Meteorology and Geodynamics, University of Vienna), the supervisor of this thesis, Dr. Gerhard Wotawa (Central Institute for Meteorology and Geodynamics, Austria) and Prof. Martin B. Kalinowski (Center for Science and Peace Research at the University of Hamburg) for offering me the initiating project. They all supported me greatly by answering scientific questions directly without any waiting time and giving me technical advice "on demand". I also want to thank Veronika Flöry for proofreading this thesis.

Besides I want be grateful for the interdisciplinary thinking, several possibilities (i.e. field-campaigns) and enthusiasm of the professors and staff of my department as well as external lecturers, who enabled me to view beyond the horizon and want to thank them for the constructive conversations I've been made as the students representative.

Special thanks owe to my partens who always worked hard to enable my education and deeply supported me both physically and mentally. Furthermore I want to thank Viki Kivi and her familiy, who always supported and encouraged me, especially during the STUMETA project.

Last but not least I want to thank all my colleagues, especially Johanna Bugkel and Marion Rothmüller for a friendly atmosphere and extensive as well as productive working sessions.

Curriculum Vitae

Name	Rainer Kaltenberger
Date of birth	1988/01/19
Place of birth	Vienna
Nationality	Austrian
Contact	kaltenberger.rainer@gmail.com

Education

2007 - 2013	Diploma study of meteorology at the University of Vienna
1998 - 2006	Bundesrealgymnasium, 1210 Vienna, Ödenburgerstraße 74 Matura passed with distinction (A-level)

Vacancies, projects and teaching

2012	Manager and Head of Organisation: STUMETA 2012 at Vienna (International scientific conference of meteorology students with 250 participants over several days) [i]
Since 2011	Project "WELI": Gathering of free-available real-time meteorological data for synoptic- and mesoscale analysis and forecasting [ii]
Since 2011	Member of the Austrian Society of Meteorology (ÖGM)
12/2011 - 4/2012	Joint project of ZAMG, Centre of Science and Peace Research (ZNF, University of Hamburg) funded by the German National Support Program of the International Atomic Energy Agency (IAEA): Prepatory study for a measurement program of krypton-85 to detect clandestine nuclear reprocessing activities via backward-modelling with the Lagrangian particle dispersion model FLEXPART.
2011 - 2013	Student Representative of Meteorology and Geophysics, National Union of Students (ÖH)
2011	Obtaining a performance scholarship
2010 - 2012	Teaching: University tutor at the Department of Meteorlgy and Geophysics of the University of Vienna (forecasting course, field experiments in Costa Rica, sinkhole)
2008 - 2011	Several national und international field-campaigns (University of Vienna and University of Natural Resources and Applied Life Sciences Vienna (BOKU)) • Microclimates of rainforests, coastal- and mountainous regions/Costa Rica [iii] • Mass balance measurements of an Austrian glacier • Aviation meteorology field-campaigns (balloning, gliding) • Sinkhole field experiments in the Eastern Alps • Stormchasing
2009 & 2011	Internships at Austrians air traffic control Austrocontrol (verification of nowcasting products)
2008	Internship at the Institute of Quantum Opics, Quantum Nanophysics and Quantum Information (IQOQI), University of Vienna
2008	Receptionist at diamond:dogs webconsulting GmbH
2007 & 2008	Internships at the Institute for Horticulture, Fruit-Growing and Viticulture, University of Natural Resources and Applied Life Sciences Vienna (BOKU)
2006/2007	Civilian service: Administrative assistant at the Police Directorate Vienna
2006 & 2007	Internships: Assistant of general contructor for construction management at Porr Corp.
2002	Volunteer at the forecasting department of the ZAMG (Central Institute for Meteorology and Geodynamics, Austria)

Skills and research interests

Skills	Team-player, interdisciplinar approaches
Languages	German (mother tongue), English (fluent), Spanish und French (basics)
Programming skills	Web programming (HTML, CSS, PHP) , Fortran, Unix shell-scripts, Matlab, familiar working environments: Linux, Windows
Certificates	EBDL (European Business Competence License)
Research interests	Synoptic meteorology, environmental meteorology, aviation meteorology

---

References (accessed on 2013/01/07)

[i] http://univie.ac.at/stumeta (official conference page)
[ii] http://www.unet.univie.ac.at/~a0704905/weli (poject page)
[iii] http://univie.ac.at/amk/costaricablog (blog of students of the Costa Rica campaign)